

Carbon dioxide methanation in a catalytic microchannel reactor

N Engelbrecht
22800433

Dissertation submitted in fulfilment of the requirements for the degree **Master of Engineering in Chemical Engineering** at the Potchefstroom Campus of the North-West University


Supervisor: Prof RC Everson
Co-supervisor: Dr S Chiuta
Assistant supervisor: Dr DG Bessarabov
Assistant supervisor: Prof HWJP Neomagus

May 2017

DECLARATION

I, Nicolaas Engelbrecht, declare herewith that the dissertation entitled: “**Carbon dioxide methanation in a catalytic microchannel reactor**”, submitted in fulfilment of the requirements for the degree Master of Engineering in Chemical Engineering, is my own work, except where acknowledged in the text, and has not been submitted to any other tertiary institution in whole or in part.

Signed at North-West University (Potchefstroom Campus)



Nicolaas Engelbrecht

14/11/2016

Date

ACKNOWLEDGEMENTS

The author would like to thank a number of people for their assistance and contributions during this study. Your continuous support and guidance proved invaluable during this period.

Project related acknowledgements:

- Prof. Raymond Everson for the leadership and support you provided during the course of this study. Thank you for your involvement and constant mentorship in every weekly meeting. Your contributions and recommendations was greatly appreciated.
- Dr. Steven Chiuta for your continual assistance and contributions in all aspects of this study. Your inputs were truly helpful. Furthermore, you always made time for me and I truly appreciate that. In addition, the valuable life lessons I learned from you will always be cherished.
- Dr. Dmitri Bessarabov for the opportunity I had to be part of HySA Infrastructure Centre of Competence. In addition, the financial support you provided through the Department of Science and Technology is much appreciated. Your valuable inputs during this study are also acknowledged.
- Prof. Hein Neomagus for your valuable insight and guidance during weekly meetings. It is greatly appreciated.
- Prof. Schalk Vorster for your contributions and recommendations during language editing of this dissertation.
- Ted Paarlberg for building experimental apparatus used during this study. Thank you for your assistance in this regard.
- Hennie Coetzee and Frikkie Conradie for making CFD modelling possible and providing assistance whenever needed.
- Dr. Andries Krüger and Phillimon Modisha for technical assistance and contributions with regards to my experimental setup.
- Isabella Ndlovu for teaching me the basics of operating a gas chromatograph and your assistance with CFD modelling.
- Louise, Lara, Tony and Neels for your help and support with regards to general administration and the handling of orders.

Personal acknowledgements:

- Firstly, to our Heavenly Father for His end-less love and daily guidance. All the glory to Him who blessed me with abilities beyond imagination, who gives me strength during difficult times and whose love constantly surrounds me. Without Him, nothing would have been possible.
- Yvonne, my mother, and Frits, my father, for your never-ending love and support. Your nurture and guidance made me the man I am today.
- Carla, my sister, for your love and support throughout. Your positive attitude inspired me when I needed it most.
- Finally, to all other family and friends for your constant support and motivation during tough times.

ABSTRACT

The work reported in this dissertation demonstrated the practicality of a catalytic microchannel reactor for CO₂ methanation implemented via the Sabatier reaction for potential power-to-gas applications. A combined experimental and computational fluid dynamic (CFD) modelling approach was used to evaluate the microchannel reactor washcoated with an 8.5 wt.% Ru/Al₂O₃ catalyst. For the experiments, a stoichiometric feed ratio (1:4) of CO₂ and H₂ was used. The reactor was evaluated for CO₂ methanation at different reaction temperatures (250–400°C), pressures (atmospheric, 5 bar and 10 bar), and gas hourly space velocities (32.6–97.8 NL.g_{cat}⁻¹.h⁻¹). The highest CO₂ conversion of 96.8% was achieved for the lowest space velocity (32.6 NL.g_{cat}⁻¹.h⁻¹) and conditions corresponding to 375°C and 10 bar. The CH₄ production was however maximised operating the reactor at conditions corresponding to high space velocity (97.8 NL.g_{cat}⁻¹.h⁻¹), high temperature (400°C) and at 5 bar. At this operating point the reactor showed 83.4% CO₂ conversion, 83.5% CH₄ yield and high CH₄ productivity (16.9 NL.g_{cat}⁻¹.h⁻¹). The microchannel reactor demonstrated good long-term performance and no observable catalyst deactivation even after start-stop and continuous cycles, thereby proving its ability to handle dynamic operation required for power-to-gas applications. A CFD model was developed and used to interpret the experimental reactor performance, as well as provide fundamental insight into the reaction-coupled transport phenomena within the reactor. Most importantly, global kinetic rate expressions were developed using model-based parameter estimation. Results from the CFD model corresponded with good agreement to the experimental reactor performance in terms of CO₂ conversion and CH₄ yield over a wide range of operating parameters. The model also provided velocity and concentration distributions to better understand the transport principles established within the reactor. Overall, the results presented in this dissertation pinpointed the important aspects of realising CO₂ methanation at the micro-scale and could provide a platform for future studies using microchannel reactors for power-to-gas applications.

Keywords: Power-to-gas concept, CO₂ methanation, Sabatier reaction, experimental reactor evaluation, microchannel reactor, Ru/Al₂O₃ catalyst, computational fluid dynamic (CFD) modelling, kinetic parameter estimation

TABLE OF CONTENTS

DECLARATION.....	I
ACKNOWLEDGEMENTS.....	II
ABSTRACT	IV
TABLE OF CONTENTS	V
LIST OF TABLES.....	IX
LIST OF FIGURES	X
LIST OF SYMBOLS.....	XIV
LIST OF PUBLICATIONS RELATED TO THIS STUDY	XV
CHAPTER 1: INTRODUCTION.....	1
1.1 Background and problem statement	1
1.2 Motivation	3
1.3 Objectives	4
1.4 Scope of the dissertation.....	4
CHAPTER 2: LITERATURE REVIEW.....	6
2.1 Introduction	6
2.2 Technology pathways for implementing power-to-gas	8
2.2.1 Renewable H ₂ blending a natural gas network.....	9
2.2.2 Chemical methanation	9
2.2.3 Biological methanation	9
2.2.4 Dual-fuel gas turbines.....	10
2.3 CO ₂ methanation via the Sabatier reaction.....	10
2.3.1 Reaction mechanism	12

2.3.1.1	Successive CO ₂ and CO dissociation to form surface carbon.....	12
2.3.1.2	Direct hydrogenation of adsorbed CO	13
2.3.1.3	Considerations on reaction mechanism.....	13
2.3.2	Thermodynamics of CO₂ methanation.....	13
2.4	Current status of CO₂ methanation	15
2.5	Reactor technology options for CO₂ methanation	21
2.5.1	Fluidized-bed reactor	21
2.5.2	Slurry bubble column reactor.....	21
2.5.3	Fixed-bed reactor	21
2.5.4	Microchannel reactor	22
2.5.5	Summary.....	22
2.6	Microchannel reactor technology	23
2.6.1	Advantages of microchannel reactors.....	23
2.6.2	Differences of microchannel reactors to conventional reactor types	24
2.6.3	Limitations and design challenges of microchannel reactor technology.....	25
2.7	Reactor modelling and simulations for CO₂ methanation	25
2.7.1	Computational fluid dynamic (CFD) modelling of microchannel reactors for CO ₂ methanation.....	29
2.7.2	Reaction kinetics of CO ₂ methanation on supported Ru catalysts.....	29
2.7.3	Summary.....	30
CHAPTER 3: EXPERIMENTAL APPARATUS		31
3.1	Microchannel reactor design.....	31
3.2	Catalyst preparation.....	33
3.3	Experimental planning.....	33
3.3.1	Thermodynamic equilibrium	33
3.4	Experimental apparatus.....	35
3.5	Experimental procedure	37

CHAPTER 4: RESULTS AND DISCUSSION: EXPERIMENTAL RESULTS	38
4.1 Reactor performance parameters	38
4.2 Effect of reactor temperature on CO ₂ methanation performance	38
4.3 Effect of reactor pressure on CO ₂ methanation performance.....	40
4.4 Effect of space velocity on CO ₂ methanation performance.....	41
4.5 Reactor pressure drop analysis	42
4.6 Durability test of reactor performance.....	42
4.7 Repeatability of experimental data points	43
4.8 Optimum reactor conditions for CH ₄ production	44
CHAPTER 5: COMPUTATIONAL FLUID DYNAMIC (CFD) MODEL DEVELOPMENT, RESULTS AND DISCUSSION	45
5.1 CFD model development	45
5.1.1 Model geometry.....	45
5.1.2 Model assumptions.....	46
5.1.3 Governing equations	47
5.1.4 Boundary conditions	48
5.1.5 Reaction kinetics.....	49
5.1.6 Solution method.....	49
5.2 CFD model results.....	50
5.2.1 Kinetic parameter estimation	50
5.2.2 Model validation: CO ₂ conversion and CH ₄ yield	51
5.2.3 Microchannel reactor transport phenomena.....	53
5.2.3.1 Velocity distributions.....	53
5.2.3.2 Concentration distributions.....	55
CHAPTER 6: CONCLUSIONS AND RECOMMENDATIONS	61
6.1 Conclusions.....	61
6.2 Contributions to current knowledge	62
6.3 Recommendations	62

BIBLIOGRAPHY	64
APPENDIX A: GAS CALIBRATION CURVES	76
APPENDIX B: FULL SET OF EXPERIMENTAL DATA.....	80
APPENDIX C: PARITY PLOTS	81

LIST OF TABLES

Table 2.1: Liquid volumetric energy densities of common hydrogen-containing fuels	8
Table 2.2: Summary of experimental CO ₂ methanation reactors reported in literature	15
Table 2.3: A summary of literature on mathematical modelling for CO ₂ methanation	25
Table 4.1: Optimum reactor conditions and performance parameters of microchannel reactor	44
Table 5.1: Summary of catalyst physical properties used for modelling the porous catalyst computational domain	47
Table 5.2: Summary of governing equations for modelling the free-fluid and porous catalyst computational domains	47
Table 5.3: Best-fitting kinetic parameters at different operating pressures.....	51
Table A.1: Example of the data collection table used during the experimental investigation.....	79

LIST OF FIGURES

Figure 1.1: P2G technology implementation.....	2
Figure 2.1: Discharge time and capacity of different energy storage methods.....	7
Figure 2.2: Equilibrium product formation (d.b.) of CO ₂ methanation at atmospheric pressure.....	14
Figure 2.3: Effect of temperature and pressure on equilibrium CO ₂ conversion.....	15
Figure 2.4: Rates of CH ₄ formation as a function of residence time at different temperature conditions	27
Figure 3.1: (a) Depiction of reactor platelet with 80 microchannels and fluid distribution manifolds engraved (b) second reactor platelet with only fluid distribution manifolds engraved for laser welding to complete the reactor (c) magnified view of 5 microchannels with applied catalyst washcoat and (d) a single, uncoated microchannel with dimensions.....	32
Figure 3.2: Microchannel reactor used during experimental investigation.....	32
Figure 3.3: Equilibrium product formation (d.b.) of CO ₂ methanation (stoichiometric H ₂ :CO ₂ molar feed ratio)	34
Figure 3.4: Effect of temperature on equilibrium CO ₂ conversion	34
Figure 3.5: Effect of temperature on equilibrium CH ₄ yield (stoichiometric H ₂ :CO ₂ molar feed ratio)	35
Figure 3.6: Flow diagram of CO ₂ methanation setup	36
Figure 3.7: Experimental setup used for conducting CO ₂ methanation experiments. (1) Control box (2) mass flow controllers (3) continuous gas analyser (4) microchannel reactor unit (5) water condenser and (6) online GC.....	36
Figure 4.1: Effect of reactor temperature on CO ₂ conversion (left) and CH ₄ yield (right) at atmospheric pressure and GHSVs of 32.6, 65.2 and 97.8 NL.g _{cat} ⁻¹ .h ⁻¹	39
Figure 4.2: Effect of reactor temperature on CO ₂ conversion (left) and CH ₄ yield (right) at 10 bar pressure and GHSVs of 32.6, 65.2 and 97.8 NL.g _{cat} ⁻¹ .h ⁻¹	40

Figure 4.3: Effect of reactor pressure on CO ₂ conversion (left) and CH ₄ yield (right) at 400°C and GHSVs of 32.6, 65.2 and 97.8 NL.g _{cat} ⁻¹ .h ⁻¹	40
Figure 4.4: Effect of GHSV on CO ₂ conversion (left) and CH ₄ yield (right) at atmospheric pressure and reactor temperatures of 250°C, 325°C and 400°C	41
Figure 4.5: Effect of GHSV on CO ₂ conversion (left) and CH ₄ yield (right) at 10 bar pressure and reactor temperatures of 250°C, 325°C and 400°C	42
Figure 4.6: Reactor pressure drop analysis at 10 bar pressure and GHSVs of 32.6, 65.2 and 97.8 NL.g _{cat} ⁻¹ .h ⁻¹	42
Figure 4.7: CO ₂ conversion (left) and CH ₄ yield (right) over an extended test period of 150 h at reactor temperature of 375°C, 10 bar pressure and GHSV of 65.2 NL.g _{cat} ⁻¹ .h ⁻¹	43
Figure 4.8: Repeatability of CO ₂ conversion (left) and CH ₄ yield (right) at atmospheric pressure and reactor temperatures of 275°C, 350°C and 400°C	43
Figure 5.1: Discretized model geometry used during CFD modelling containing 43 520 free-triangular domain elements	46
Figure 5.2: Model fit on CO ₂ conversion (left) and CH ₄ yield (right) at atmospheric pressure and GHSVs of 32.6, 65.2 and 97.8 NL.g _{cat} ⁻¹ .h ⁻¹	52
Figure 5.3: Model fit on CO ₂ conversion (left) and CH ₄ yield (right) at 5 bar pressure and GHSVs of 32.6, 65.2 and 97.8 NL.g _{cat} ⁻¹ .h ⁻¹	52
Figure 5.4: Model fit on CO ₂ conversion (left) and CH ₄ yield (right) at 10 bar pressure and GHSVs of 32.6, 65.2 and 97.8 NL.g _{cat} ⁻¹ .h ⁻¹	53
Figure 5.5: Axial velocity (v _x) profile at the mid-xz plane for 250°C (left) and 400°C (right) at atmospheric pressure and GHSV of 32.6 NL.g _{cat} ⁻¹ .h ⁻¹	54
Figure 5.6: Axial velocity (v _x) profile at the mid-xz plane for 250°C (left) and 400°C (right) at 10 bar pressure and GHSV of 32.6 NL.g _{cat} ⁻¹ .h ⁻¹	55
Figure 5.7: Species mole fraction (d.b.) along normalised microchannel length (x/L) for 32.6 NL.g _{cat} ⁻¹ .h ⁻¹ (left) and 97.8 NL.g _{cat} ⁻¹ .h ⁻¹ (right) at 400°C and atmospheric pressure	56

Figure 5.8: Species mole fraction (d.b.) along normalised microchannel length (x/L) for 32.6 $\text{NL.g}_{\text{cat}}^{-1}.\text{h}^{-1}$ (left) and 97.8 $\text{NL.g}_{\text{cat}}^{-1}.\text{h}^{-1}$ (right) at 400°C and 10 bar pressure.....	57
Figure 5.9: Reaction rate along normalised microchannel length (x/L) for atmospheric (left) and 10 bar pressure (right) at 400°C and 32.6 $\text{NL.g}_{\text{cat}}^{-1}.\text{h}^{-1}$	58
Figure 5.10: Axial CO_2 mass flux at the mid-xz plane for 32.6 $\text{NL.g}_{\text{cat}}^{-1}.\text{h}^{-1}$ (left) and 97.8 $\text{NL.g}_{\text{cat}}^{-1}.\text{h}^{-1}$ (right) at 400°C and atmospheric pressure	58
Figure 5.11: Axial CO_2 mass flux at the mid-xz plane for 32.6 $\text{NL.g}_{\text{cat}}^{-1}.\text{h}^{-1}$ (left) and 97.8 $\text{NL.g}_{\text{cat}}^{-1}.\text{h}^{-1}$ (right) at 400°C and 10 bar pressure.....	59
Figure 5.12: CH_4 concentration along normalised microchannel height (z/H) for atmospheric (left) and 10 bar pressure (right) at different x-coordinates (10, 100, 300 and 500 μm) from the microchannel inlet at 400°C.....	60
Figure A.1: Hydrogen calibration curve used to calculate H_2 mole fraction in product gas during experiments.....	76
Figure A.2: Carbon dioxide calibration curve used to calculate CO_2 mole fraction in product gas during experiments.....	77
Figure A.3: Methane calibration curve used to calculate CH_4 mole fraction in product gas during experiments.....	77
Figure A.4: Carbon monoxide calibration curve used to calculate CO mole fraction in product gas during experiments.....	78
Figure B.1: Effect of reactor temperature on CO_2 conversion (left) and CH_4 yield (right) at atmospheric pressure and GHSVs of 32.6, 48.9, 65.2, 81.5 and 97.8 $\text{NL.g}_{\text{cat}}^{-1}.\text{h}^{-1}$	80
Figure B.2: Effect of reactor temperature on CO_2 conversion (left) and CH_4 yield (right) at 5 bar pressure and GHSVs of 32.6, 48.9, 65.2, 81.5 and 97.8 $\text{NL.g}_{\text{cat}}^{-1}.\text{h}^{-1}$	80
Figure B.3: Effect of reactor temperature on CO_2 conversion (left) and CH_4 yield (right) at 10 bar pressure and GHSVs of 32.6, 48.9, 65.2, 81.5 and 97.8 $\text{NL.g}_{\text{cat}}^{-1}.\text{h}^{-1}$	80

Figure C.1: Parity plot of model predicted vs experimental CO ₂ conversion at atmospheric pressure	81
Figure C.2: Parity plot of model predicted vs experimental CO ₂ conversion at 5 bar pressure.....	81
Figure C.3: Parity plot of model predicted vs experimental CO ₂ conversion at 10 bar pressure.....	81

LIST OF PUBLICATIONS RELATED TO THIS STUDY

Peer-reviewed journal publications

Engelbrecht, N., Chiuta, S., Everson, R.C., Neomagus, H.W.J.P. & Bessarabov D.G. 2017. Experimentation and CFD modelling of a microchannel reactor for carbon dioxide methanation. *Chemical Engineering Journal*, 313:847-857.

<http://dx.doi.org/10.1016/j.cej.2016.10.131>

Chemical Engineering Journal 313 (2017) 847–857



Experimentation and CFD modelling of a microchannel reactor for carbon dioxide methanation



Nicolaas Engelbrecht, Steven Chiuta*, Raymond C. Everson, Hein W.J.P. Neomagus, Dmitri G. Bessarabov*

HySA Infrastructure Centre of Competence, North-West University, Faculty of Engineering, Private Bag X6001, Potchefstroom Campus, 2531, South Africa

HIGHLIGHTS

- Sabatier reaction is successfully demonstrated in a microchannel reactor.
- A combined approach with experiments and computational fluid dynamics is presented.
- Microchannel reactor showed high CO₂ conversion and CH₄ productivity.
- Global methanation kinetic rate law to predict experimental data is developed.
- CFD model identified operational limits and reaction-coupled transport phenomena.

ARTICLE INFO

Article history:

Received 30 August 2016
Received in revised form 24 October 2016
Accepted 29 October 2016
Available online 2 November 2016

Keywords:

Renewable hydrogen
Power-to-gas
CO₂ methanation
Sabatier reaction
Microchannel reactor
CFD modelling

ABSTRACT

The methanation of carbon dioxide (CO₂) via the Sabatier process is increasingly gaining interest for power-to-gas application. In this investigation, a microchannel reactor was evaluated for CO₂ methanation at different operational pressures (atmospheric, 5 bar, and 10 bar), reaction temperatures (250–400 °C) and space velocities (32.6–97.8 L_{gas}⁻¹h⁻¹). The recommended operation point was identified at reactor conditions corresponding to 5 bar, 400 °C, and 97.8 L_{gas}⁻¹h⁻¹. At this condition, the microchannel reactor yielded good CO₂ conversion (83.4%) and high methane (CH₄) productivity (16.9 L_{gas}⁻¹h⁻¹). The microchannel reactor also demonstrated good long-term performance at demanding operation conditions relating to high space velocity and high temperature. Subsequently, a CFD model was developed to describe the reaction-coupled transport phenomena within the microchannel reactor. Kinetic rate expressions were developed and validated for all reaction conditions to provide reaction source terms for the CFD modelling. Velocity and concentration profiles were discussed at different reaction conditions to interpret experimental results and provide insight into reactor operation. Overall, the results reported in this paper could give fundamental design and operational insight to the further development of microchannel reactors for CO₂ methanation in power-to-gas applications.

© 2016 Elsevier B.V. All rights reserved.

1. Introduction

Renewable energy sources (RES) such as solar and wind are increasingly gaining acceptance as a significant portion of sustainable energy portfolios across many countries. Indeed, various developments have recently been made on photovoltaic (PV) and wind turbine technologies to exploit renewable sources for large-scale power generation [1]. Despite the recent technological advancements, the intermittency and fluctuation of solar and wind remain arguably the most important challenge in integrating renewable energy sources to the existing grid [2,3]. Recently,

Sterner [4] introduced the concept of power-to-gas (P2G) in Germany's "Energiewende" with the idea of storing excess renewable energy generated using renewable hydrogen. Essentially, the excess power generated by these renewables is harnessed in producing hydrogen (H₂) through the water electrolysis process [5]. Since its first inception, the P2G concept has evolved to include various alternative implementation pathways extended to renewable methane (substitute natural gas) production specifically to enable sustainable capture and utilization of carbon dioxide (CO₂) [1,6–8]. Carbon dioxide is widely recognized as a major greenhouse gas causing global warming.

Renewable methane production achieved via methanation of CO₂ in the Sabatier process (Eq. (1)) is a particularly viable option for P2G implementation owing to an already existing natural gas infrastructure as well as the wide variety of applications (e.g.

* Corresponding authors.

E-mail addresses: 21876533@nwu.ac.za (S. Chiuta), Dmitri.Bessarabov@nwu.ac.za (D.G. Bessarabov).

<http://dx.doi.org/10.1016/j.cej.2016.10.131>
1385-8947/© 2016 Elsevier B.V. All rights reserved.

Conferences attended during this study period

Engelbrecht, N., Chiuta, S., Everson, R.C., Neomagus, H.W.J.P. & Bessarabov D.G. 2016. Carbon dioxide methanation in a catalytic microchannel reactor. 27th Annual Conference of the Catalysis Society of South Africa, 6-9 November, Champagne Sports Resort, KwaZulu-Natal, South Africa.

Engelbrecht, N., Everson, R.C., Neomagus, H.W.J.P., Chiuta, S. & Bessarabov D.G. 2015. CO₂ methanation using renewable hydrogen in a microchannel reactor. 26th Annual Conference of the Catalysis Society of South Africa, 15-18 November, Arabella Country Estate, Western Cape, South Africa.

CHAPTER 1: INTRODUCTION

In Section 1.1 an overview is presented of the important aspects of the background and problem statement of this work. The motivation for this work is provided in Section 1.2. Then the overall and specific objectives of this work are presented in Section 1.3. Finally, the scope of this dissertation is given in Section 1.4.

1.1 Background and problem statement

The ever-expanding global industrial and commercial sectors raise questions about the supply capacity of existing energy resources, e.g. coal and crude-oil (deLlano-Paz *et al.*, 2015:50). Moreover, social and environmental sustainability is of major concern, as currently fossil fuel combustion emits harmful greenhouse gases (GHGs). Carbon dioxide (CO₂) is widely regarded as the biggest contributor to GHGs produced by human activity. In 2013 South Africa emitted 420.4 million tons of CO₂, the 15th highest by country globally (IEA, 2015:49). According to Zhao *et al.* (2015:916) South Africa's high CO₂ emission rate is largely attributed to vast coal resources and considerable subsidies granted to the energy sector by the government. In addition, South Africa started benefiting from a carbon tax policy only in 2015 (National Treasury, 2013:58). The necessity of alternative energy resources is therefore evident, as the dependency on fossil fuels needs to be decreased (Awan & Khan, 2014:237).

Renewable energy sources (RES) such as solar and wind are widely considered as some of the high-ranking potential solutions to the current energy crisis (Ludig *et al.*, 2011:6674). Renewable energy technologies provide sustainable and cleaner sources of energy, which will ultimately reduce humanity's carbon footprint. However, the natural intermittency of solar and wind energy, as well as instances of power oversupply, complicates the sustainability of renewable energy as a base load power source (Finn & Fitzpatrick, 2014:11). The fact that power generated by RES cannot be stored on a large scale and used during times of limited supply (night-time or periods of low wind speed) suggests that an alternative medium for energy storage is required (Scamman & Newborough, 2016:10080). In view of this, the power-to-gas (P2G) technology concept was initially proposed in Germany under the "Energiewende" (energy-turnaround) as a power-grid balancing mechanism to capture and store surplus energy and then used during times of low supply capacity such as night-time or periods of low wind speed (Sterner, 2009:104,106; Ludig *et al.*, 2011:6674; Gahleitner, 2013:2040; Pregger *et al.*, 2013:350; Henning & Palzer, 2014:1004; Vandewalle *et al.*, 2015:28; Götz *et al.*, 2016:1371; Scamman & Newborough, 2016:10080; Chiuta, Engelbrecht, *et al.*, 2016:400). Essentially, P2G

converts excess renewable power into a valuable chemical energy carrier such as hydrogen (H_2) or methane (CH_4), that can be used in different sectors, i.e. the chemical industry, the mobility sector, the gas sector (e.g. for domestic heating) or used to reproduce electricity back into the power grid. The integration of renewable power through P2G and possible implementation pathways of the technology are illustrated in Figure 1.1.

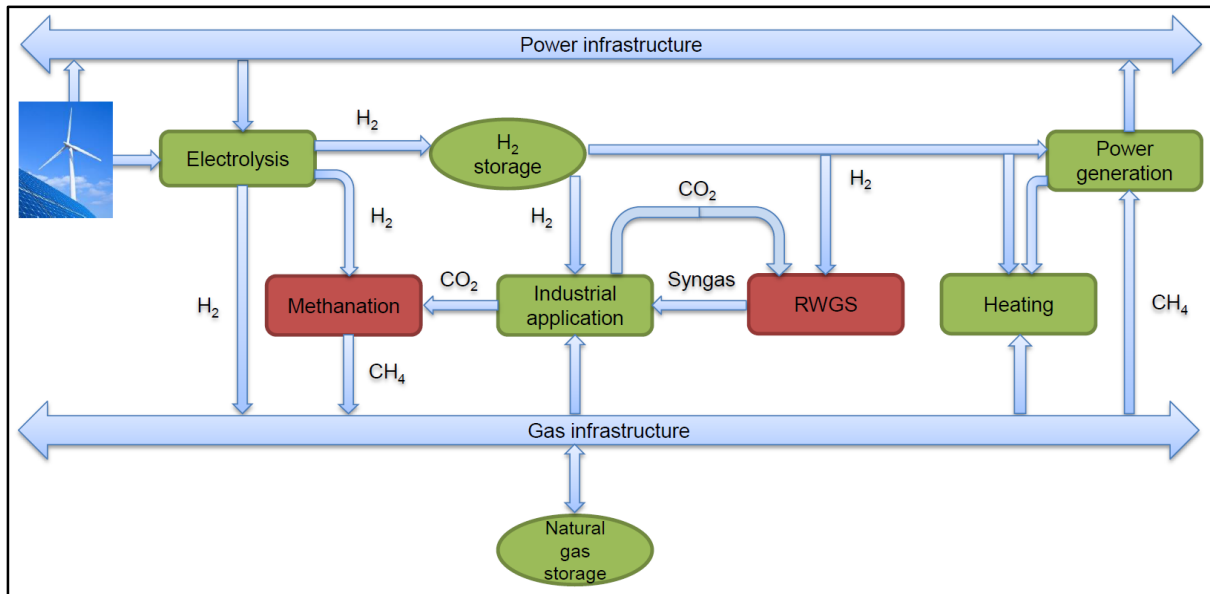


Figure 1.1: P2G technology implementation

To implement the concept of P2G two crucial steps are necessary to produce CH_4 . Firstly, the excess power generated by RES during periods of oversupply is used in the water electrolysis process to produce renewable hydrogen (power-to-hydrogen). If a CO_2 point source is available (e.g. biogas plant, fossil-fuel combustion plant or cement manufacturing process), the CO_2 is subsequently combined with H_2 according to the well-known Sabatier process (Bensmann *et al.*, 2014:413; Vandewalle *et al.*, 2015:28; Rossi *et al.*, 2015:341). Methane is produced with a relatively high volumetric energy density, typically used in the transport sector, energy storage and power generation applications (Hoekman *et al.*, 2010:45). In this manner P2G technology therefore provides a method of converting and storing renewable energy in chemical energy carriers whilst also consuming CO_2 , thereby promoting carbon-neutral and clean energy solutions.

Despite its attractiveness, the implementation of the Sabatier process in P2G setups requires reactors that can operate efficiently in dynamic and frequent start-stop scenarios. Conventional reactors, such as fixed-bed reactors, are well-known for industrial methanation, but are generally intended for continuous operation. It is noteworthy that reactors having fast response times, as well as load-following capabilities, are used for CO_2 methanation in the context of power-to-gas applications. Also, the highly exothermic nature of the Sabatier

reaction is of significance as reactors should have high heat transfer characteristics. As a result, conventional reactors have heat and mass transfer properties that will limit the methanation reaction under demanding reactor conditions (Liu & Ji, 2013:742,743). Microchannel reactors however can sustain the dynamic operation required and provide the quick start-up times necessary for effective operation (Men *et al.*, 2007:82). Microchannel reactor technology essentially demonstrates the concept of process intensification through improved heat and mass transfer properties. Furthermore, reactor units are generally more compact, and by applying a “number-up” approach offers modular-based plants with medium to large-scale capacity for P2G applications. According to Brooks *et al.* (2007:1162) microchannel reactors provide benefits, such as improved catalyst stability and precise temperature control over the reactor. These characteristics coupled with high heat and mass transfer properties will ensure that microchannel reactors deliver improved reactor performance over extended time periods (Fogler, 2012:201).

1.2 Motivation

Solar and wind energy are able to provide clean energy solutions on a large scale if methods providing energy storage are established. An effort is made to prove the feasibility of CO₂ methanation in which CH₄ is produced as an energy storage media in power-to-gas applications. Carbon dioxide is readily available from concentrated industrial point sources and currently considered as a waste product (Vandewalle *et al.*, 2015:28). In contrast to previous studies, this dissertation focuses specifically on the implementation of the Sabatier process in a microchannel reactor. Microchannel reactor technology is generally process-intensifying in nature as high surface-to-volume ratios support improved heat and mass transfer properties (Hessel *et al.*, 2004:202; Holladay *et al.*, 2004:4768). Dynamic and intermittent (start-stop) operation is another advantage critical for application in P2G processes (Chiuta *et al.*, 2013:14988). A thorough analysis of the existing literature indicated very few studies on Sabatier-based microchannel reactors, as only the work previously reported by Brooks *et al.* (2007:1161) investigated a pure feed of CO₂ in a microchannel reactor.

This study will investigate, experimentally as well as numerically, the effects of reactor temperature, pressure and space velocity on the performance of the reactor (i.e. CO₂ conversion, CH₄ yield and specific CH₄ productivity). The work reported by Brooks *et al.* (2007:1161) used a simple one-dimensional plug-flow model to describe their microchannel reactor. The current investigation however will provide a detailed computational fluid dynamic (CFD) model of the reactor in the three-dimensional space. The mathematical modelling of the Sabatier reactor will assist in describing experimental data obtained in this

investigation and define reactor performance at optimum reactor conditions. In essence, using CFD modelling to describe the microchannel reactor will also contribute to a better understanding of the reaction-coupled transport phenomena within the reactor.

1.3 Objectives

The overall objective of this study is to establish the performance of a laboratory-scale microchannel reactor for the methanation of CO₂ over a suitable reaction catalyst. Furthermore, to develop a three-dimensional model of the microchannel reactor and validate the results obtained using experimental data.

The specific objectives of this work are:

- i. To design, develop and demonstrate a microchannel reactor with a commercial Ru/Al₂O₃ catalyst washcoat for the methanation of CO₂.
- ii. To determine the optimum reactor conditions that produce high CO₂ conversion, CH₄ yield and CH₄ throughput.
- iii. To develop a CFD model that describes and provides fundamental insight into the reaction-coupled transport phenomena occurring within the microchannel reactor.
- iv. To validate the CFD model with experimental performance parameters defined as CO₂ conversion and CH₄ yield.

1.4 Scope of the dissertation

Chapter 1 presents an introduction on the background and motivation for the work done in this dissertation. The specific objectives of this study are also listed in this chapter.

Chapter 2 presents relevant literature on the concept and implementation of P2G technology using renewable energies. Previous accounts of literature on the methanation of CO₂ using conventional and sophisticated reactors are summarised, as well as relevant modelling studies of Sabatier-based reactors.

Chapter 3 presents the experimental setup used during this investigation. The experimental microchannel reactor is described, as well as details on other apparatus and procedures followed during the experimental investigation.

Chapter 4 presents the results obtained during the experimental investigation of the microchannel reactor and discusses the influence of reactor temperature, pressure and space velocity on the performance parameters defined as CO₂ conversion, CH₄ yield and specific CH₄ production rate.

Chapter 5 presents a detailed CFD model development of the Sabatier-based microchannel reactor. Through kinetic parameter estimation, the mathematical model is validated on data gained through the experimental investigation. In addition, this chapter serves to explain the reaction-coupled transport phenomena encountered in the microchannel reactor.

Chapter 6 summarises this dissertation with an overview of conclusions related to the objectives set out for this investigation and proposes recommendations for further research done on the subject of CO₂ methanation using microchannel reactor technology.

CHAPTER 2: LITERATURE REVIEW

This chapter serves as a review of relevant literature and presents a concise background to the present study. In Section 2.1 an overview of the current energy crisis and renewable energy as a possible solution is presented. The power-to-gas concept is also introduced in this section. In Section 2.2 a discussion of possible technology implementation pathways for power-to-gas is given. In Section 2.3 the background of the Sabatier process, the reaction mechanism and thermodynamics are presented. In Section 2.4 a comprehensive discussion of previously reported literature on CO₂ methanation in laboratory-scale reactors is given. In Section 2.5 an overview is given of possible reactor technology options considered for implementing the Sabatier process in power-to-gas applications. Section 2.6 focuses on the advantages, differences from conventional reactors and possible technology limitations of microchannel reactor technology. Lastly, in Section 2.7 relevant literature on modelling and simulation of microchannel reactors for CO₂ methanation is presented. Also, appropriate reaction kinetics is discussed in this section.

2.1 Introduction

Recently the focus on adequate energy supply has been highlighted as global economies continue to develop. These developments have raised questions about the sustainable use and supply capacity of current fossil fuel resources. Furthermore, as efforts have been made to meet global energy demands, CO₂ emissions have increased significantly as a result. All of these factors are therefore incentives for the current development of renewable and low-carbon energy technologies (Wang *et al.*, 2011:3703).

Renewable energy sources (RES) are often regarded as the solution to increasing global energy demand, as the scenario of using fossil fuels as primary energy resource is weakening (Schiebahn *et al.*, 2015:4285). Renewable energy sources (e.g. solar and wind) are effectively infinite sources of energy with predictable and therefore reliable patterns. Solar and wind farms can be employed in virtually any location supporting these technologies, with minimal environmental or social impact. In recent years there has been a considerable growth in the advancement of renewable energy technologies such as solar and wind power (Varone & Ferrari, 2015:208). These technologies have made substantial progress in terms of technical development and commercial implementation worldwide.

The daily intermittency (night-time or periods of low wind speed) of RES is arguably the greatest restriction regarding continuous power supply from renewables. During periods of oversupply from renewable energy sources, many power-grids are not able to handle the

supply capacity from these power sources. In addition, the share of renewables are ever-increasing in global energy portfolios. As an example, in Germany peak supply from renewable power sources supplied nearly all of the country's power demand momentarily on 15 May 2016 (Shankleman, 2016). In another case, Scotland's energy demand was fulfilled by wind power on 7 August 2016, as 106% of the country's demand was generated by wind turbines (Johnston, 2016). On the contrary, during night-time or periods of low wind speed, renewable energy sources will be unable to supply any electricity to the power grid. It is therefore evident that methods of large-scale renewable energy storage are desired to provide grid-balancing.

The storage of energy (Figure 2.1) has previously been implemented with methods such as pumped hydro-storage (PHS), flywheels, compressed air energy storage (CAES), electrochemical (e.g. batteries) and thermal energy storage. These systems however provide only small to medium scale energy storage for limited time periods. Currently, alternative methods of storing energy on a large scale are researched (Koochi-Kamali *et al.*, 2013:140,143,155; Judd & Pinchbeck, 2013:3). Promising methods of energy storage such as renewable hydrogen and synthetic natural gas (SNG) provide storage capacity in the GWh range (Figure 2.1).

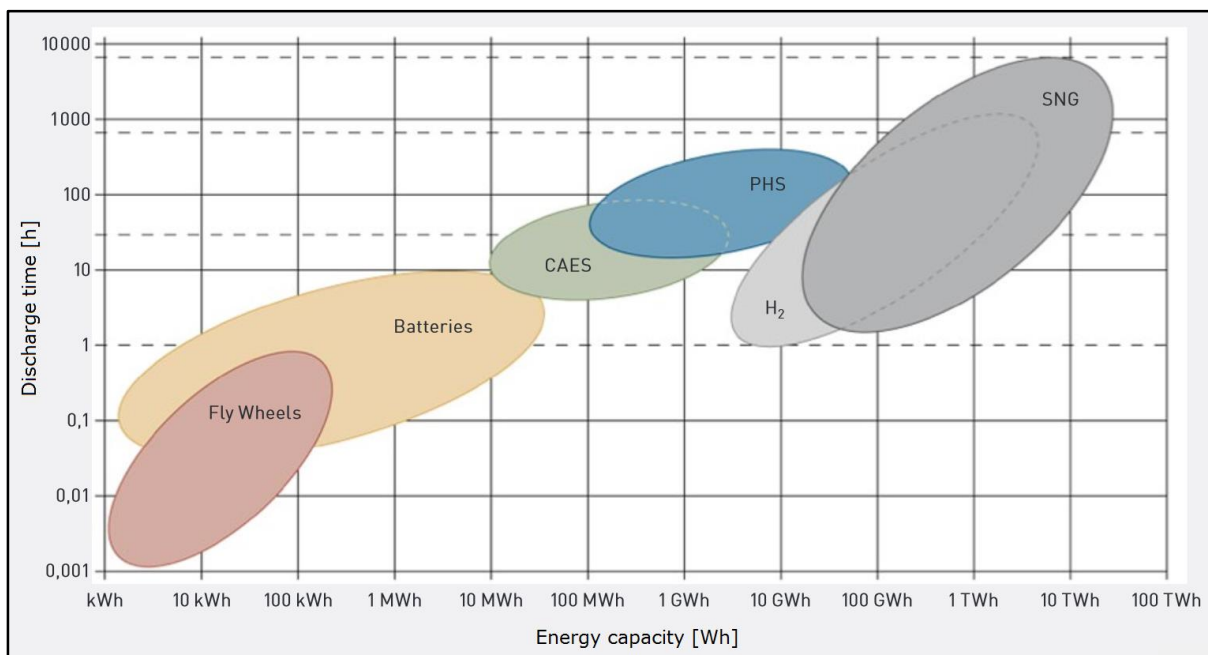


Figure 2.1: Discharge time and capacity of different energy storage methods (adapted from Judd & Pinchbeck, 2013:3)

To compensate for the naturally intermittent supply of solar and wind energy, the power-to-gas (P2G) concept is proposed. The P2G process makes use of excess renewable energy during periods of peak energy supply and stores the energy in the form of chemical

energy carriers (Sterner, 2009:104,106). This energy conversion is achieved through the water electrolysis process and subsequently produces H₂. An additional methanation step using CO₂ can be implemented to produce CH₄, given a ready source of CO₂ (Figure 1.1). With the implementation of P2G technology, fossil fuels and their use in industrial applications can be reduced, possibly providing cleaner energy solutions. The power-to-gas concept can be extended to power-to-X as other chemicals (e.g. syngas, methanol, dimethyl ether etc.) can be used as possible energy carriers depending on the end-use application (Varone & Ferrari, 2015:208; Wang *et al.*, 2011:3704; Yang *et al.*, 2014:1135).

2.2 Technology pathways for implementing power-to-gas

Methane is a particularly attractive option for P2G implementation, as possible applications for CH₄ include the transport and chemical industries. The application of renewable CH₄ is supported as it is a hydrogen-dense energy source and has a substantially higher liquid volumetric energy density than hydrogen (Table 2.1). In addition, synthetic produced CH₄ (SNG) can be stored on a large scale in natural gas networks, as SNG complies with specifications to CH₄ quality in natural gas networks (90–95% CH₄) (Vandewalle *et al.*, 2015:29; Gabbar *et al.*, 2015:188). By converting the excess renewable energy into CH₄ as chemical energy carrier, grid balancing can be achieved through a conventional gas-turbine combustion process, regenerating electrical power (Garmsiri *et al.*, 2014:2507). As mentioned by Sterner (2009:104) the P2G concept therefore has the ability to increase the dependency on RES-based generation methods i.e. scenarios where the majority of an energy portfolio consists of renewables. Energy storage can be achieved through a number of chemical energy carriers. Table 2.1 presents the liquid volumetric energy densities of typical hydrogen-containing fuels.

Table 2.1: Liquid volumetric energy densities of common hydrogen-containing fuels (adapted from U.S. DOE, 2001)

Fuel	Liquid volumetric energy density (MJ.L ⁻¹)
Hydrogen	8.49
Methane	20.92
Propane	23.49
Gasoline	31.15
Diesel	31.44
Methanol	15.80

2.2.1 Renewable H₂ blending a natural gas network

Hydrogen produced through water electrolysis is used as chemical energy carrier and supplied to a natural gas network. On the other hand, this implementation method has its shortcomings. According to Altfeld & Pinchbeck (2013:12) H₂ blends of up to 10 vol.% can be tolerated by general end-use applications. Also, in applications using modern gas turbines supporting premixed burners (i.e. power generation), H₂ blend ratios are restricted to below 5% (Judd & Pinchbeck, 2013:4). Likewise, limitations on components sensitive to H₂ (e.g. steel pipelines and SNG storage tanks) restrict any high H₂ blend ratios (to <10%) as long-term material durability and embrittlement pose safety concerns (Altfeld & Pinchbeck, 2013:12; Garmsiri *et al.*, 2014:2512).

2.2.2 Chemical methanation

In the case of chemical methanation, renewable energy is stored in the form of CH₄. Methane is produced involving the following two conversion steps:

- i. Water electrolysis using excess renewable energy, producing H₂ and O₂.
- ii. The successive use of H₂ in the Sabatier methanation reaction supplied by a concentrated point source of CO₂. A suitable catalyst is used in this reaction step.

As CH₄ is produced through two simple conversion steps, the round-trip energy conservation is reasonably higher (i.e. energy losses are minimal) as for the production of other hydrocarbons comprising more reaction steps. Also, CH₄ has an attractive liquid volumetric energy density (Table 2.1) and various industrial applications. Combined with the incentive of CH₄ for production and large-scale storage capacity in natural gas networks, it has great potential in the application of P2G technology. Chemical methanation will therefore be the focus area of this dissertation.

2.2.3 Biological methanation

Integrating renewable H₂ in conventional biogas plants offers a resulting upgrade of biogas CH₄ quality through biological methanation. Biological methanation is a relatively new prospect of producing CH₄ for energy storage and large-scale application. Instead of chemically synthesised CH₄, methanogenic archaea is used to biochemically catalyse biogas (Burkhardt & Busch, 2013:74). Biogas generally consists of up to 50% CO₂ (CH₄ being the major fraction) and is commonly encountered in applications such as anaerobic biomass digesters and sewage treatment plants (Bensmann *et al.*, 2014:413; Yang *et al.*, 2014:1135).

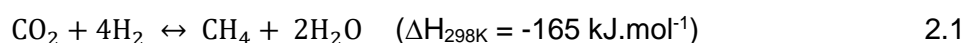
There are however a few disadvantages to the methanation of biogas. Firstly, biogas contains some impurities. Among others, NH₃, H₂S and O₂ have negative impacts such as toxicity to anaerobic bacteria, corrosiveness on process equipment and flammability in the presence of CH₄, respectively (Yang *et al.*, 2014:1136). Prior to the methanation process, a cleaning and purification stage is therefore necessary which adds to increased capital costs. Secondly, only a few studies reported in the literature were devoted to the upgrading of biogas, which is therefore a relatively new P2G implementation pathway (Bensmann *et al.*, 2014:414).

2.2.4 Dual-fuel gas turbines

Dual-fuel gas turbines have capabilities of incorporating different combustion fuels for operation. Natural gas and liquid fuels, in particular diesel, are appropriate fuels for combustion, although liquid fuels are expensive and rarely used. The purpose of these turbines is to explore compact power generation units for on- and offshore use, while ensuring reliable operation (Stambler, 2003:25). High quality SNG produced through methanation is therefore appropriate for combustion. The use of conventional gas turbines operating on natural gas is more realistic as lower operating and maintenance costs are supported.

2.3 CO₂ methanation via the Sabatier reaction

The Sabatier reaction was first reported by Paul Sabatier, a French chemist whose work on the catalytic hydrogenation of organic species was published in 1913 (Sterner, 2009:109). The Sabatier reaction (Equation 2.1) is a highly exothermic reaction between H₂ and CO₂. The forward Sabatier reaction is frequently described in literature as CO₂ methanation or CO₂ hydrogenation, whilst the reverse reaction is referred to as steam-methane reforming, implemented industrially to produce H₂ (Lunde & Kester, 1974:27). In past the Sabatier reaction was regularly investigated in the temperature range of 200–400°C using Group VIII metal supported catalysts such as Ni, Ru, Rh or Pd (Brooks *et al.*, 2007:1162; Gogate & Davies, 2010:903; Goodman, 2013:8; Lunde & Kester, 1973:423; Park & McFarland, 2009:92; Wang & Gong, 2011:5,6).



Nickel has generally been used as a CO₂ methanation catalyst due to its low cost and widespread use (Schaaf *et al.*, 2014:5; Koschany *et al.*, 2016:505). Nickel has the ability to convert about 40–70% CO₂, but with rather varying selectivities towards CH₄. Lunde & Kester (1974:27) reported that several problems were encountered with the use of a Ni-

based catalyst. To ensure Ni is in its most active form, hydrogen reduction at reactor start-up is compulsory. Carbon deposition may occur at higher temperatures and slow catalyst deactivation can be expected as a result of sulphur poisoning due to the presence of feedgas impurities such as hydrogen sulphide (H₂S). The use of Rh and Pd as active supported catalysts for CO₂ methanation was also investigated, but showed undesirable CO₂ conversions in fixed-bed reactors (Gogate & Davies, 2010:903; Park & McFarland, 2009:92).

Generally, it is recognised that the highest CO₂ conversions are obtained on supported Ru catalysts (Lunde & Kester, 1974:27; Solymosi *et al.*, 1981:166; Prairie *et al.*, 1991:130; Duyar *et al.*, 2015:27). Moreover, catalyst supports such as Al₂O₃, TiO₂, SiO₂ and ZrO₂ are commonly used. However, TiO₂ and Al₂O₃ are considered best with ZrO₂, also providing reasonable CO₂ conversions (Lunde & Kester, 1974:27; VanderWiel *et al.*, 2000:3; Brooks *et al.*, 2007:1161). Also, according to Lunde (1974:229) and Zamani *et al.* (2014:145) Ru catalytic activity increases as higher metal loadings are used at low reaction temperatures. Brooks *et al.* (2007:1162) noted that supported Ru is a stable catalyst during lifetime testing. However, the catalytic activity of Ru is best exploited as a single-metal catalyst, unlike in studies done by Luo *et al.* (2005:1421) and Zamani *et al.* (2014:143) where Ru was studied as a multi-metallic catalyst.

Although the Sabatier reaction was discovered in 1913, the interest in its use began to gain momentum in the 1970s, when it was successfully implemented in a laboratory-scale reactor by Lunde & Kester (1973:423). Since then, the Sabatier process has been used as motivation to produce CH₄ for synthetic fuel applications, as an effective method of storing renewable energy and in space-based applications to revitalise confined atmospheres of metabolically generated CO₂.

Recently, the National Aeronautics and Space Administration agency (NASA) has explored the Sabatier process on the International Space Station (ISS) in order to convert metabolically generated CO₂ into drinkable water and CH₄. In 2010 a Sabatier-based system was successfully installed on the ISS in combination with the atmosphere revitalisation system (NASA, 2011; Junaedi *et al.*, 2014:2). This system improves the efficiency of the ISS's resupply capabilities, as less water has to be transported from Earth. Previously, CO₂ generated by the CO₂ removal assembly and H₂ produced by the oxygen generator assembly were vented into space. In future long-distance space missions, the Sabatier process may well utilise CO₂ from the Martian atmosphere to produce CH₄ and used as propellant on the return journey to Earth (Brooks *et al.*, 2007:1161).

In 2012 a P2G demonstration plant was inaugurated by the German Centre for Solar Energy and Hydrogen Research (ZSW) in Stuttgart, Germany. The 250 kW pilot plant produced CH₄ at a rate of 300 m³/d (ZSW, 2016). According to the researchers at ZSW, the pilot plant would provide much-needed data for scale-up of P2G technology. With the support of ZSW, Audi AG in 2013 initiated the world's first industrial-scale P2G methanation plant (6 MW) in Werlte, Germany. The plant was constructed in collaboration with ETOGAS GmbH and is able to produce an annual 1 000 metric tonnes of Audi's so-called "e-gas" (Audi AG, 2013; ZSW, 2016).

2.3.1 Reaction mechanism

In the past, there was difficulty to establish the exact Sabatier reaction mechanism being followed (Wei & Jinlong, 2011:6). Uncertainties about the intermediate compound present during the rate-determining step have led to two main reaction mechanisms being proposed. The first proposed mechanism for CO₂ methanation involves the conversion of adsorbed CO₂ into adsorbed carbon monoxide (CO). Consequently CO undergoes dissociation to form surface carbon. The successive elementary steps are based on the same reaction mechanism as CO methanation originally proposed by Bahr (1928:2177). With the formation of adsorbed CO, there is still no definite proof for the mechanism of CO methanation either. The second proposed mechanism is based on the formation of CO and carbon formates as reaction intermediates (Marwood *et al.*, 1997:244).

2.3.1.1 Successive CO₂ and CO dissociation to form surface carbon

The dissociation of CO₂ leads to the formation of adsorbed CO (Weatherbee & Bartholomew, 1982:466). The dissociation of CO occurs, forming surface carbon. In both these steps surface oxygen is also produced and successively hydrogenated to form H₂O. On the other hand, surface carbon is hydrogenated to form CH₄. In previous work Weatherbee & Bartholomew (1981:67) witnessed that the methanation of CO₂ had almost the exact specific reaction rate than that of CO below 300°C on a Ni/SiO₂ catalyst. This leads to the conclusion that both these reaction mechanisms are governed by the same rate-controlled step. The dissociation of CO₂ is thus unlikely to be the rate-determining step. Indeed, Peebles & Goodman (1983:4384,4385) also determined that the rate-limiting step in this reaction mechanism is either the dissociation of CO to form surface carbon or the hydrogenation of surface carbon, depending on different reaction conditions. The theory that the rate-limiting step is the dissociation of CO is also supported by Choe *et al.* (2005:1687).

2.3.1.2 Direct hydrogenation of adsorbed CO

The second proposed mechanism for CO₂ methanation was suggested by Marwood *et al.* (1997:244). In this mechanism, a hydrogen carbonate species (HCO₃⁻) is observed on the catalyst surface as CO₂ reacts with a surface hydroxyl (OH⁻) group (Wei & Jinlong, 2011:6,7). The adsorbed hydrogen carbonate provides a pathway for the formation of an interfacial formate (HCOO⁻) through reaction with adsorbed hydrogen. The decomposition of the formate produces adsorbed CO and re-establishes the surface hydroxyl group. The subsequent hydrogenation of CO produces CH₄.

2.3.1.3 Considerations on reaction mechanism

In general, there are many factors to consider when attempting to pinpoint the exact reaction mechanism for CO₂ methanation. The reverse-water-gas-shift (RWGS) reaction (Equation 2.2) is thermodynamically favoured at high temperatures to form CO. Therefore, operating conditions, different catalysts and support materials, catalyst loading, preparation method and morphological properties (e.g. catalyst surface area and pore volume) etc. may all contribute to the specific reaction mechanism. Also, the presence of gas impurities in the feedstream may alter the reaction mechanism (Goodman, 2013:25). Consequently, products such as CO and CH₃OH might be obtained. By considering all these factors, it becomes evident that a consensus cannot be reached with respect to the reaction mechanism for CO₂ methanation (Goodman, 2013:21; Park & McFarland, 2009:97).

2.3.2 Thermodynamics of CO₂ methanation

Gao *et al.* (2012:2364) investigated the equilibrium product formation of CO₂ methanation via the Gibbs free energy minimization method. Their work investigated, *inter alia*, a stoichiometric 1:4 (CO₂:H₂) molar feed ratio at atmospheric pressure. The effect of temperature is illustrated (Figure 2.2) on the equilibrium product distribution. At low temperature (<400°C) the formation of CH₄ is dominant through the exothermic Sabatier reaction (Equation 2.1).

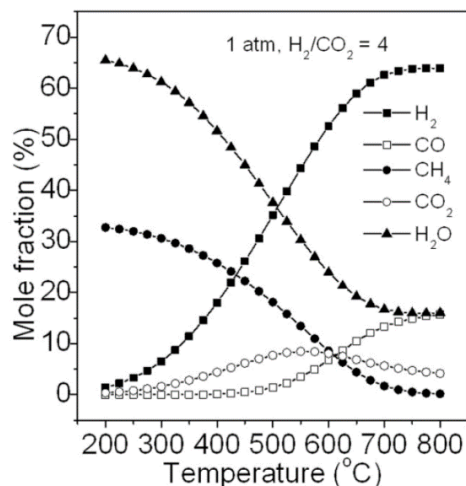


Figure 2.2: Equilibrium product formation (d.b.) of CO₂ methanation at atmospheric pressure (taken from Gao *et al.*, 2012:2364)

The reaction between H₂ and CO₂ may also produce CO through the slightly endothermic RWGS reaction (Equation 2.2). At higher temperatures (>600°C) CO occurs as the major carbon-containing product as the endothermicity of the RWGS reaction increases reaction extent with increasing temperature. To focus on CH₄ formation, low temperature is therefore essential.



The overall CO₂ conversion is illustrated (Figure 2.3) with a variation in temperature and pressure. According to Le Châtelier's principle, higher operating pressure favours greater CO₂ conversions as the Sabatier reaction involves a reduction in number of moles with reaction extent. The effect of a pressure increase from 1 to 10 atm proved significant as the CO₂ conversion increased substantially in the 300–600°C temperature range. Higher pressures (30 and 100 atm) resulted only in a slight increase in CO₂ conversion. In the temperature region (200-600°C) where the Sabatier reaction is dominant, CO₂ conversion decreased with increasing temperature. A trade-off situation is therefore required. Conditions which should favour CO₂ conversion are low temperature and high pressure although an adequate temperature is required to provide an equilibrium-limited reaction rate.

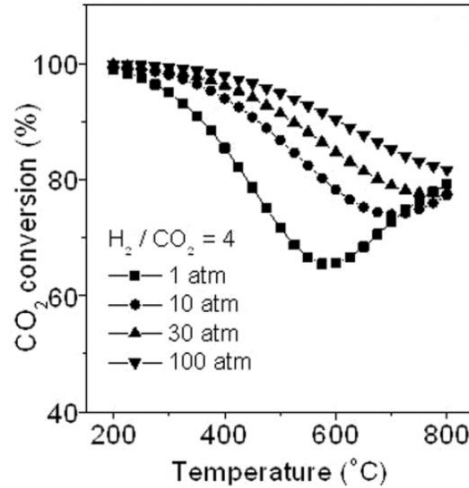


Figure 2.3: Effect of temperature and pressure on equilibrium CO₂ conversion (taken from Gao *et al.*, 2012:2365)

2.4 Current status of CO₂ methanation

Table 2.2 presents a summary of previously reported literature, in chronological order, on experimental CO₂ methanation reactors. A brief discussion of each contribution will then be presented.

Table 2.2: Summary of experimental CO₂ methanation reactors reported in literature

Source	Reactor type	Reactor conditions ¹	Catalyst used (wt.%)	Highest CO ₂ conversion
Lunde & Kester (1974:31)	Packed-bed	0.3:0.7 (CO ₂ :H ₂), 204-371°C	0.5% Ru/Al ₂ O ₃	85%
Weatherbee & Bartholomew (1982:461)	Packed-bed	dilute feed, 227-327°C, 0.4 bar	3% Ni/SiO ₂	<10%
Peebles & Goodman (1983:4383)	Batch	dilute feed, 279-437°C	Ni(100)	78%
Ohya <i>et al.</i> (1997:242)	Packed-bed with integrated membrane	206-446°C, 1 bar	0.5% Ru/Al ₂ O ₃	87%
VanderWiel <i>et al.</i> (2000:3)	Packed-bed	110-350°C	5% Ru/ZrO ₂	90%
Luo <i>et al.</i> (2005:1421)	Integrated micro-reactor	360-400°C, 2 bar	1% Ru-Y/sepiolite	32.4%
Brooks <i>et al.</i> (2007:1167)	Microchannel	254-347°C	3% Ru/TiO ₂	89.5%
Hwang <i>et al.</i> (2008:119)	Packed-bed with integrated membrane	225-300°C, 1-3 atm	35% Ni-based	±92%
Park & McFarland (2009:92)	Fixed-bed	450°C	6.2% Pd-Mg/SiO ₂	59%

¹ Stoichiometric feed ratio (CO₂:H₂) and atmospheric pressure unless specified otherwise

Table 2.2: (continued): Summary of experimental CO₂ methanation reactors reported in literature

Source	Reactor type	Reactor conditions ²	Catalyst used (wt.%)	Highest CO ₂ conversion
Gogate & Davies (2010:903)	Fixed-bed	1:1 (CO ₂ :H ₂), 270°C, 20 atm	2% Rh/TiO ₂	19.2%
Hoekman <i>et al.</i> (2010:49)	Packed-bed	dilute feed, 200-350°C	20% Ni/Al ₂ O ₃	60%
Bakar & Toemen (2012:527)	Packed-bed	100-400°C	Ni/Ru/Pd (90:8:2)/Al ₂ O ₃	53%
Müller <i>et al.</i> (2013:3776)	Packed-bed	275-500°C	0.5% Ru/Al ₂ O ₃	93.3%
Schoder <i>et al.</i> (2013:344)	Packed-bed	300-400°C	5% Ru/Al ₂ O ₃	89.1%
Junaedi <i>et al.</i> (2014:9)	Monolithic	1:4.5 (CO ₂ :H ₂), 250-400°C	Ru-microlith	96.2%
Schaaf <i>et al.</i> (2014:13)	Fixed-bed	400-500°C, 20 bar	Ni-based	70%
Tada <i>et al.</i> (2014:10093)	Fixed-bed	250-500°C	1.8% Ru/CeO ₂	±90%
Zamani <i>et al.</i> (2014:146)	Packed-bed	100-300°C	Ru/Mn/Cu(10:30:60)/Al ₂ O ₃	98.5%
Duyar <i>et al.</i> (2015:32)	Packed-bed	dilute feed, 230-245°C	10% Ru/Al ₂ O ₃	89%
Rossi <i>et al.</i> (2015:344)	Monolithic	300-350°C, 2 bar	Ni-based	81%
Garbarino <i>et al.</i> (2015:9172)	Fixed-bed	dilute feed, 250-500°C	3% Ru/Al ₂ O ₃	91%
Martin (2015:35)	Packed-bed	350-500°C, 1 bar	Ni-based	63%
Lim <i>et al.</i> (2016:33)	Batch	1:3 (CO ₂ :H ₂), 180-210°C, 10-20 bar	12% Ni/Al ₂ O ₃	±98%
Pandey & Deo (2016:102)	Fixed-bed	dilute feed, 250°C	10% Ni/Fe (75:25)/Al ₂ O ₃	±22%
Xu <i>et al.</i> (2016:141)	Fixed-bed	150-400°C	5% Ru/TiO ₂ -Al ₂ O ₃	±85%
Ducamp <i>et al.</i> (2016)	Fixed-bed	200-275°C, 4-8 bar	14% Ni/Al ₂ O ₃	89%

Lunde & Kester (1974:27) investigated CO₂ methanation on a 0.5 wt.% Ru/Al₂O₃ catalyst to explore methods of CH₄ synthesis for fuel applications. A packed-bed reactor was used to conduct the experimental investigation. The reactor showed a CO₂ conversion of 85% at approximately 371°C. Weatherbee & Bartholomew (1982:461) investigated the Sabatier reaction at low reactant partial pressures to determine reaction kinetics and the

² Stoichiometric feed ratio (CO₂:H₂) and atmospheric pressure unless specified otherwise

mechanism on a 3 wt.% Ni/SiO₂ catalyst. Experiments were conducted at high space velocities (30 000–90 000 h⁻¹). Consequently, CO₂ conversions below 10% were reported.

Peebles & Goodman (1983:4378) investigated the rate of reaction of CO₂ methanation in a batch reaction chamber in order to identify reaction kinetics and possible reaction intermediates for a mechanism. A Ni(100) catalyst surface was used in their experiments for quick alteration between a reaction and analysis chamber. A CO₂ conversion of 78% was achieved at 437°C. Also, the effect of surface modifiers (potassium (K) and sulphur (S)) was investigated on the production rate of CO and CH₄. These surface modifiers however did not have considerable effect on the mechanism for CO₂ methanation. The study by Ohya *et al.* (1997:237) investigated a 0.5 wt.% Ru/Al₂O₃ catalyst for CO₂ methanation in a packed-bed as part of a larger water vapour permselective membrane reactor. Among other, the effect of the selective removal of water vapour during reaction and the ratio of feed gas were investigated. At 300°C a CO₂ conversion of 87% was obtained. With the inclusion of the membrane, the CO₂ conversion increased to 98%.

VanderWiel *et al.* (2000:3) investigated three supported Ru catalysts of variable loading (1 wt.% Ru/G1-80, 3 wt.% Ru/TiO₂ and 5 wt.% Ru/ZrO₂) in a packed-bed reactor. An attempt was made to prove the feasibility of microreactors for space-based applications employing the Sabatier or RWGS reaction to convert CO₂ from the Martian atmosphere into useful fuels. Conversions approaching 90% were achieved at 250°C and space velocities lower than 18 000 h⁻¹. At high space velocities (>36 000 h⁻¹) some CO formation was observed. In an investigation by Luo *et al.* (2005:1419) the effect of yttrium (Y) addition was determined on the CO₂ methanation performance of a 1 wt.% Ru/sepiolite catalyst. At 420°C the addition of Y increased the CO₂ conversion from 16.4% to 32.4%. Also, the 1 wt.% Ru–Y/sepiolite catalyst showed better resistance against S poisoning and a larger surface area during CO chemisorption experiments.

Brooks *et al.* (2007:1161) studied a microchannel reactor with 3 wt.% Ru/TiO₂ catalyst for its possible use in space applications for fuel production. The microchannel reactor also incorporated a counter-flow of cooling-oil to remove heat from the reaction zone. It was found that a CO₂ conversion of 89.5% was achievable at reaction temperatures above 300°C. It was noted that the microchannel reactor provided good performance and catalyst durability during the investigation. Hwang *et al.* (2008:119) investigated a packed-bed reactor for CO₂ methanation using a commercial 35 wt.% Ni-based catalyst. The packed-bed of catalyst forms part of a larger CO₂-selective membrane reactor assembly for space-related air revitalisation systems. The reactor showed good CO₂ conversion (±92%) at

atmospheric pressure and 250°C. A successive reaction step using a Ni/SiO₂ catalyst was incorporated to convert CH₄ to graphitic carbon as an effective carbon capture strategy.

Park & McFarland (2009:92) investigated several Pd-based catalysts for CO₂ methanation activity in a fixed-bed reactor. The best CO₂ conversion (59%) and CH₄ selectivity (95%) was obtained for a 6.2 wt.% Pd–Mg/SiO₂ catalyst at 450°C. Their work serves to identify an appropriate mechanism for the CO₂ methanation reaction and would provide a better understanding of the reaction pathways on Pd-based catalysts. In an investigation by Gogate & Davies (2010:901) Rh-based catalysts were evaluated in a fixed-bed reactor for CO methanation, CO₂ methanation and co-methanation of CO and CO₂. Their work evaluated these methanation strategies as possible methods of utilising CO and CO₂ to produce valuable chemicals. The best catalyst identified for CO₂ methanation was a 2 wt.% Rh/TiO₂ catalyst. A CO₂ conversion of 19.2% was achieved with high CH₄ selectivity (93.3%) at 270°C and 20 atm. However, small fractions of ethane (C₂H₆), propane (C₃H₈) and CO were detected.

Hoekman *et al.* (2010:44) investigated the methanation of CO₂ as an effective method of carbon capture and sequestration (CCS) of diluted CO₂ in a simulated flue gas stream. A packed-bed reactor with 20 wt.% Ni/Al₂O₃ catalyst was used. The effect of different feed gas ratios, a variation in reaction temperature and space velocity were investigated. A CO₂ conversion of 60% was achieved at reaction conditions corresponding to 350°C and 10 000 h⁻¹. A stoichiometric feed ratio of 1:4 (CO₂:H₂) was recommended as H₂ is utilised efficiently while maintaining a high CO₂ conversion. Bakar & Toemen (2012:525) investigated CO₂ methanation as a purification technique of a simulated natural gas stream in a packed-bed microreactor. Various Ni-based catalysts were developed of which a Ni/Ru/Pd(90:8:2)/Al₂O₃ catalyst was identified as providing the best performance. At 400°C a CO₂ conversion of 53% and CH₄ yield of 39.7% was achieved. The effect of adding H₂S as a catalyst poisoning agent to the feed gas was also investigated. The CO₂ conversion was seen to decrease to 35% with low CH₄ yield (3.6%). However, in the 140–300°C temperature range 100% H₂S desulphurisation was achieved.

Müller *et al.* (2013:3771) investigated the catalytic performance of a packed-bed reactor with 0.5 wt.% Ru/Al₂O₃ catalyst for P2G applications. In particular, a thermo-desorption study was done to determine adsorbed CO₂ amounts and SEM images taken to investigate the long-term stability of the catalyst. It was found that the reactor performed best at 350°C. At this temperature condition, the reactor produced a CO₂ conversion of 93.3% and CH₄ yield of 91.7%. Schoder *et al.* (2013:349) investigated Ni and Ru-based catalysts in a packed-bed reactor to produce CH₄ as chemical energy carrier. A 5 wt.% Ru/Al₂O₃ catalyst

provided the best CO₂ conversion (89.1%) with 99.7% selectivity towards CH₄ at 300°C and low space velocity (6 000 h⁻¹). The best-performing Ni catalyst (5 wt.% Ni/Al₂O₃) exhibited a CO₂ conversion of 72.8% and CH₄ selectivity of 99.1% at 375°C.

Junaedi *et al.* (2014:1) reported on a microlithic reactor demonstrated in earlier work by the same authors (Junaedi *et al.*, 2011:5033) for ground demonstration which can be incorporated in the ISS's CO₂ reduction assembly. The reactor with Ru-based Microlith catalyst substrate was specifically designed to operate at low temperature (<400°C) and space velocities up to 30 000 h⁻¹. A CO₂ conversion of 96.2% with 100% CH₄ selectivity was achieved at 360°C and a 1:4.5 (CO₂:H₂) feed ratio. For a stoichiometric feed ratio of 1:4, a CO₂ conversion of 89.3% was reported at 370°C. Vibration tests and a 1 000 h durability test to investigate long-term catalyst performance were also performed. Schaaf *et al.* (2014:1) evaluated a fixed-bed reactor for CO₂ methanation as a possible method of renewable energy storage with CH₄ in natural gas networks. A Ni-based catalyst was used. At 400°C and 20 bar, a CO₂ conversion of 70% was achieved at low space velocity (5 000 h⁻¹). Two possible scale-up strategies were also proposed in AspenPlus® to produce CH₄ at production rates of 1 000 m³.h⁻¹ and 10 000 m³.h⁻¹, respectively.

Tada *et al.* (2014:10090) investigated the activity of different Ru/CeO₂/Al₂O₃ catalysts on CO₂ methanation performance and CH₄ selectivity in a fixed-bed tube reactor. In particular, the CeO₂ loading on these catalysts were varied. For a 1.8 wt.% Ru/CeO₂ catalyst, it was found that a CO₂ conversion of ±90% was achievable at 350°C. The Ru/30%CeO₂/Al₂O₃ and Ru/60%CeO₂/Al₂O₃ catalysts showed CH₄ selectivities close the 100% in the 300–400°C temperature range. Zamani *et al.* (2014:143) investigated different loadings of Ru in Ru/Mn/Cu/Al₂O₃ catalysts to purify natural gas from CO₂. At 220°C 70% selectivity towards CH₄ was achieved. Other products such as methanol (CH₃OH) contributed to a total CO₂ conversion of 98.5%. A reaction mechanism was also proposed for the Ru/Mn/Cu(10:30:60)/Al₂O₃ catalyst.

Duyar *et al.* (2015:27) performed a kinetic study on a 10 wt.% Ru/Al₂O₃ catalyst in an effort to produce CH₄ as an effective method of utilising CO₂. A fixed-bed reactor was used to conduct experiments at low CO₂ partial pressure (1–25 kPa). CO₂ conversions up to 89% were achieved at 230°C. Rossi *et al.* (2015:341) also investigated CO₂ methanation as an effective method of renewable energy storage and reducing CO₂ emissions. A Ni-based catalyst was used in a monolithic reactor system. At 300°C a maximum CO₂ conversion of 81% was achieved. Moreover, an economic evaluation was done to determine financial benefits of a power-to-gas set-up linked to an already existing commercial PV system. Producing CH₄ proved economically viable during periods of excess solar power supply.

Garbarino *et al.* (2015:9171) evaluated a 3 wt.% Ru/Al₂O₃ and 20 wt.% Ni/Al₂O₃ catalyst for CO₂ methanation. At 350°C and high space velocity (55 000 h⁻¹) the Ru catalyst showed 86% CO₂ conversion, with the Ni catalyst only achieving 59%. At 450°C however, the Ni catalyst performed better (79% vs 76% CO₂ conversion). The Ru catalyst's stability in particular was evident and recommended for possible applications relating to intermittent reactor operation. The dissertation by Martin (2015:35,60) considered CO₂ methanation as a P2G application to produce CH₄ for energy storage in natural gas networks. Different Ni-based catalysts were used in a 4 mm diameter tube reactor. The first reactor configuration evaluated was a packed-bed reactor. Alternatively, washcoated metallic strips were used in such a way as to line the inside wall of the tube. Through this method, a single channel with catalyst washcoat was established. At 500°C the packed-bed reactor provided a CO₂ conversion of ±63% and the channel reactor ±60% CO₂ conversion.

Lim *et al.* (2016:28) used a batch reactor for CO₂ methanation experiments. A 12 wt.% Ni/Al₂O₃ catalyst was used in a spinning basket contained within the batch reactor volume. Experiments were conducted at low temperature (180–210°C) and above atmospheric pressure conditions. At 190°C a CO₂ conversion of ±98% was achieved with a high CH₄ yield (±99.5%) at initial CO₂ and H₂ partial pressures of 2.4 and 11.2 bar, respectively. Additional experimental results were used to estimate kinetic parameters. In a study conducted by Pandey & Deo (2016:99) different catalyst supports (Al₂O₃, ZrO₂, TiO₂ and SiO₂) were evaluated for CO₂ methanation using 10 wt.% Ni/Fe-based catalysts. A Ni/Fe(75:25)/Al₂O₃ catalyst was identified as providing the best CH₄ yield (22%) with greater than 90% of CO₂ converted contributing to CH₄ formation.

Xu *et al.* (2016:140) investigated the effect of TiO₂ addition to the catalyst support and calcination temperature of a 5 wt.% Ru/Al₂O₃ catalyst in a fixed-bed reactor. The Ru/TiO₂-Al₂O₃ catalyst did show better CO₂ conversions in the 175–350°C temperature range compared to the reference Ru/Al₂O₃ catalyst. At 375°C both catalysts provided CO₂ conversions of approximately 82%. A CO₂ conversion of 85% was achieved when the catalyst calcination temperature was increased to 1 100°C. This is a result of a phase change of TiO₂ from anatase to rutile promoting a smaller Ru particle size. Ducamp *et al.* (2016) investigated a fixed-bed reactor with annular cooling for CO₂ methanation using a commercial 14 wt.% Ni/Al₂O₃ catalyst. Their work was also an effort to produce CH₄ for renewable energy storage applications. At 275°C and 4 bar pressure the reactor performed well with a CO₂ conversion of 85%. When the pressure was increased to 5 bar, a CO₂ conversion of 89% was obtained.

2.5 Reactor technology options for CO₂ methanation

Reactor technologies suitable for power-to-gas applications should have dynamic and fast response times (load-following abilities) as renewable energy sources, in particular solar and wind, fluctuate regularly and are naturally intermittent. It is also required that the reactor cold start-up time is rapid. Moreover, the CO₂ methanation reaction is highly exothermic, which requires the reactor to have efficient heat removal capabilities and precise temperature control.

2.5.1 Fluidized-bed reactor

Fluidized-bed reactors are industrially used in applications such as coal gasification, production of various chemicals and waste water treatment. Research on fluidized-bed reactors for the highly exothermic methanation of CO and CO₂ found that fluidized-bed reactors have good heat transfer characteristics allowing for one-step operation (Kopyscinski *et al.*, 2011:925; Schaaf *et al.*, 2014:5). However, since fluidized-bed dynamics incorporate turbulent gas-solid suspensions, a requirement for attrition resistant catalysts is evident (Kopyscinski *et al.*, 2011:925).

2.5.2 Slurry bubble column reactor

Slurry bubble column reactors utilise gas sparging through liquid-solid suspensions and are often used in the biochemical and petrochemical industries (Kantarci *et al.*, 2005:2263). Slurry bubble column reactors in particular have gained much attention for its use in the well-known Fischer-Tropsch synthesis and methanol synthesis processes (Degaleesan *et al.*, 2001:1913). Three-phase slurry reactors provide high heat transfer characteristics coupled with low operating costs and minimal maintenance (Behkish *et al.*, 2002:3307; Kumar *et al.*, 2012:783). These reactors however have one major disadvantage, namely liquid-side mass transfer limitations, effectively causing a decrease in reaction rate (Götz *et al.*, 2014:6). Recently, laboratory-scale slurry reactors have been investigated for CO methanation (Zhang *et al.*, 2014:211) and co-methanation of CO and CO₂ (Götz *et al.*, 2013:1147).

2.5.3 Fixed-bed reactor

Fixed-bed reactors have a wide variety of industrial application. Similar to slurry bubble column reactors, multi-tubular fixed-bed reactors are commonly used for Fischer-Tropsch synthesis in the petrochemical industry (Jess & Kern, 2009:1164). Since conventional fixed-bed reactors have limited axial and radial heat transfer characteristics,

operation under isothermal conditions is compromised (Schaaf *et al.*, 2014:5). Therefore, a strategy of two or more adiabatic fixed-bed reactors in series is proposed for effective temperature control. According to Schildhauer & Biollaz (2015:605) the 6 MW P2G plant in Werlte, Germany makes use of a fixed-bed reactor. The reactor incorporates molten salt cooling for temperature control as the CO₂ methanation reaction is highly exothermic.

2.5.4 Microchannel reactor

Microchannel technology is comparatively new to research on catalytic reactor systems; however it has the potential to be used in various process intensifying applications (Stankiewicz & Moulijn, 2000:23,26). Essentially small microchannels in the 50–5 000 µm range significantly increases the surface-to-volume ratio of catalysts, thus allowing the reduction of equipment size while providing the same reactor throughput. (Pattison & Baldea, 2015:171; Tonkovich *et al.*, 2004:4819). Generally, microchannel reactors are utilised in modular plants which exposes the possibility of easy scale-up to industrial-scale plants. (Tonkovich *et al.*, 2004:4819). The American company Velocys developed the first commercial-scale gas-to-liquid (Fischer-Tropsch) reactor incorporating microchannel technology, capable of 125 b/d production capacity (Roberts, 2013:103). Linking these reactors will produce plant capacities as demanded by clients. In collaboration with Haldor Topsøe and Ventech, a modular-based Fischer-Tropsch plant was built using Ventech's modular design and fabrication technologies. Haldor Topsøe will produce syngas feedstock for the Fischer-Tropsch plant. The first such facility, a 1 000 b/d capacity gas-to-liquid plant was manufactured for Calumet Specialty Products Partners to produce paraffinic hydrocarbons as feedstock in the further production of waxes and solvents.

2.5.5 Summary

Fluidized-bed and fixed-bed reactors have previously been considered for industrial-scale CO methanation processes. Both these reactor types have unique advantages, but there are shortcomings in each with respect to microchannel reactor technology. In the case of fluidized-bed reactor types, very good mass and heat transfer properties are achieved with intimate mixing between the gas-phase and solid catalyst particles (Kopyscinski *et al.*, 2011:925). However, particle abrasion and entrainment are some of the challenges faced. On the other hand, fixed-bed reactors have limited heat transfer characteristics, making the operation of a single adiabatic reactor unrealistic. Microchannel reactors provide excellent heat and mass transfer and superior catalyst durability (Tonkovich *et al.*, 2004:4819). Also, the scale-up of processing capacity is realistic with modular-based microchannel reactors.

2.6 Microchannel reactor technology

Since the 1990s, organisations such as Fraunhofer ICT-IMM, Forschungszentrum Karlsruhe GmbH, DuPont, Massachusetts Institute of Technology (MIT) and Pacific Northwest National Laboratory (PNNL) have been exploring methods of process intensification and provided an upsurge in interest and technological advancements, especially in the field of microchannel technology (Holladay *et al.*, 2004:4768). In 1996 PNNL developed a microchannel heat exchanger that provided heat transfer coefficients in the range of 5 000 to 16 000 W.m⁻².K⁻¹, almost an order of magnitude higher than any other conventional heat exchanger for similar fluids (Tonkovich *et al.*, 1996:119).

Microreactors originally developed through research conducted in the field of microfabrication methods for small-scale electronic units (Holladay *et al.*, 2004:4768). Ultimately, the microfabrication methods combined with process intensification approaches gave rise to microchannel reactors and their use in catalytic reactor development. (Stankiewicz & Moulijn, 2000:26). As for reactors, process intensification refers to improved design and implementation of unit operations e.g. a reduction in reactor size whilst maintaining performance and volumetric throughput (Pattison & Baldea, 2015:171). Reactor units smaller in size therefore reduce the cost of equipment significantly. Moreover, chemical process intensification not only refers to the reduction of design dimensions, but also the incorporation of multiple unit operations into one compact, multifunctional element. The method of intensification ensures better heat management, intimate mixing as well as high chemical conversions, leading to more efficient reactor technologies (Delparish & Avci, 2016:73).

2.6.1 Advantages of microchannel reactors

Microchannel reactor technology provides many design and operational advantages over more conventional reaction types. These advantages include:

- i. Very high mass transfer rates due to high surface-to-volume ratios (Holladay *et al.*, 2004:4768). In some cases, microchannel reactors provide surface-to-volume ratios several orders of magnitude higher than conventional reactors (Hessel *et al.*, 2004:202). VanderWiel *et al.* (2000:5,6) noted that high mass transfer rates are typically achieved in microchannel reactors as the characteristic path length for reaction to take place is physically reduced. Microchannel reactors can therefore be significantly smaller than other reactor types providing the same throughput, e.g. in cases of reactions being mass transfer limited (Holladay *et al.*, 2004:4768).

- ii. Microchannel reactors provide improved heat transfer characteristics (Fogler, 2012:201). This property of microchannel reactors is very useful in applications where good temperature control is essential, e.g. in highly endothermic or exothermic reactions (Holladay *et al.*, 2004:4768). Consequently, the occurrence of cold or hot regions within the microchannel reactor are avoided and near-isothermal operation is attained (Delparish & Avci, 2016:73).
- iii. Improved catalyst stability and performance during long-term operation with minimal thermal degradation as a result of very good heat transfer properties (Liu *et al.*, 2012:600).
- iv. The scale-up of microchannel reactors is simplified with the so-called “number-up” technique (Liu *et al.*, 2012:600; Roberts, 2013:103). Microchannel reactors can therefore be custom designed and delivered on site for specific application or throughput capability.
- v. Flexibility in terms of changes in feed composition and reactor conditions (Deshmukh *et al.*, 2010:10883). Also, the quick response time (dynamic operation) of microchannel reactors ensures that this technology is practical in handling load changes due to the natural intermittency of RES (Chiuta *et al.*, 2013:14988).

2.6.2 Differences of microchannel reactors to conventional reactor types

Microchannel reactors support many differences in design and operation to conventional reactor types such as fluidized or fixed-bed technologies. Some of these differences are listed below:

- i. Microchannel units are usually smaller compared to conventional reactor types providing the same volumetric throughput. This attribute is largely due to the intensifying nature of microchannel reactor technology (Pattison & Baldea, 2015:171; Delparish & Avci, 2016:73).
- ii. According to Chiuta *et al.* (2013:14971) reaction rates in microchannel reactors are generally governed by intrinsic reaction kinetics as opposed to mass or heat transfer limitations.
- iii. The number of degrees of freedom is significantly reduced over the reactor unit compared to other reactor types, since microchannel reactors are generally operated as multifunctional units (Pattison & Baldea, 2015:171).

2.6.3 Limitations and design challenges of microchannel reactor technology

Microchannel reactor technology supports many advantages that make this reactor technology superior to conventional reactor technology. In general, microchannel reactors however have a few limitations due to their process intensifying nature:

- i. Generally, introducing measurement instrumentation (e.g. thermocouples) to microchannel reactors proves difficult as reactor geometrics are physically reduced (Pattison & Baldea, 2015:171).
- ii. Microchannel reactors are generally prone to increased sensitivity to fouling because of the reactor's intensification of the overall reaction kinetics (Holladay *et al.*, 2004:171).
- iii. According to Holladay *et al.* (2004:171) increased pressure drops may occur in microchannel reactors when high space velocities are initiated. This is mainly due to the reduction in microchannel cross-sections.

As the field of microchannel technology is ever expanding, these limitations and design challenges will be addressed to a point where improved reactor designs provide enhanced reactor performance without any restraining factors.

2.7 Reactor modelling and simulations for CO₂ methanation

Table 2.3 presents a summary of previously reported modelling evaluations, in chronological order, on the methanation of CO₂. A brief discussion of each contribution will then be presented.

Table 2.3: A summary of literature on mathematical modelling for CO₂ methanation

Source	Reactor type	Reactor conditions ³	Catalyst used in describing kinetic model (wt.%)	Model
Lunde (1974:228)	Packed-bed	0.3:0.7 (CO ₂ :H ₂), 204-360°C	0.5% Ru/Al ₂ O ₃	1D mathematical
Ohya <i>et al.</i> (1997:242)	Packed-bed-permselective membrane	206-446°C, 1 bar	0.5% Ru/Al ₂ O ₃	1D mathematical
Brooks <i>et al.</i> (2007:1164)	Microchannel	254-347°C	3% Ru/TiO ₂	1D reactive plug flow
Schlereth & Hinrichsen (2014:704)	Fixed-bed	250-350°C, 10 bar	Ni/Mg/Al ₂ O ₄ and 5% Ru/ZrO ₂	1D plug flow and 2D
Kiewidt & Thöming (2015:61)	Fixed-bed	250-450°C, 1-20 bar	5% Ru/ZrO ₂	1D plug flow

³ Stoichiometric feed ratio (CO₂:H₂) and atmospheric pressure unless specified otherwise

Table 2.3: (continued): A summary of literature on mathematical modelling for CO₂ methanation

Source	Reactor type	Reactor conditions ⁴	Catalyst used in describing kinetic model (wt.%)	Model
Chein <i>et al.</i> (2016:245)	Fixed-bed	200-500°C, 1-5 atm	Ni/Mg/Al ₂ O ₄	2D CFD
Ducamp <i>et al.</i> (2016)	Fixed-bed	200-275°C, 4-8 bar	14% Ni/Al ₂ O ₃	2D CFD
Lim <i>et al.</i> (2016:33)	Batch	1:3 (CO ₂ :H ₂), 180-210°C, 10-20 bar	12% Ni/Al ₂ O ₃	1D mathematical

The one-dimensional mathematical model derived by Lunde (1974:228) was constructed using a simplified thermal and chemical model. The thermal model considered partial differential equations to describe heat balances in the reactor's thermal zones (reactor catalyst, gas flow, reactor wall and coolant flow). The chemical model involved the reaction rate equation (Equation 2.6) previously derived by Lunde & Kester (1974:30) and was used to describe species generation/consumption. The thermal and chemical model was linked by the heat generated through reaction at different temperatures.

The investigation by Ohya *et al.* (1997:242) used ordinary differential equations to describe species formation along the length of the packed-bed reactor. The assumption of plug-flow was made for these differential equations to be valid. No correlations were used to estimate heat, mass and momentum transport. Their work was based on the same global Sabatier rate equation reported by Lunde & Kester (1974:30). However, Ohya *et al.* (1997:242) refitted kinetic rate parameters to validate the experimental data points obtained in their work.

Brooks *et al.* (2007:1164) developed a one-dimensional reactive porous-media model describing the methanation of CO₂ in a microchannel reactor over a 3% Ru/TiO₂ catalyst. Partial differential equations were used as governing equations for energy, mass and momentum continuity. These partial differential equations were based on one-dimensional plug-flow approximations in the axial direction. In essence, any variation in gas density, species composition, velocity, temperature and pressure was neglected in radial (transverse) directions. This investigation also used the rate equation of Lunde & Kester (1974:30). Kinetic rate parameters were adjusted to provide a good fit to their data. Figure 2.4 illustrates the model fitted to experimental rates of CH₄ formation as a function of residence time.

⁴ Stoichiometric feed ratio (CO₂:H₂) and atmospheric pressure unless specified otherwise

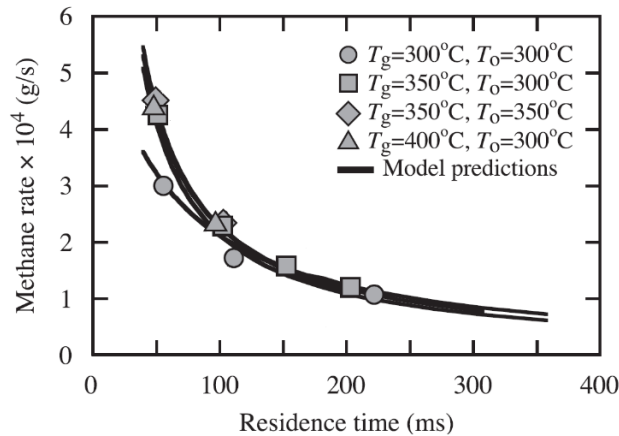


Figure 2.4: Rates of CH₄ formation as a function of residence time at different temperature conditions (adapted from Brooks *et al.*, 2007:1162)

Schlereth & Hinrichsen (2014:704) developed four different models to describe CO₂ methanation in a fixed-bed membrane reactor. The first pseudo-homogeneous plug-flow model was one-dimensional with ordinary differential equations to describe mass and heat balances. In this model, pressure drop, diffusional effects and wall resistance were neglected. The second pseudo-homogeneous model was two-dimensional, as radial effects were incorporated in the heat and mass balance equations developed for the first model. However, porosity and dispersion coefficients were assumed constant. The third pseudo-homogeneous model used empirical correlations to estimate the porosity and heat transfer coefficient in the radial direction. In addition, the extended Brinkman equation was incorporated to describe the momentum balance. The fourth model was based on a dusty-gas approach to describe a one-dimensional heterogeneous reactor model. Molecular and Knudsen diffusion and differential equations were accounted for and used to describe flux densities, mole fractions and pressure drops. For all models developed, kinetic rate equations described by Xu & Froment (1989:92) for a Ni/Mg/Al₂O₄ catalyst and Schoder *et al.* (2013:344) for a 5 wt.% Ru/ZrO₂ catalyst were separately used.

The modelling study by Kiewidt & Thöming (2015:61) was based on a pseudo-homogeneous plug-flow model to describe CO₂ methanation in a fixed-bed reactor. Ordinary differential equations were used for mass, momentum, species concentration and energy balances to describe a single homogeneous phase within the reactor. Axial pressure drop was modelled using a Darcy-Forchheimer expression, while Newton's law of cooling was used to describe the reactor wall cooling rate. To account for intraparticle diffusion, the effectiveness factor and the Thiele modulus were used. The effective diffusivity was calculated using the Bosanquet equation. To describe species formation, the elementary rate law developed by Lunde & Kester (1974:30) was used. Model validation was based on

experimental results presented by Schoder *et al.* (2013:344) on a 5 wt.% Ru/ZrO₂ catalyst. Kiewidt & Thöming (2015:61) used the Semenov number to predict optimum temperature profiles within the reactor. Subsequently, maximised CH₄ yield within the fixed-bed reactor was modelled.

Chein *et al.* (2016:243) used a two-dimensional CFD model to estimate CH₄ formation in a fixed-bed reactor. Partial differential equations were used as governing equations for energy, mass, momentum and species transport. In addition, the Brinkman-Forchheimer extended Darcy equation was used to describe fluid flow in the porous medium. In addition, the Stefan-Maxwell multicomponent diffusion model was used. The Hougen-Watson rate equation was used to describe reaction kinetics on the Ni-based catalyst (Xu & Froment, 1989:92). COMSOL Multiphysics was used to solve the mathematical model. The model was validated on experimental CO₂ methanation results presented by Hwang *et al.* (2008:119) on a 35 wt.% Ni-based catalyst. The effect of a different catalyst was studied as the rate law from Lunde & Kester (1974:30) was used to investigate the performance of a Ru catalyst for CO₂ methanation. From the results reported it is evident that the Ru catalyst showed better CO₂ conversion than the Ni-based catalyst.

Ducamp *et al.* (2016) developed a heterogeneous two-dimensional CFD model in COMSOL Multiphysics to model a fixed-bed reactor with annular cooling. Mass and heat balance equations were developed for the respective gas-phase and catalyst particle domains. The gas-phase and catalyst particle models were subsequently linked by the Satterfield correlations for mass and heat transfer coefficients. Similar to Chein *et al.* (2016:243), the Brinkman-Forchheimer extended Darcy equation was used to describe fluid flow in the porous phase. Radial diffusion was accounted for with the Gunn correlation, while the axial diffusion was estimated with the Edward and Richardson correlation. Also, reaction kinetics for the CO₂ methanation, CO methanation and RWGS reactions were included. Temperature and species concentration were then modelled in the axial and radial directions.

Lim *et al.* (2016:38) used ordinary differential equations to describe the rate of species formation and consumption in a batch reactor. The time-dependent differential equations were solved using MATLAB software based on the sum of least squares between experimental and model-predicted partial pressures. In particular, it was noted that the high selectivity (>99%) towards CH₄ production warranted the development of the model exclusively for the Sabatier reaction.

2.7.1 Computational fluid dynamic (CFD) modelling of microchannel reactors for CO₂ methanation

Modelling studies often differ in complexity from simple one-dimensional models to advanced modelling techniques such as CFD modelling. Model-based interpretation serves to define the reaction coupled transport phenomena within a reactor. An understanding of the dynamic profiles is obtained, which cannot be described by experimental results. No full CFD models have been developed for Sabatier-based microchannel reactors. In this dissertation, however, we follow the approach used recently by Chiuta *et al.* (2014:11390) where they developed a mathematical CFD model in the finite element-based COMSOL Multiphysics® to describe a microchannel reactor for ammonia decomposition using a 4.7 wt.% Ni-Pt/Al₂O₃ catalyst. A single-channel modelling approach was followed in which a free-fluid phase and porous catalyst washcoat were introduced as computational domains. A follow-up study by the same authors investigated an identical reactor but with 8.5 wt.% Ru-Cs/Al₂O₃ catalyst (Chiuta, Everson, *et al.*, 2016:3774). A similar modelling approach was followed in this dissertation. A detailed description and model development is further discussed in Section 5.1.

2.7.2 Reaction kinetics of CO₂ methanation on supported Ru catalysts

Recently, Duyar *et al.* (2015:31,32) used two rate equations to describe CH₄ formation on a 10 wt.% Ru/Al₂O₃ catalyst at atmospheric pressure. The first, an Eley-Rideal rate law incorporating the equilibrium constant ($K(T)$) for CO₂ adsorption was used in a kinetic study at low CO₂ and H₂ partial pressures. Consistent with the Eley-Rideal mechanism, it was concluded that gas-phase H₂ reacted directly with adsorbed CO₂. The reaction rate per catalyst mass is given by Equation 2.3.

$$r_{\text{Sabatier}} = \frac{(k(T))(K(T))(p_{\text{CO}_2})(p_{\text{H}_2})}{1+(K(T))(p_{\text{CO}_2})} \quad 2.3$$

The temperature-dependent reaction rate constant ($k(T)$) is expressed in Arrhenius form as Equation 2.4.

$$k(T) = A e^{\frac{-E_a}{RT}} \quad 2.4$$

The second proposed rate law is in empirical form to describe CH₄ formation at more realistic reactant partial pressures. It was found that the reaction rate showed strong dependence on the partial pressure of H₂ at the conditions investigated. With increasing CO₂

partial pressure, the order dependence on CO₂ approached zero. The reaction rate per catalyst mass is given by Equation 2.5.

$$r_{Sabatier} = \frac{(k(T))(p_{CO_2})^{0.34}(p_{H_2})^{0.88}}{(p_{CH_4})^{0.11}(p_{H_2O})^{0.23}} \quad 2.5$$

The kinetic rate expression for the global Sabatier reaction is commonly described in literature as a reversible elementary rate law. Initial work done by Lunde & Kester (1974:30) developed the rate equation incorporating an empirical factor (n) to describe experimental data points obtained over a 0.5 wt.% Ru/Al₂O₃ catalyst in a packed-bed reactor. The general form of this reversible elementary rate law is given by Equation 2.6 (Lunde, 1974:228; Lunde & Kester, 1974:30).

$$-\frac{dp_{CO_2}}{dt} = k(T) \times \left[(p_{CO_2})^n (p_{H_2})^{4n} - \frac{(p_{CH_4})^n (p_{H_2O})^{2n}}{(K(T))^n} \right] \quad 2.6$$

Under the assumption of an ideal gas mixture, the reaction rate is expressed per unit volume in Equation 2.7.

$$r_{Sabatier} = \frac{1}{RT} \frac{dp_{CO_2}}{dt} \quad 2.7$$

2.7.3 Summary

Numerous accounts of the relevant literature are discussed in Section 2.7, all of which used simple plug-flow or two-dimensional models to describe CO₂ methanation. These models, however, fail to describe energy, mass and momentum transfer in the three-dimensional space. An opportunity to model a reactor system for CO₂ methanation using three-dimensional full CFD is presented. CFD modelling is superior as it will enable a comprehensive evaluation of the reaction-coupled transport characteristics in the microchannel reactor. Identification of suitable governing equations for energy, mass, momentum and species continuity will enable the accurate modelling of both free-fluid and porous media phases. In addition, through parameter refinement the mathematical model will be validated on data gained through the experimental investigation of the reactor.

CHAPTER 3: EXPERIMENTAL APPARATUS

This chapter serves to describe the experimental apparatus used and methods followed during the experimental investigation of the microchannel reactor. The design of the microchannel reactor is described in Section 3.1. In Section 3.2 a summary of the morphological properties and preparation method of the reaction catalyst is specified. In Section 3.3 a discussion is given on initial planning done before experimentation was started. Section 3.4 provides detail on the apparatus used, while Section 3.5 describes the procedures followed during the experimental investigation.

3.1 Microchannel reactor design

The microchannel reactor was designed and fabricated in association with Fraunhofer-ICT-IMM (Mainz, Germany), constructed from SS314 stainless steel with a plate thickness of 2 mm. The microchannel reactor platelet was constructed with 80 microchannels engraved into its face (Figure 3.1: a) using a wet chemical etching method described elsewhere (O'Connell *et al.*, 2012:12). Each channel had a width of 450 μm , height of 150 μm and length of 50 mm (Figure 3.1: d). Channels were separated by a fin with width of 250 μm . To allow for distributed fluid flow across the channels, inlet and outlet distribution manifolds with right-angled triangular shapes were fabricated at the respective reactor inlet and outlet (Figure 3.1: a,b). The microchannel reactor was laser welded with a second platelet, equally-sized with distribution manifolds (Figure 3.1: b), but without microchannels engraved into its face.

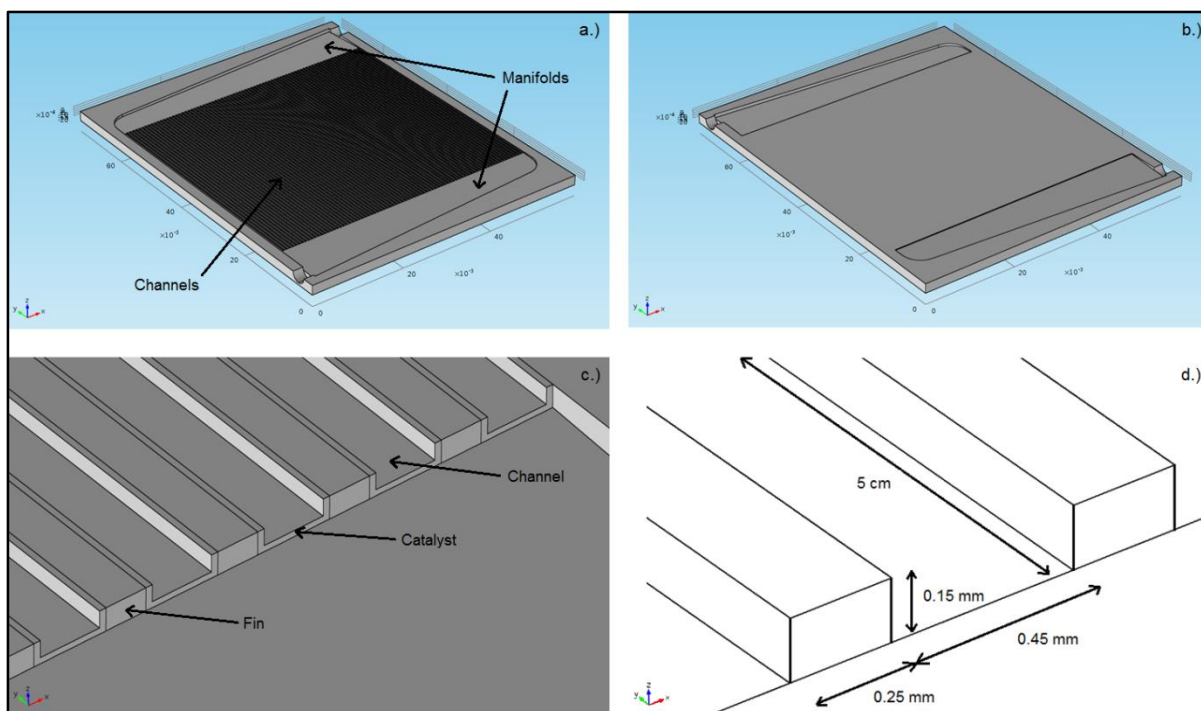


Figure 3.1: (a) Depiction of reactor platelet with 80 microchannels and fluid distribution manifolds engraved (b) second reactor platelet with only fluid distribution manifolds engraved for laser welding to complete the reactor (c) magnified view of 5 microchannels with applied catalyst washcoat and (d) a single, uncoated microchannel with dimensions

The reactor body was supported by a reactor casing containing two heating cartridges (Figure 3.2). The heating cartridges incorporated integrated thermocouples to allow for accurate temperature control. The reactor casing also included 2 small holes of 1 mm diameter for thermocouples to be inserted into the casing. The holes were positioned such that the thermocouples were next to the reactor wall. Lastly, stainless steel inlet and outlet piping was welded to the reactor's respective inlet and outlet points.

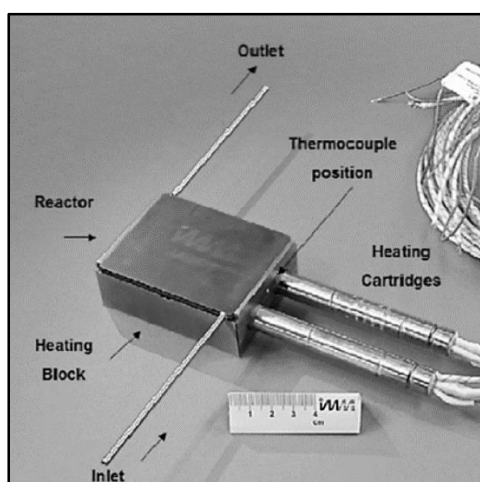


Figure 3.2: Microchannel reactor used during experimental investigation (taken from Chiuta *et al.*, 2015:2922)

3.2 Catalyst preparation

A commercial 8.5 wt.% Ru-Cs/Al₂O₃ catalyst (10010™, Acta S.p.A, Italy) was supplied by Acta S.p.A. (2016). The microchannel reactor with Cs-promoted Ru catalyst was originally used for work on H₂ production via ammonia decomposition by Chiuta *et al.* (2015:2921), but showed adequate performance towards the methanation of CO₂. The catalyst had a BET surface area of 113 m².g⁻¹ and a pore volume of 0.30 cm³.g⁻¹. The successive catalyst washcoating, drying and calcination were done according to literature described by O'Connell *et al.* (2012:13). The catalyst washcoat was applied to each microchannel with a layer thickness (δ) of 40 μ m, amounting to a total mass of 92 mg Ru on the entire reactor platelet.

3.3 Experimental planning

Experimental preparation included the manufacture of the controller stand comprising the box for temperature and flow controller instrumentation. This stand moreover featured an array of mass flow controllers providing controlled flow of CO₂ and H₂ to the reactor. A second stand was also manufactured containing the differential pressure (DP) transmitter. This stand was manufactured in a way as to provide support for the microchannel reactor within thermally insulating material, while the pressure transmitter was connected to the reactor's inlet and outlet piping.

To investigate the performance of the microchannel reactor, the variation of operating parameters was considered. Firstly, reactor temperature was a key parameter identified to investigate the rate of reaction taking place within the microchannel reactor. Along with temperature, the effect of varying reactor pressure allowed for an investigation where thermodynamic equilibrium was considered to be a limiting factor on the performance of the reactor. To operate the reactor close to thermodynamic equilibrium permits for optimal reactor performance and essentially contributes to an energy efficient process. Lastly, the effect of varying space velocity was included as an operating parameter to maximise CH₄ production, as increased space velocity will yield higher volumetric CH₄ production rates.

3.3.1 Thermodynamic equilibrium

The importance of temperature and pressure ranges and their effect on the extent of reaction were considered by exploring thermodynamic equilibrium. A replication of the work by Gao *et al.* (2012:2364) was done, using the AspenPlus® V8.6 simulation package. Components for both the Sabatier and the RWGS reactions were considered as possible products in the equilibrium calculations. The Peng-Robinson fluid property package was

used in these equilibrium calculations. Figure 3.3 illustrates the equilibrium product formation as a function of temperature.

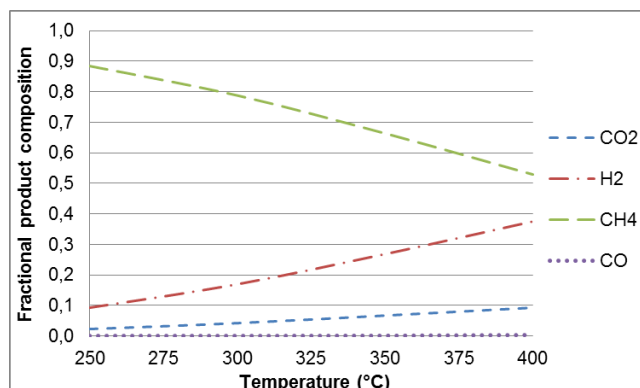


Figure 3.3: Equilibrium product formation (d.b.) of CO₂ methanation (stoichiometric H₂:CO₂ molar feed ratio)

As established by Gao *et al.* (2012:2364) the extent of reaction towards CH₄ formation (Sabatier reaction) dominates in the 250–400°C temperature range. The CO₂ conversion at atmospheric, 5 bar and 10 bar pressure is illustrated in Figure 3.4. Also, it is apparent that CO₂ conversion decreases with increasing temperature as the Sabatier reaction is exothermic. However, it is worthy to consider the actual rate of reaction before any assumptions are made on the optimum temperature for CH₄ formation. At atmospheric pressure and 400°C, the equilibrium CO₂ conversion is 85.4%, while at 10 bar pressure the CO₂ conversion increases to 94.1%.

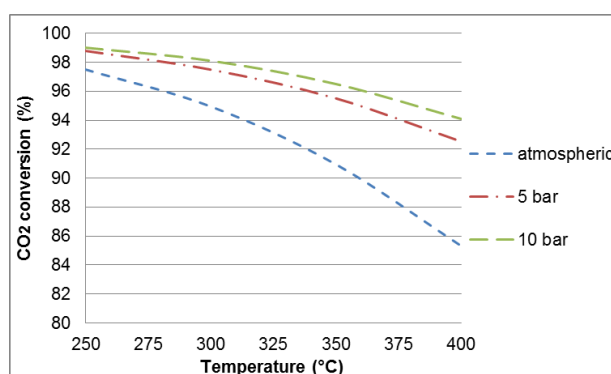


Figure 3.4: Effect of temperature on equilibrium CO₂ conversion

The mildly endothermic RWGS reaction encourages CO formation at high temperature and low pressures. During the CO₂ methanation process, the RWGS reaction is seen as a secondary reaction as CO is an unfavorable carbon-containing product. The effect of increased pressure on the equilibrium CH₄ yield is illustrated in Figure 3.5. In the 250–400°C temperature range, CO formation is minimal. Consequently, the CH₄ yield is only slightly lower than the overall CO₂ conversion in this temperature range. The CH₄ yield is

seen to improve with increased pressure over the entire temperature range, while the equimolar stoichiometry of the RWGS reaction causes minimal effect with varying pressure. At atmospheric pressure and 400°C, the equilibrium CH₄ yield is 84.9%, while at 10 bar pressure the CH₄ yield increases to 94.0%.

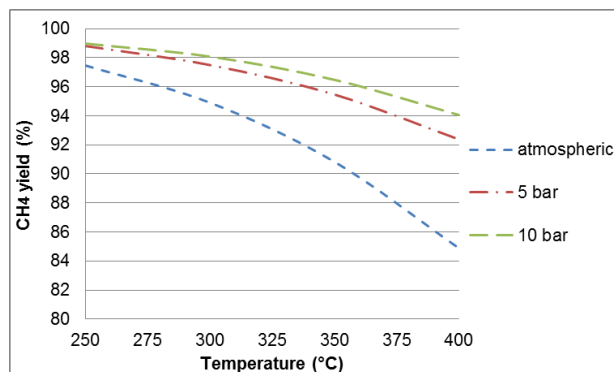


Figure 3.5: Effect of temperature on equilibrium CH₄ yield (stoichiometric H₂:CO₂ molar feed ratio)

3.4 Experimental apparatus

A flow diagram of the experimental setup is illustrated in Figure 3.6. A flow of pure N₂ was used during heat-up and cool down procedures, being regulated by a thermal mass flow controller (Brooks SLA5850). The reactor temperature was maintained using two Watlow FIREROD[®] electric heating cartridges (300 W) inside the reactor casing, incorporating K-type thermocouples. Two more K-type thermocouples were used to measure temperature in the heating block near the reactor wall. These thermocouples were positioned on opposite ends of the reactor. The flow of H₂ and CO₂ was controlled by corresponding thermal mass flow controllers (Brooks SLA5850). An ABB continuous gas analyzer (Model EL3020) was used to confirm a stoichiometric feed ratio of 1:4 (CO₂:H₂) to the reactor. The reactor pressure drop was measured by an AT9000 DP transmitter (GTX31D) connected to the respective reactor inlet and outlet piping. A needle valve was used at the reactor outlet to create a back-pressure for experiments performed at 5 bar and 10 bar. Water vapour produced through both the Sabatier and RWGS reactions was condensed from the product gas using a Julabo F12 condenser with Thermal H5 coolant in order to protect the GC columns from moisture damage. Lastly, the flow of dry product gas was measured by an Aalborg digital mass flow meter in series to an online gas chromatograph (SRI8610C GC).

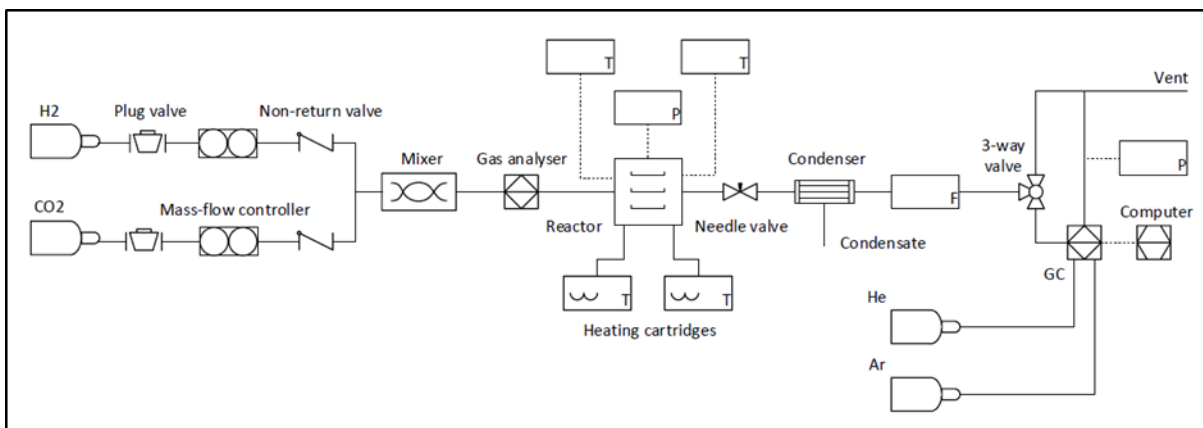


Figure 3.6: Flow diagram of CO₂ methanation setup

A photograph of the actual experimental setup is displayed in Figure 3.7. The online GC was used to analyse the composition (d.b.) of the product gas downstream from the reactor. The GC was fitted with a 1.8 m HayeSep D column, two molecular sieve (MS) 13X columns (1.8 m and 0.9 m), two TCDs and one HID. The first GC channel used He as carrier gas and made use of the HayeSep D and 1.8 m MS column in series. The first channel was equipped with a TCD and HID detector; however only the TCD was used. Carbon dioxide was trapped using the HayeSep D column and detected with an event program that incorporated the activation of the stop-flow solenoid. The second channel made use of the 0.9 m MS column and was used to separate H₂, CH₄ and CO. This channel used Ar as carrier gas and was equipped with the second TCD.

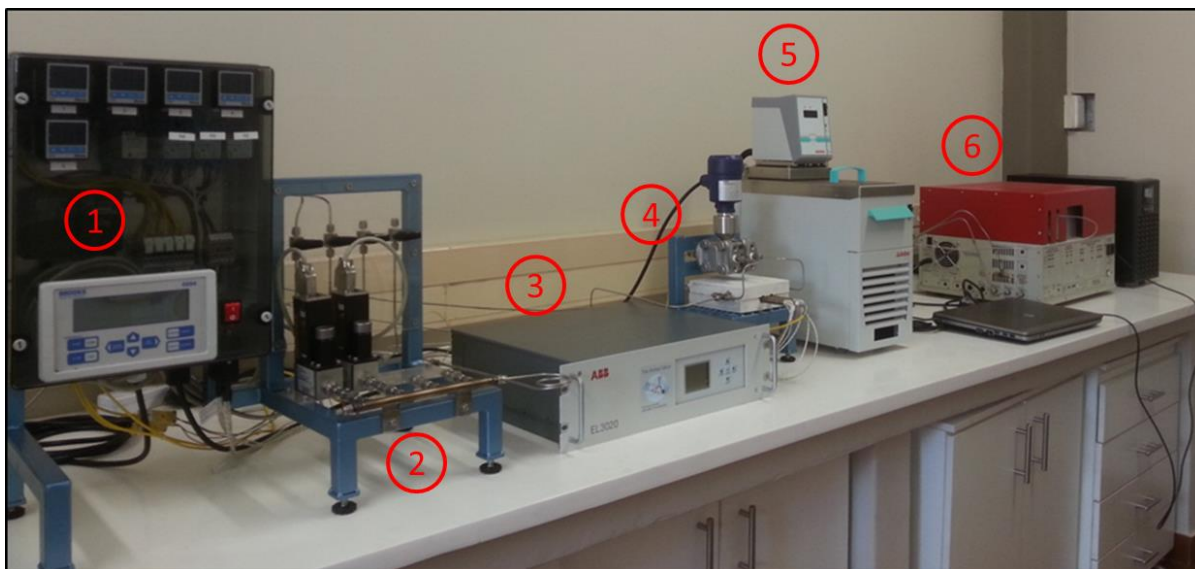


Figure 3.7: Experimental setup used for conducting CO₂ methanation experiments. (1) Control box (2) mass flow controllers (3) continuous gas analyser (4) microchannel reactor unit (5) water condenser and (6) online GC

3.5 Experimental procedure

Firstly, to activate the catalyst before any experiments were done, the catalyst was reduced at a reactor temperature of 400°C under a pure H₂ flow rate of 50 NmL.min⁻¹ for 1 h. After reduction, a N₂ flow rate of 50 NmL.min⁻¹ was induced for 30 min to drive off any excess H₂ before experiments were started. A constant molar stoichiometric (Sabatier reaction) feed ratio of 1:4 (CO₂:H₂) was used for all experiments conducted. Preliminary experimental runs at atmospheric pressure indicated that CH₄ formation initiated at temperatures of 250°C and higher. The highest CO₂ conversion was achieved at 400°C, at which point thermodynamic reversibility restricted CO₂ conversion at temperatures above 400°C. Investigation of the effect of moderate pressure increases was also undertaken as equilibrium calculations indicated increased CO₂ conversion (Figure 3.4). An initial flow rate of 50 Nml.min⁻¹ showed an adequate reaction rate whilst 150 Nml.min⁻¹ was regarded as the maximum flow rate due to pressure drop restrictions and minimum contact time with the catalyst surface. Consequently, to evaluate the reactor's performance, seven reactor temperatures, three reactor pressures and five inlet flow rates were used. The reactor temperature was varied from 250 to 400°C in increments of 25°C, the reactor pressure between atmospheric, 5 bar and 10 bar pressure and the combined flow rate of H₂ and CO₂ from 50 to 150 NmL.min⁻¹ in increments of 25 NmL.min⁻¹ corresponding to space velocities (GHSV) of 32.6–97.8 NL.g_{cat}⁻¹.h⁻¹.

During every experimental heat-up and cool-down procedure, a N₂ flow rate of 50 Nml.min⁻¹ was used until the desired reactor temperature was achieved. The reactor was operated in daily cycles to simulate the natural intermittency of renewable energy sources (e.g. solar and wind) in power-to-gas scenarios. The experimental investigation involved varying one parameter per experiment whilst keeping both other parameters constant. The performance of the reactor was based on quantitative data provided by the GC, the online digital flow meter as well as pressure drop measurements taken at regular intervals. Each experiment involved 2.5 h of continuous operation, with a GC sample being taken every 15 min. In total 10 data points were averaged to give one experimental data point. The repeatability of experimental data points was also investigated with 15 experiments at atmospheric pressure being repeated. In total 120 experiments totalling to 300 h were done during approximately 40 daily start-up and shutdown cycles. The reactor's stability was assessed through a durability test lasting 150 h of continuous operation after the 120 experiments had been completed. The durability test was done at a reactor temperature of 375°C, reactor pressure of 10 bar and GHSV of 65.2 NL.g_{cat}⁻¹.h⁻¹ to simulate demanding reactor conditions.

CHAPTER 4: RESULTS AND DISCUSSION: EXPERIMENTAL RESULTS

The results obtained from the experimental evaluation of the microchannel reactor are discussed in this chapter. A definition of the performance parameters used during this investigation is given in Section 4.1. The method followed to obtain equilibrium data is also discussed in Section 4.1. The effect of reactor temperature on CO₂ methanation performance is discussed in Section 4.2. In Section 4.3 the effect of varying the operating pressure on the reactor's performance is considered. In Section 4.4 the effect of a variation in the space velocity on the reactor's performance is established. An analysis on the reactor's pressure drop characteristics is investigated in Section 4.5, while the durability test performed on the reactor is discussed in Section 4.6. The reproducibility of experimental data is considered in Section 4.7 using repeated experimental data points. Lastly, a discussion on the optimal reactor conditions for CH₄ production follows in Section 4.8.

4.1 Reactor performance parameters

The microchannel reactor's performance was evaluated on the performance parameters defined as CO₂ conversion, CH₄ yield and specific CH₄ productivity. These parameters are defined by Equations 4.1–4.3.

$$X_{CO_2} (\%) = \frac{\dot{n}_{T_{in}} y_{CO_2} - \dot{n}_{T_{out}} y_{CO_2}}{\dot{n}_{T_{in}} y_{CO_2}} \times 100 \quad 4.1$$

$$Y_{CH_4} (\%) = \frac{\dot{n}_{T_{out}} y_{CH_4}}{\dot{n}_{T_{out}} y_{CO_2} + \dot{n}_{T_{out}} y_{CH_4} + \dot{n}_{T_{out}} y_{CO}} \times 100 \quad 4.2$$

$$CH_4 \text{ productivity (NL.g}_{cat}^{-1}.h^{-1}) = \frac{\dot{v}_{T_{out}} y_{CH_4}}{m_{cat}} \quad 4.3$$

4.2 Effect of reactor temperature on CO₂ methanation performance

The effect of reaction temperature on the reactor's methanation ability is discussed using three space velocities and two reactor pressures (Figure 4.1 and Figure 4.2, respectively). At atmospheric pressure CO₂ conversion increased significantly with temperature for all space velocities (Figure 4.1: left). However, the effective CO₂ reaction rate at atmospheric pressure was too low for any thermodynamically-limited reaction to take place at all temperatures investigated. The highest CO₂ conversion (80.4%) was observed at the lowest GHSV (32.6 NL.g_{cat}⁻¹.h⁻¹) and a temperature of 400°C, while the thermodynamic equilibrium conversion at the same temperature was 85.3%. As shown in Figure 4.2: (left), at higher pressure (10 bar) a similar trend in CO₂ conversion with increased temperature was

observed. At temperatures of 350–400°C the lowest GHSV (32.6 NL.g_{cat}⁻¹.h⁻¹) is strongly affected by thermodynamic limitations with equilibrium CO₂ conversions of 95.4–94.5%. Calculated equilibrium values of 96.5–94.1% for this temperature range found that equilibrium conversion was achieved. At these temperatures, the intermediate and highest GHSV (65.2–97.8 NL.g_{cat}⁻¹.h⁻¹) did not show strong equilibrium limitations, with the exception of 65.2 NL.g_{cat}⁻¹.h⁻¹ at 400°C.

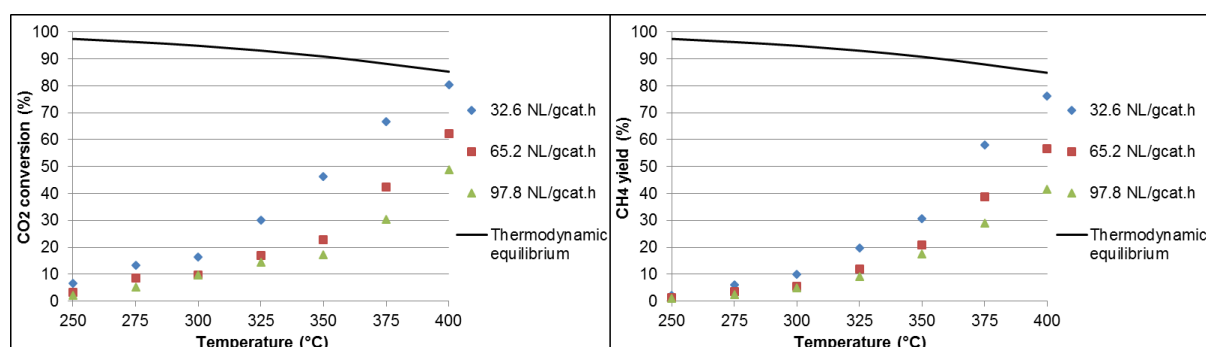


Figure 4.1: Effect of reactor temperature on CO₂ conversion (left) and CH₄ yield (right) at atmospheric pressure and GHSVs of 32.6, 65.2 and 97.8 NL.g_{cat}⁻¹.h⁻¹

For CH₄ yield, a trend similar to that of CO₂ conversion at both atmospheric (Figure 4.1: right) and 10 bar pressures (Figure 4.2: right) was observed. In general a CH₄ yield slightly lower than CO₂ conversion was achieved across the entire temperature range investigated (250–400°C). This observation leads to the conclusion that CO formation according to the RWGS reaction (Equation 2.2) contributes to the total rate of CO₂ converted. At atmospheric pressure the highest CH₄ yield (76.3%) was also obtained at 400°C for 32.6 NL.g_{cat}⁻¹.h⁻¹ (Figure 4.1: right). Although the RWGS reaction produces CO as a secondary product to CH₄, the CH₄-producing Sabatier reaction (Equation 2.1) is dominant in the higher temperature range (300–400°C) where greater CO₂ conversions were observed. At a pressure of 10 bar, the lowest space velocity (32.6 NL.g_{cat}⁻¹.h⁻¹) showed marginal to zero CO formation at temperatures of 300–400°C, as the CH₄ yield obtained is similar to the CO₂ converted (Figure 4.2). A temperature of 375°C and space velocity of 32.6 NL.g_{cat}⁻¹.h⁻¹ provided a CH₄ yield of 97.5%, which was the highest CH₄ yield calculated at 10 bar pressure. The intermediate and highest space velocities (65.2 and 97.8 NL.g_{cat}⁻¹.h⁻¹) however did yield CH₄ percentages lower than the total amount of CO₂ converted due to CO formation across the entire temperature range (250–400°C) investigated.

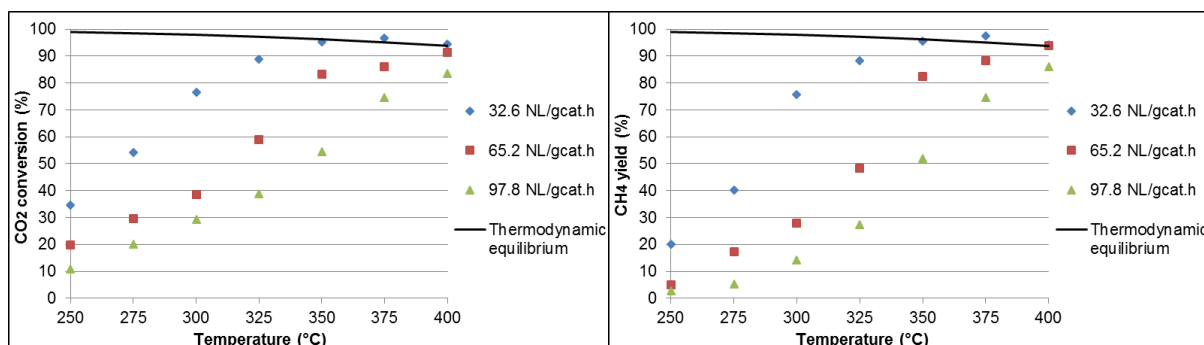


Figure 4.2: Effect of reactor temperature on CO₂ conversion (left) and CH₄ yield (right) at 10 bar pressure and GHSVs of 32.6, 65.2 and 97.8 NL.g_{cat}⁻¹.h⁻¹

4.3 Effect of reactor pressure on CO₂ methanation performance

The effect of reactor pressure is illustrated in Figure 4.3 at a reaction temperature of 400°C. With an increase in reactor pressure, a general increase in CO₂ conversion was observed (Figure 4.3: left) at all the space velocities investigated. The effect of increased reactor pressure is significant between atmospheric and 5 bar pressure while an increase in pressure from 5 bar to 10 bar pressure shows only a slight improvement in CO₂ conversion. To improve CH₄ production, a strategy of high pressure, high flow rate is proposed. However, the highest space velocity (97.8 NL.g_{cat}⁻¹.h⁻¹) shows an insignificant increase in CO₂ conversion from 5 bar to 10 bar pressure (83.4–83.6%). Operation at 5 bar will therefore be more efficient due to saving on overheads related to gas compression.

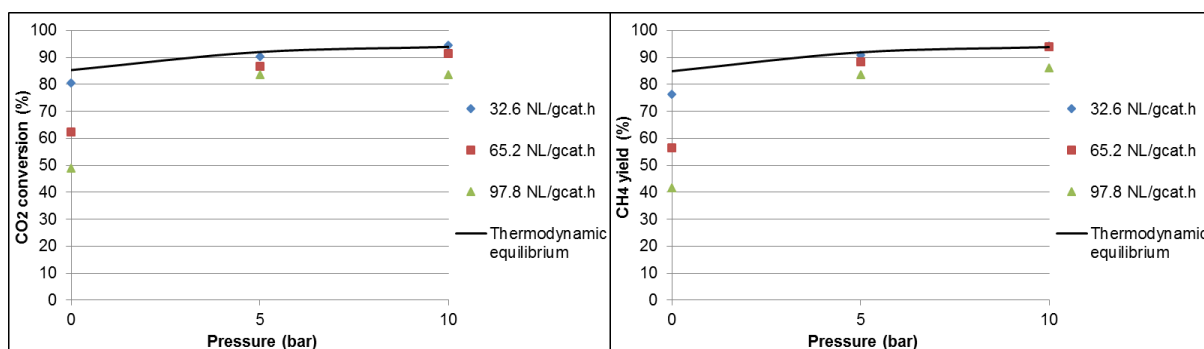


Figure 4.3: Effect of reactor pressure on CO₂ conversion (left) and CH₄ yield (right) at 400°C and GHSVs of 32.6, 65.2 and 97.8 NL.g_{cat}⁻¹.h⁻¹

Increasing pressure had a positive influence on the CH₄ yield at 400°C for all three space velocities investigated, as seen in Figure 4.3: (right). The lowest and intermediate space velocities (32.6 and 65.2 NL.g_{cat}⁻¹.h⁻¹) shows equilibrium limitation of the CH₄ yield at 5 and 10 bar as increasing pressure promotes the rate at which reaction takes place. At 5 and 10 bar the effect of space velocity on the CH₄ yield is significantly less than that observed at atmospheric pressure.

4.4 Effect of space velocity on CO₂ methanation performance

The effect of altering GHSV is illustrated at atmospheric (Figure 4.4) and 10 bar pressure (Figure 4.5). In general, CO₂ conversion was found to decrease with increasing space velocity for both pressures presented. At atmospheric pressure (Figure 4.4: left), CO₂ conversion decreases significantly with increasing space velocity (32.6–97.8 NL.g_{cat}⁻¹.h⁻¹) at 400°C (80.4–48.9%), while at low temperature (250°C) only a slight decrease in CO₂ conversion is observed (6.6–2.2%). It is evident that operating the reactor at higher temperatures improved CO₂ conversion significantly. However, high flow rates are required to maximise CH₄ production and, at atmospheric pressure, undesirable conversions occur at high GHSVs. Elevating the reactor pressure to 10 bar proved that the conversion of CO₂ at 400°C was not affected appreciably by GHSV (Figure 4.5: left). A decrease in CO₂ conversion of only 10.9% (from 94.5% to 83.6%) was observed with a threefold increase in GHSV from 32.6–97.8 NL.g_{cat}⁻¹.h⁻¹. Thus, operating the reactor at 10 bar, 400°C and 97.8 NL.g_{cat}⁻¹.h⁻¹ will enable a high CH₄ production rate.

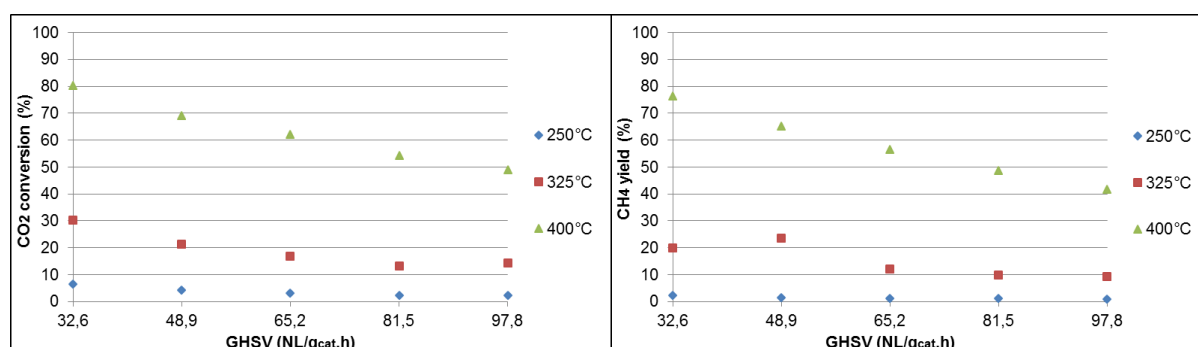


Figure 4.4: Effect of GHSV on CO₂ conversion (left) and CH₄ yield (right) at atmospheric pressure and reactor temperatures of 250°C, 325°C and 400°C

At 10 bar pressure and 325°C the effect of GHSV is pronounced, as the CH₄ yield is found to decrease by 60.9% (88.4–27.5%) when comparing the CH₄ yield at a GHSV of 32.6 NL.g_{cat}⁻¹.h⁻¹ with the yield at a GHSV of 97.8 NL.g_{cat}⁻¹.h⁻¹ (Figure 4.5: right). A similar trend is also seen in the CO₂ conversion (Figure 4.5: left). At 325°C the kinetic rate of reaction is slower than at 400°C where equilibrium limitation plays a significantly larger role. Consequently an increase in space velocity has a greater influence on CO₂ conversion and CH₄ yield at 325°C than at 400°C. In other words, at 400°C an increase in space velocity (32.6–97.8 NL.g_{cat}⁻¹.h⁻¹) is able to maintain the rate of the reaction with a substantially smaller drop in CH₄ yield of only 8.2% (94.2–86.0%). From another perspective, the effect of GHSV on CO₂ conversion and CH₄ yield can be seen in Figure 4.2 where at 325°C a great variation in these parameters is visible with increasing space velocity at 10 bar pressure. This effect is not so prominent at a lower (250°C) or a higher temperature (400°C).

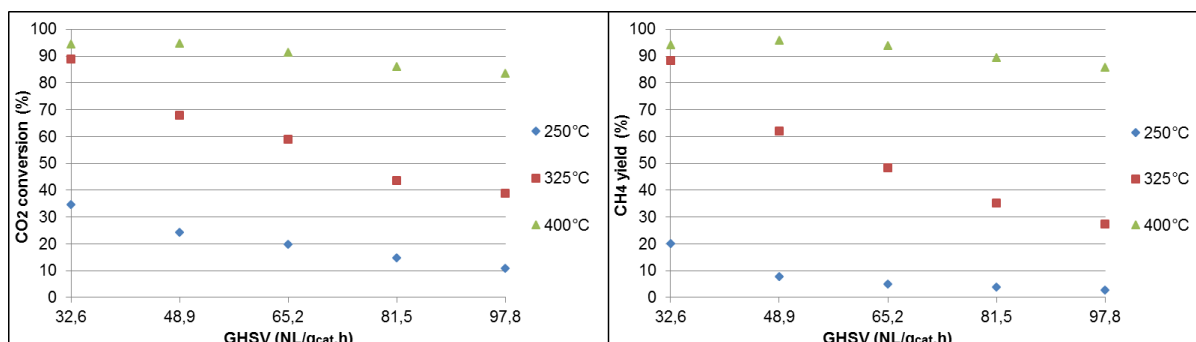


Figure 4.5: Effect of GHSV on CO₂ conversion (left) and CH₄ yield (right) at 10 bar pressure and reactor temperatures of 250°C, 325°C and 400°C

4.5 Reactor pressure drop analysis

Pressure drop measurements over the microchannel reactor using three GHSVs (32.6, 65.2 and 97.8 NL.g_{cat}⁻¹.h⁻¹) at 10 bar pressure are shown in Figure 4.6. As expected the pressure drop across the reactor increases with increasing space velocity. The pressure drop is also dependent on the combined effect of temperature and reaction stoichiometry linked to the kinetic reaction rate. With increasing temperature a general trend of increasing pressure drop is observed. The largest pressure drop at 10 bar pressure is found to be 5.40 kPa (108 Pa.mm⁻¹) at 400°C and a GHSV of 97.8 NL.g_{cat}⁻¹.h⁻¹. Considering the high throughput of product gas that the microchannel reactor allows under these conditions, the loss in process pressure is marginal. An advantage of operating a reactor scheme with low pressure drop characteristics is increased process efficiency obtained by avoiding additional operational costs to create a forced-flow system.

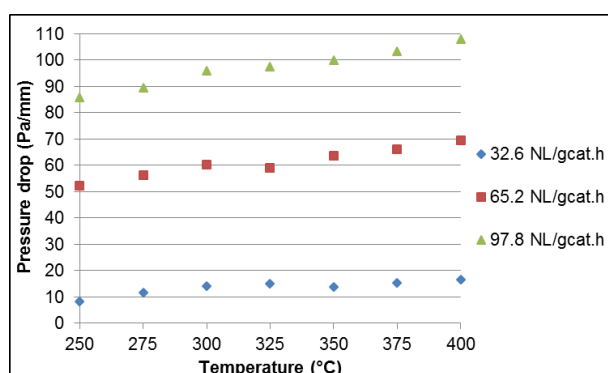


Figure 4.6: Reactor pressure drop analysis at 10 bar pressure and GHSVs of 32.6, 65.2 and 97.8 NL.g_{cat}⁻¹.h⁻¹

4.6 Durability test of reactor performance

A durability test of 150 h was performed in the microchannel reactor to investigate the possibility of catalyst deactivation due to thermal degradation or catalyst poisoning. The test was initiated at a reactor temperature of 375°C, reactor pressure of 10 bar and GHSV of 65.2 NL.g_{cat}⁻¹.h⁻¹ to simulate harsh reactor conditions. The results from the durability test

(Figure 4.7) indicate that stability in terms of CO₂ conversion and CH₄ yield is maintained throughout the time period. The CO₂ conversion and CH₄ yield obtained throughout the test fall within a band of 4% from the calculated average CO₂ conversion (86.0%) and CH₄ yield (86.6%). The random scatter of data points around the calculated averages during the entire test period leads to the conclusion that the catalyst remains active and stable over prolonged periods of rigorous reactor operation. After the test period the microchannel reactor was inspected for mechanical or structural failure, but did not show any such deficiencies.

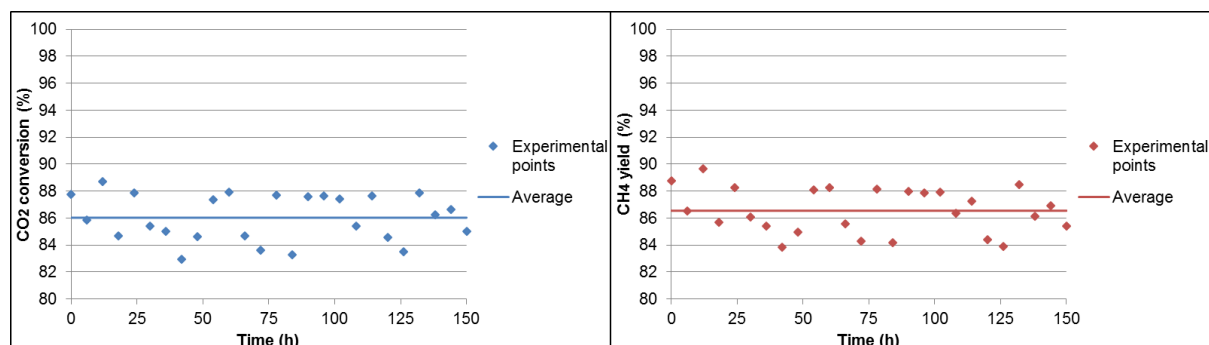


Figure 4.7: CO₂ conversion (left) and CH₄ yield (right) over an extended test period of 150 h at reactor temperature of 375°C, 10 bar pressure and GHSV of 65.2 NL_{g_{cat}}⁻¹.h⁻¹

4.7 Repeatability of experimental data points

To determine whether experimental data points were repeatable, 15 data points were repeated at atmospheric pressure. The repeated data points for reactor temperatures of 275°C, 350°C and 400°C as functions of GHSV were plotted against the experimental data points for comparison purposes (Figure 4.8). These three temperatures were picked at random to investigate data repeatability over the entire temperature range. For both CO₂ conversion (Figure 4.8: left) and CH₄ yield (Figure 4.8: right) the repeated points fall within an error margin of 6% from the experimental data points. From the comparison between the repeated and experimental data points it can be concluded that experiments conducted in the microchannel reactor are reproducible as shown by the relatively small error margin.

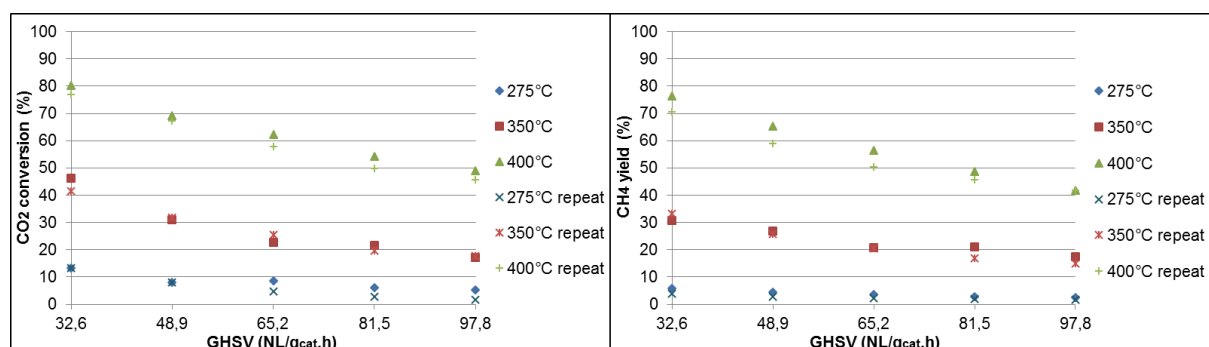


Figure 4.8: Repeatability of CO₂ conversion (left) and CH₄ yield (right) at atmospheric pressure and reactor temperatures of 275°C, 350°C and 400°C

4.8 Optimum reactor conditions for CH₄ production

To consider the feasibility of CO₂ methanation using renewable hydrogen, a strategy must be implemented to improve the production of CH₄. To achieve optimal production of CH₄ a balance between CO₂ conversion and reactor throughput is required. Considerations regarding the energy efficiency of reactor operation had also been considered before decisions were taken regarding the optimal reactor conditions. The best reactor performance for the highest space velocity (97.8 NL.g_{cat}⁻¹.h⁻¹) was achieved at 400°C for all pressures investigated. The effect of increasing pressure was found to improve reactor performance significantly, compared to results found with atmospheric pressure experiments. However, as discussed in Section 4.3, increasing pressure from 5 bar to 10 bar had an insignificant effect on CO₂ conversion and CH₄ yield under these conditions. Operating the reactor at 5 bar pressure will therefore minimise operational expenditures while producing a satisfactory rate of CH₄ production. The optimal conditions for CH₄ production are summarised in Table 4.1.

Table 4.1: Optimum reactor conditions and performance parameters of microchannel reactor

Parameter/Condition	
Catalyst	8.5 wt.% Ru/Al ₂ O ₃
Catalyst loading (mg)	92
Feed ratio (CO ₂ :H ₂)	1:4
Reactor temperature (°C)	400
Reactor pressure (bar)	5
GHSV (NL.g _{cat} ⁻¹ .h ⁻¹)	97.8
CO ₂ conversion (%)	83.4
CH ₄ yield (%)	83.5
Reactor pressure drop (Pa.mm ⁻¹)	245
CH ₄ production rate (NL.g _{cat} ⁻¹ .h ⁻¹)	16.9

CHAPTER 5: COMPUTATIONAL FLUID DYNAMIC (CFD) MODEL DEVELOPMENT, RESULTS AND DISCUSSION

Computational fluid dynamic (CFD) modelling was used to describe the microchannel reactor for the purpose of CO₂ methanation in addition to the experimentally evaluated microchannel reactor. The CFD model development is presented in Section 5.1. The model geometry, assumptions, governing equations, boundary conditions, reaction kinetics and the model solution method is discussed. The results obtained from the microchannel reactor model are presented in Section 5.2. The kinetic parameters obtained, model validation on experimental data and reaction-coupled transport phenomena are presented.

5.1 CFD model development

The microchannel reactor-based CFD model demanded the definition of a free-fluid phase, as well as a porous catalyst layer as computational domains in the model geometry. Identifying suitable governing equations was essential in the development of the mathematical model, while certain assumptions were required regarding species continuity, momentum, mass and energy calculations. Recognition must be given to Chiuta *et al.* (2014:11390), as the specific microchannel model geometry used during this work was originally constructed by them. Chemical reaction kinetics for the Sabatier reaction along with the reverse-water-gas-shift (RWGS) reaction (modelled as a secondary reaction to the Sabatier reaction) were included to predict the respective formation of CH₄ and CO as observed during the experimental evaluation of the microchannel reactor. A suitable solution method was identified to solve the mathematical model and subsequently compare with the experimental results in order to identify the accuracy of the CFD model.

5.1.1 Model geometry

To obtain an accurate representation of the microchannel reactor used during the experimental investigation (Section 3.1) identical microchannel dimensions was used in this modelling study. The model geometry for CFD simulation consisted of a single microchannel with a width of 450 μm , height of 150 μm and length of 50 mm. It was assumed that microchannels within the reactor were identical, allowing the modelling approach of a single microchannel to describe the entire reactor. The even dispersal of volumetric flow by the distribution manifold is a common assumption to calculate the flow rate through a single channel and is described in the literature (Chen *et al.*, 2008:4; Commenge *et al.*, 2002:355). To simplify the model even further, a symmetrical approach was adopted where only half the width of the channel was modelled. The model consisted of a free-fluid region, as well as a

porous catalyst washcoat ($\delta = 40 \mu\text{m}$) lining the inside faces of the microchannel. Figure 5.1 illustrates a depiction of the discretized model geometry containing 43 520 free-triangular domain elements used to describe the geometry mesh. The half-width cross-section of the discretized free-fluid phase and porous catalyst layer is visible in the yz -plane (Figure 5.1).

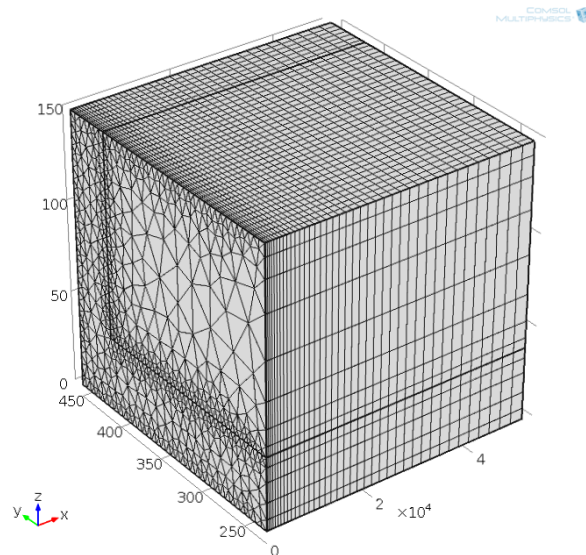


Figure 5.1: Discretized model geometry used during CFD modelling containing 43 520 free-triangular domain elements

5.1.2 Model assumptions

The assumption was made that flow within the channel was weakly compressible, steady and laminar. It was assumed that the ideal gas law was valid for the multicomponent mixture and the gas density calculated accordingly. Temperature-dependent correlations for the heat capacity, thermal conductivity and viscosity of each species were obtained from the Korean Thermophysical Properties Data Bank and with the mass fraction weighted rule, used to describe each property at local points along the microchannel (CHERIC, 2016). Isothermal reactor operation was assumed, therefore asserting thermal equilibrium between the gas phase and the porous catalyst layer. The assumption was made that the homogeneous gas-phase reaction was insignificant and that reaction only took place in the porous catalyst washcoat. The catalyst washcoat properties was assumed uniform throughout the porous layer and summarised in Table 5.1.

Table 5.1: Summary of catalyst physical properties used for modelling the porous catalyst computational domain (taken from Chiuta *et al.*, 2016:3778)

Parameter	
Layer thickness, δ (μm)	40
Density, ρ ($\text{kg}\cdot\text{m}^{-3}$)	980
Porosity, ε	0.4
Permeability, κ (m^2)	1e-12
Thermal conductivity, λ ($\text{W}\cdot\text{m}^{-1}\cdot\text{K}^{-1}$)	44
Heat capacity, C_p ($\text{J}\cdot\text{kg}^{-1}\cdot\text{K}^{-1}$)	890

5.1.3 Governing equations

Partial differential equations (in vector form) were used to describe the respective continuity, momentum, mass and energy conservation equations in the free-fluid and porous catalyst computational domains (Table 5.2). To describe momentum conservation in the free-fluid region, the Navier-Stokes equation for compressible fluids was used, while the Brinkman-Forchheimer extended Darcy model was used to describe momentum conservation in the porous catalyst layer. Species continuity within the free-fluid, as well as the porous catalyst phase was estimated using the Stefan-Maxwell multicomponent diffusion model, with the term describing species generation and consumption only applying to the porous catalyst phase. Furthermore, convective mass transfer was assumed in both these regions.

Table 5.2: Summary of governing equations for modelling the free-fluid and porous catalyst computational domains (taken from Chiuta *et al.*, 2014:11392–11395)

Free-fluid phase	
Ideal gas law	$\rho = \frac{P}{RT} \sum_{i=1}^5 y_i M_i$
Continuity equation	$\nabla \cdot (\rho \mathbf{u}) = 0$
Navier-Stokes momentum equation	$\mathbf{u} \cdot \nabla (\rho \mathbf{u}) = -\nabla P + \nabla \cdot (\mu \nabla \mathbf{u})$
Energy equation	$\mathbf{u} \cdot \nabla T (\rho C_p) = \nabla \cdot (k \nabla T)$
Species continuity equation	$\mathbf{u} \cdot \nabla (\rho \omega_i) = \nabla \cdot (\rho D_{ij} \nabla \omega_i)$
Porous-catalyst phase	
Ideal gas law	$\rho = \frac{P}{RT} \sum_{i=1}^5 y_i M_i$
Continuity equation	$\nabla \cdot (\varepsilon \rho \mathbf{u}) = 0$
Brinkman-Forchheimer extended Darcy equation	$\mathbf{u} \cdot \nabla (\varepsilon \rho \mathbf{u}) = -\nabla P + \nabla \cdot (\mu_{eff} \nabla \mathbf{u}) - \frac{\mu}{\kappa} \mathbf{u} - \frac{\varepsilon \rho C_F}{\sqrt{\kappa}} \mathbf{u} \mathbf{u}$
Energy equation	$\mathbf{u} \cdot \nabla T (\varepsilon \rho C_p) = \nabla \cdot (k_{eff} \nabla T) + (1 - \varepsilon) \Delta H_r \rho_s R_r$
Species continuity equation	$\mathbf{u} \cdot \nabla (\varepsilon \rho \omega_i) = \nabla \cdot (\varepsilon \rho D_{ij_{eff}} \nabla \omega_i) + (1 - \varepsilon) \sum_{i=1}^5 a_i M_i \rho_s R_r$

The Fuller-Schettler-Giddings (FSG) equation (Equation 5.1) was used to estimate binary gas-phase diffusion coefficients based on atomic diffusion volumes (Fuller *et al.*, 1966:21; Fuller *et al.*, 1969:3683). This correlation was found to be the most accurate for estimating binary diffusion coefficients, based on the smallest average error compared to experimentally determined coefficients (Reid *et al.*, 1987:634).

$$D_{ij} = \frac{10^{-3} T^{1.75} \left(\frac{1}{M_i} + \frac{1}{M_j} \right)^{\frac{1}{2}}}{P_{atm} \left[(\sum v_i)^{\frac{1}{3}} + (\sum v_j)^{\frac{1}{3}} \right]^2} \quad 5.1$$

To estimate the effective binary diffusion coefficients in the porous catalyst phase, the Bruggeman correlation (Equation 5.2) was used to account for the effects of catalyst porosity on binary interactions (Fuller *et al.*, 2009:336).

$$D_{ij_{eff}} = D_{ij} \left(\frac{T}{T_0} \right)^{1.5} \varepsilon^{1.5} \quad 5.2$$

5.1.4 Boundary conditions

The mathematical model was solved subject to certain initial and boundary conditions. Firstly, a constant stoichiometric molar ratio of 1:4 (CO₂:H₂) at the inlet of the microchannel was used as in the case of the experimental reactor evaluation (Section 3.4). The reactants entered the microchannel through the free-fluid inlet boundary with a flat velocity profile (Cao *et al.*, 2015:277). As a result, the magnitude of the average inlet velocity was calculated, based on the cross-sectional area of the free-fluid region. At the free-fluid exit boundary, the outlet pressure was defined as the reference operational pressure for the specific reactor condition, while viscous stress at the outlet boundary was assumed to disappear. Furthermore, velocity, temperature and species mass fluxes in the normal (outward) direction were set to zero at the microchannel exit boundary. Along the channel walls the no-slip boundary condition was applied, while no flux in terms of species mass was imposed in the normal directions on wall boundaries. Also, a constant wall-temperature boundary condition was implemented, since the assumption of isothermal reactor operation was made. A symmetric boundary condition was applied at the centre-plane to impose zero normal gradients in velocity, pressure, temperature and species mass fraction across the symmetrical boundary. Lastly, continuity in velocity, pressure, temperature and species mass were assumed at the interface between the free-fluid and porous catalyst phases.

5.1.5 Reaction kinetics

In this dissertation, the reversible elementary rate law (Equation 5.3) will be used to describe the Sabatier reaction. The work by Lunde (1974:228) and Lunde & Kester (1974:33) found a value for the empirical factor (n) of 0.225 with an activation energy (E_a) of 74.46 kJ.mol⁻¹. In the work published by Brooks *et al.* (2007:1166), n and E_a were found to be 0.3 and 69.06 kJ.mol⁻¹, respectively. In their case, kinetic data was derived using a 3 wt.% Ru/TiO₂ catalyst in a packed-bed quartz tube. Subsequent experiments by Brooks *et al.* (2007:1166) were conducted in a microchannel reactor. The current investigation uses reference kinetics of Ohya *et al.* (1997:245) who also conducted an experimental investigation on a 0.5 wt.% Ru/Al₂O₃ catalyst in a packed-bed reactor. An identical E_a of 69.06 kJ.mol⁻¹ was found to that of Brooks *et al.* (2007:1166). However, the value for the empirical factor n of 0.85 differs significantly from other reported values. Ohya *et al.* (1997:245) found a value for the pre-exponential constant (A) of 4.75e5 bar^{-2.5}.s⁻¹. The general form of the reversible elementary rate law is given by Equation 5.3 (Lunde, 1974:228; Lunde & Kester, 1974:30).

$$-\frac{dp_{CO_2}}{dt} = k(T) \times \left[(p_{CO_2})^n (p_{H_2})^{4n} - \frac{(p_{CH_4})^n (p_{H_2O})^{2n}}{(K(T))^n} \right] \quad 5.3$$

$$r_{Sabatier} = \frac{1}{RT} \frac{dp_{CO_2}}{dt} \quad 5.4$$

The first order rate law in CO₂ concentration (Equation 5.5) will be used to describe the RWGS reaction (Lebarbier *et al.*, 2010:5). A similar difference in reaction rate constants as was found by Dagle *et al.* (2008:67) is expected in this investigation as to model the RWGS reaction as a secondary reaction. Respective values for A and E_a of 3.40e8 s⁻¹ and 83.2 kJ.mol⁻¹ were reported on a 10 wt.% Pd/ZnO catalyst in the 250–400°C temperature range. The current work will use these kinetic parameters as reference, noting that the 10 wt.% Pd/ZnO catalyst loading is comparable to the 8.5 wt.% Ru/Al₂O₃ catalyst used in the current study.

$$-r_{RWGS} = k(T) \times C_{CO_2} \quad 5.5$$

5.1.6 Solution method

CFD modelling was carried out using the COMSOL Multiphysics® (Version 4.3b) finite element-based simulation package. A computer with 2.9 GHz (8-core Intel) processing power and 16 GB DDR3 RAM was used to run the software package. The parallel sparse direct linear solver (PARDISO) was used to solve variables to within a relative tolerance of

10e-2. Three separate modelling studies were introduced for the different operating pressures (atmospheric, 5 bar and 10 bar). For each, a parametric sweep study (with reference kinetic parameters) over the range of temperatures (250–400°C in increments of 25°C) and space velocities (32.6–97.8 NL.g_{cat}⁻¹.h⁻¹ in increments of 16.3 NL.g_{cat}⁻¹.h⁻¹) was done in order to fit the performance parameters defined as CO₂ conversion and CH₄ yield. These experimental parameters correspond to those used in the experimental investigation (Section 3.5). Once an initial fit to the experimental data was obtained, an optimisation study using the Nelder-Mead solution method was conducted to find the best-fitting kinetic parameters for both reactions. The optimisation studies were done based on the sum of least squares method between the experimentally determined and model predicted CO₂ conversion and CH₄ yield.

5.2 CFD model results

This Section serves as a discussion of the results obtained from the CFD model. The best-fitting kinetic parameters are presented in Section 5.2.1. The model validation on experimental performance parameters defined as CO₂ conversion and CH₄ yield is presented in Section 5.2.2 as to evaluate the accurateness of the CFD model, with an evaluation of the transport phenomena encountered within the three-dimensional microchannel space following in Section 5.2.3.

5.2.1 Kinetic parameter estimation

In Appendix C a parity plot of model-predicted vs. experimental CO₂ conversion is presented for atmospheric (Figure C.1), 5 bar (Figure C.2) and 10 bar pressure (Figure C.3). A 95% prediction interval demonstrates that the mathematical model predicted experimental CO₂ conversion data with reasonable accuracy. Values for R² of 0.973, 0.989 and 0.953 were obtained for the respective operating pressures (atmospheric, 5 bar and 10 bar). The best-fitting kinetic parameters, obtained by the solution method described in Section 5.1.6, are presented for each pressure in Table 5.3.

It was found that E_a values for the Sabatier reaction slightly higher than the reference value (69.06 kJ.mol⁻¹), reported by Ohya *et al.* (1997:245), best described each pressure. At 10 bar, thermodynamic limitations from the reversible Sabatier rate law were found to exhibit a much larger role on the CO₂ conversion than at atmospheric pressure. Consequently, a decrease in E_a values was seen with increasing pressure, as the effect of temperature on the reaction rate was smaller. For 5 and 10 bar, the Sabatier reaction order was significantly smaller than the reference value (0.85) reported by Ohya *et al.* (1997:245). The best fitting

activation energies for the RWGS reaction were also seen to decrease with increasing pressure.

Table 5.3: Best-fitting kinetic parameters at different operating pressures

Atmospheric			
	Sabatier		RWGS
A ($\text{bar}^{-2.5} \cdot \text{s}^{-1}$)	6.17e7	A (s^{-1})	2.94e7
E _a ($\text{kJ} \cdot \text{mol}^{-1}$)	77.96	E _a ($\text{kJ} \cdot \text{mol}^{-1}$)	89.83
n	0.85		
5 bar			
	Sabatier		RWGS
A ($\text{bar}^{-0.92} \cdot \text{s}^{-1}$)	7.63e6	A (s^{-1})	1.76e7
E _a ($\text{kJ} \cdot \text{mol}^{-1}$)	74.73	E _a ($\text{kJ} \cdot \text{mol}^{-1}$)	85.94
n	0.305		
10 bar			
	Sabatier		RWGS
A ($\text{bar}^{-0.67} \cdot \text{s}^{-1}$)	6.83e6	A (s^{-1})	3.63e6
E _a ($\text{kJ} \cdot \text{mol}^{-1}$)	69.35	E _a ($\text{kJ} \cdot \text{mol}^{-1}$)	77.36
n	0.222		

5.2.2 Model validation: CO₂ conversion and CH₄ yield

At atmospheric pressure, the model trend for both the CO₂ conversion (Figure 5.2: left) and CH₄ yield (Figure 5.2: right) closely represented the results found in the experimental evaluation of the microchannel reactor. Only at the highest temperature (400°C) and lowest space velocity (32.6 NL.g_{cat}⁻¹.h⁻¹) the model deviated more significantly from the experimental data points. In particular, the lowest space velocity yielded a much higher experimental CH₄ yield than what was predicted by the model at this temperature. Experimentally, the Sabatier reaction (CH₄ formation) controlled CO₂ conversion more than the model predicted. This was due to a RWGS reaction rate being modelled as first order in CO₂ concentration, when in actual fact the RWGS reaction rate is governed by thermodynamic limitations. With increasing space velocity, lower reaction rates for both reactions were observed, translating to reduced CO₂ conversions (and CH₄ yields) across the entire temperature range (250–400°C).

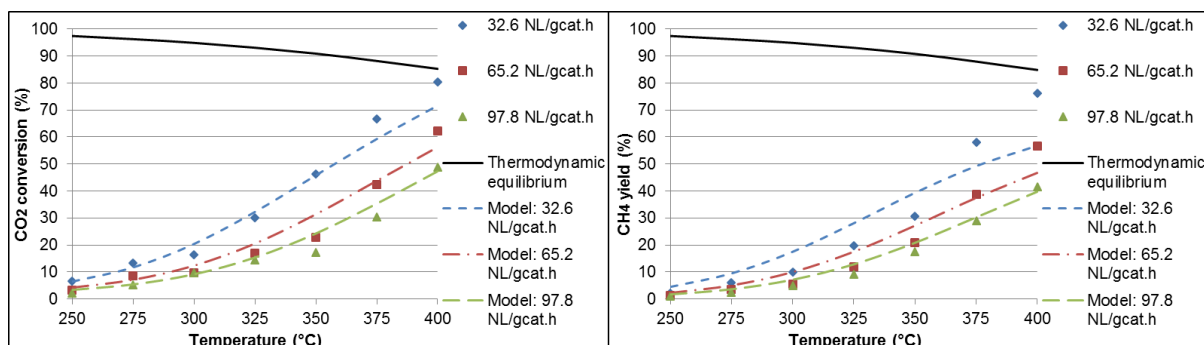


Figure 5.2: Model fit on CO₂ conversion (left) and CH₄ yield (right) at atmospheric pressure and GHSVs of 32.6, 65.2 and 97.8 NL.g_{cat}⁻¹.h⁻¹

The model-predicted CO₂ conversion (Figure 5.3: left) and CH₄ yield (Figure 5.3: right) show a good fitting to experimental data at 5 bar pressure. An important observation was made at 400°C where the model-predicted CO₂ conversion exceeded equilibrium for the lowest space velocity (32.6 NL.g_{cat}⁻¹.h⁻¹). This was due to the simplicity of the first order rate dependence in CO₂ concentration used to model the RWGS reaction rate. In reality the RWGS rate is also equilibrium-limited similar to the Sabatier reaction, and not first order as modelled in this study. To increase the accuracy of the modelled RWGS reaction rate, a more complex RWGS rate law is suggested for future studies. This was also noticed at 10 bar pressure (Figure 5.4) in the higher temperature range (375–400°C).

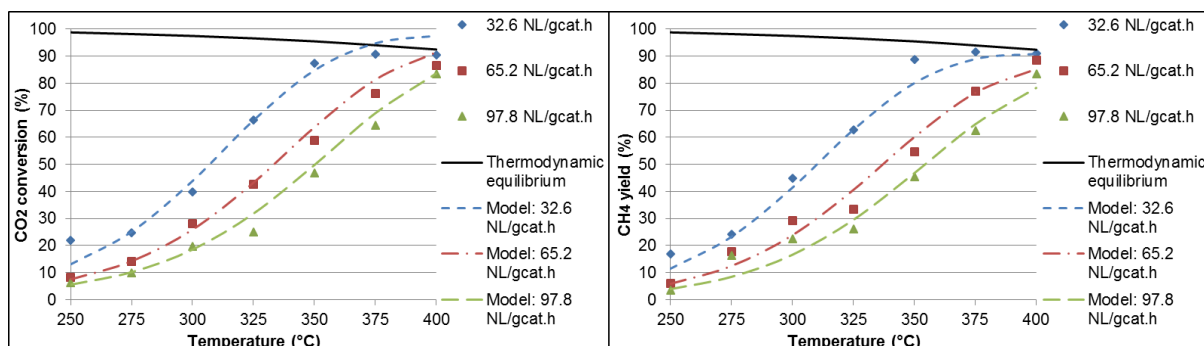


Figure 5.3: Model fit on CO₂ conversion (left) and CH₄ yield (right) at 5 bar pressure and GHSVs of 32.6, 65.2 and 97.8 NL.g_{cat}⁻¹.h⁻¹

As the stoichiometry of the Sabatier reaction allows a decrease in moles with reaction extent, an increase in conversion equilibrium was expected for increases in operating pressure for all temperatures investigated. Indeed, an increase in modelled CO₂ conversion was seen from atmospheric pressure (Figure 5.2) to 5 bar (Figure 5.3) and ultimately up to 10 bar (Figure 5.4). At 10 bar, model results for the lowest space velocity (32.6 NL.g_{cat}⁻¹.h⁻¹) showed lower CO₂ conversions (Figure 5.4: left) than experimental data in the 250–300°C temperature range, while for the highest space velocity (97.8 NL.g_{cat}⁻¹.h⁻¹) the model-predicted CO₂ conversion was found to be greater for temperatures of 325–400°C. Overall, the model fit also predicted much higher CH₄ yields (Figure 5.4: right) over the entire

temperature range for the highest space velocity (97.8 NL.g_{cat}⁻¹.h⁻¹). In general, the effect of increasing space velocity was greater during the experimental investigation of the microchannel reactor than the model predicted for both CO₂ conversion and CH₄ yield at 10 bar pressure.

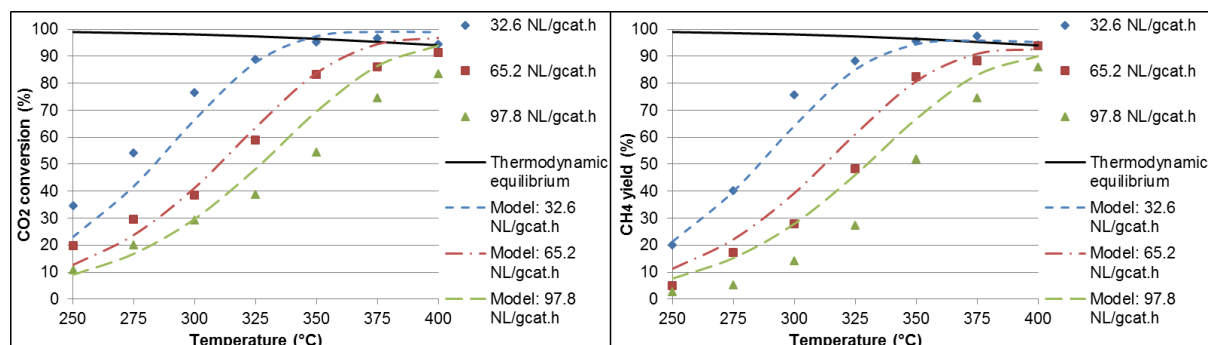


Figure 5.4: Model fit on CO₂ conversion (left) and CH₄ yield (right) at 10 bar pressure and GHSVs of 32.6, 65.2 and 97.8 NL.g_{cat}⁻¹.h⁻¹

5.2.3 Microchannel reactor transport phenomena

5.2.3.1 Velocity distributions

The axial velocity (v_x) distributions shown for atmospheric (Figure 5.5) and 10 bar pressure (Figure 5.6) provide an understanding of the reaction extent at different operating conditions. At all conditions a fully-developed laminar velocity profile was seen to develop near the inlet of the microchannel. For a GHSV of 32.6 NL.g_{cat}⁻¹.h⁻¹, a maximum axial velocity of approximately 0.41 m.s⁻¹ was observed near the inlet before the extent of reaction (CO₂ conversion), and the stoichiometry of the Sabatier reaction caused a decrease in axial velocity further down the length of the channel. At low temperature (250°C) and atmospheric pressure (Figure 5.5: left) a weakly decreasing axial velocity profile was seen down the length of the channel, as low reaction rates occurred at this temperature condition. At 400°C (Figure 5.5: right) a reduction in velocity was observed down the entire length of the channel, as higher reaction rates occurred at 400°C for both the Sabatier and RWGS reactions. It is obvious that at atmospheric pressure, thermodynamic equilibrium was not achieved as a near-constant velocity profile distinctive to equilibrium was not observed near the exit of the channel.

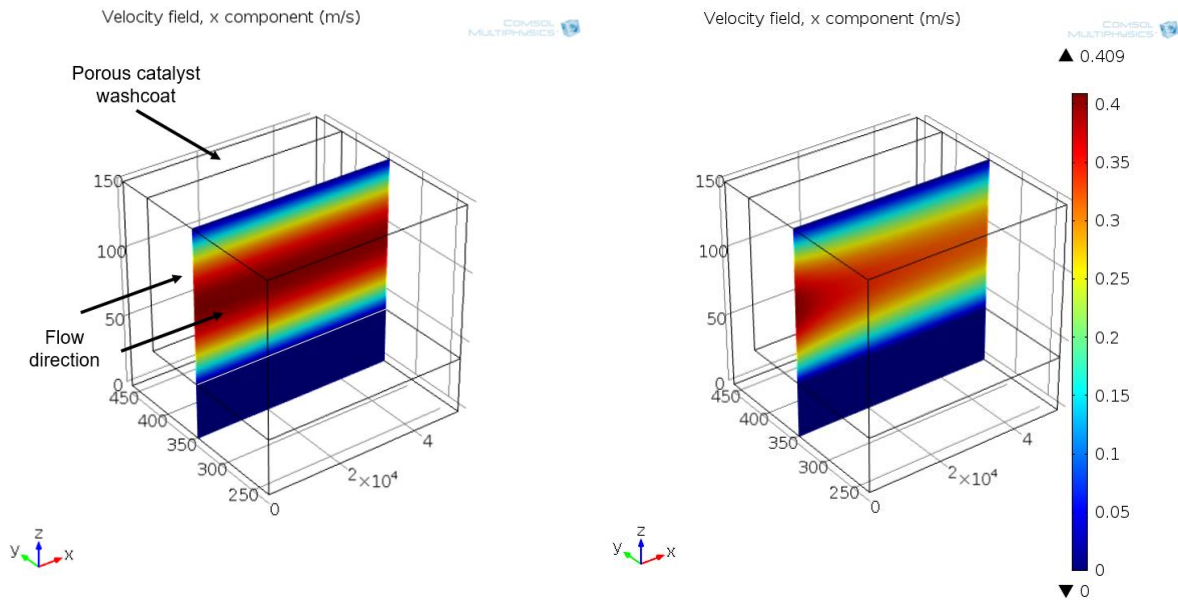


Figure 5.5: Axial velocity (v_x) profile at the mid-xz plane for 250°C (left) and 400°C (right) at atmospheric pressure and GHSV of 32.6 NL.g_{cat}⁻¹.h⁻¹

To increase overall CO₂ conversion and therefore efficient reactor operation, higher pressure operation was prerequisite. A slight decrease in axial velocity along the microchannel length was seen at the 10 bar and 250°C condition (Figure 5.6: left), however only slightly better than what was observed at atmospheric pressure (Figure 5.5: left). The best reactor performance was seen at high-pressure (10 bar) and high-temperature (400°C) operation (Figure 5.6: right) where the axial velocity reduced significantly in the first quarter of the microchannel. In the latter half of the microchannel the axial velocity tapered off towards a constant velocity magnitude as influences of equilibrium limitation hindered CO₂ conversion any further. In general, low fluid velocities were seen in the porous catalyst washcoat for all conditions investigated.

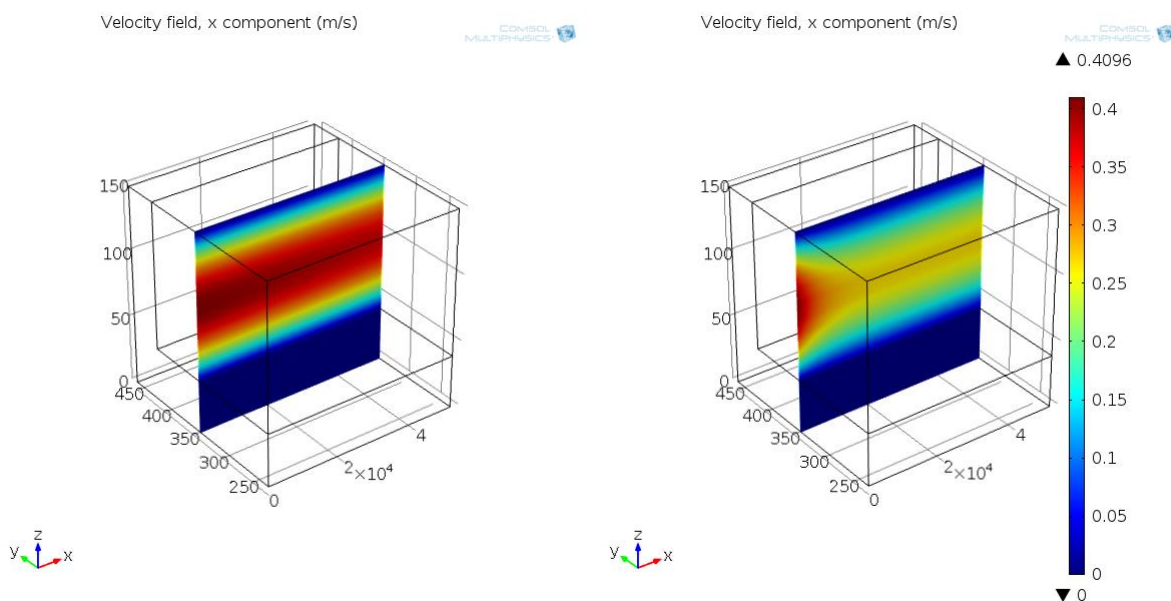


Figure 5.6: Axial velocity (v_x) profile at the mid-xz plane for 250°C (left) and 400°C (right) at 10 bar pressure and GHSV of 32.6 NL.g_{cat}⁻¹.h⁻¹

5.2.3.2 Concentration distributions

It is obvious from axial velocity distributions presented for both atmospheric (Figure 5.5) and 10 bar pressure (Figure 5.6) that reactor operation at low temperature proved to be unsatisfactory in terms of CO₂ conversion. To increase CO₂ conversion it is suggested that the microchannel reactor is operated under high-temperature conditions for all pressures investigated. To attain a quantitative understanding of the reaction extent, Figure 5.7 and Figure 5.8 provide illustrations of species mole fractions (d.b.) along the channel length for atmospheric and 10 bar pressure, respectively. At atmospheric pressure and 400°C, the best reactor performance was observed for the lowest space velocity (32.6 NL.g_{cat}⁻¹.h⁻¹) as mentioned before in Section 5.2.2. This is evident in Figure 5.7 as the highest CH₄ fraction obtained was 0.21 at the outlet of the channel (Figure 5.7: left). With increased space velocity, the CH₄ outlet fraction reduced to 0.12 (Figure 5.7: right) as reaction rates decreased due to reduced contact times with the catalyst surface. Overall, high residual H₂ and CO₂ were observed as equilibrium limitation was not achieved under any atmospheric pressure conditions.

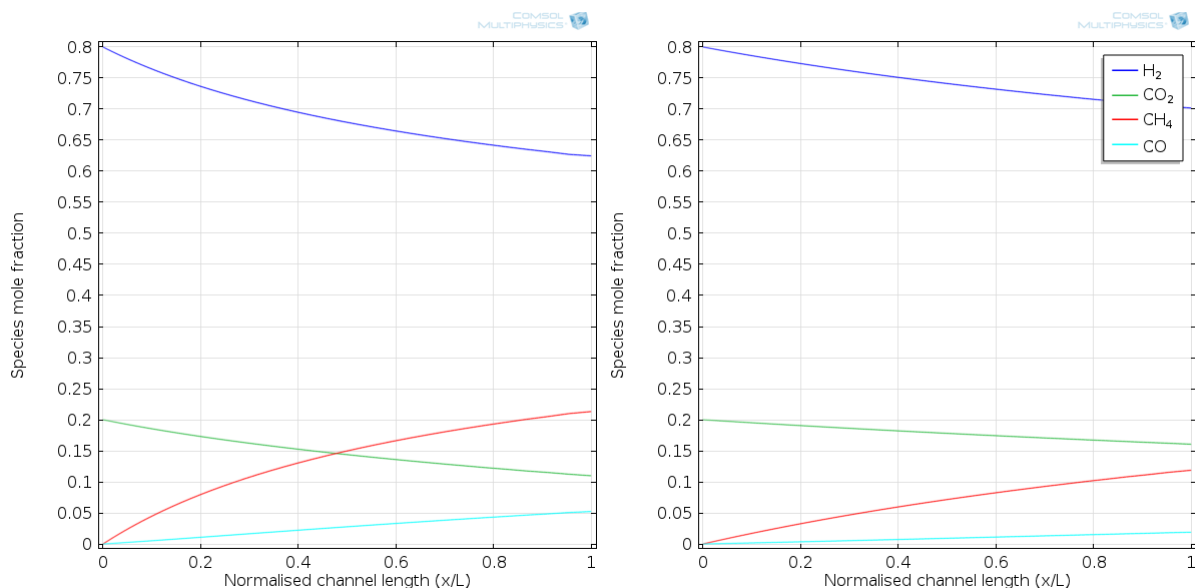


Figure 5.7: Species mole fraction (d.b.) along normalised microchannel length (x/L) for 32.6 NL.g_{cat}⁻¹.h⁻¹ (left) and 97.8 NL.g_{cat}⁻¹.h⁻¹ (right) at 400°C and atmospheric pressure

With increased pressure (10 bar) acceptable product spectra were observed at 400°C (Figure 5.8). For a GHSV of 32.6 NL.g_{cat}⁻¹.h⁻¹ a maximum CH₄ fraction of 0.68 was obtained at the channel outlet (Figure 5.8: left). Also, species mole fractions seem to form a plateau around half-way through the channel as equilibrium limitation starts. However, to increase reactor efficiency by effectively utilising the entire channel length, a high space velocity is essential. With a threefold increase in space velocity (97.8 NL.g_{cat}⁻¹.h⁻¹) the CH₄ fraction (0.65) obtained at the outlet of the channel (Figure 5.8: right) changed marginally from what was previously observed at low space velocity. Again, high-pressure, high-temperature conditions showed satisfactory reactor performance, while a high space velocity produced the best result in terms of specific CH₄ production.

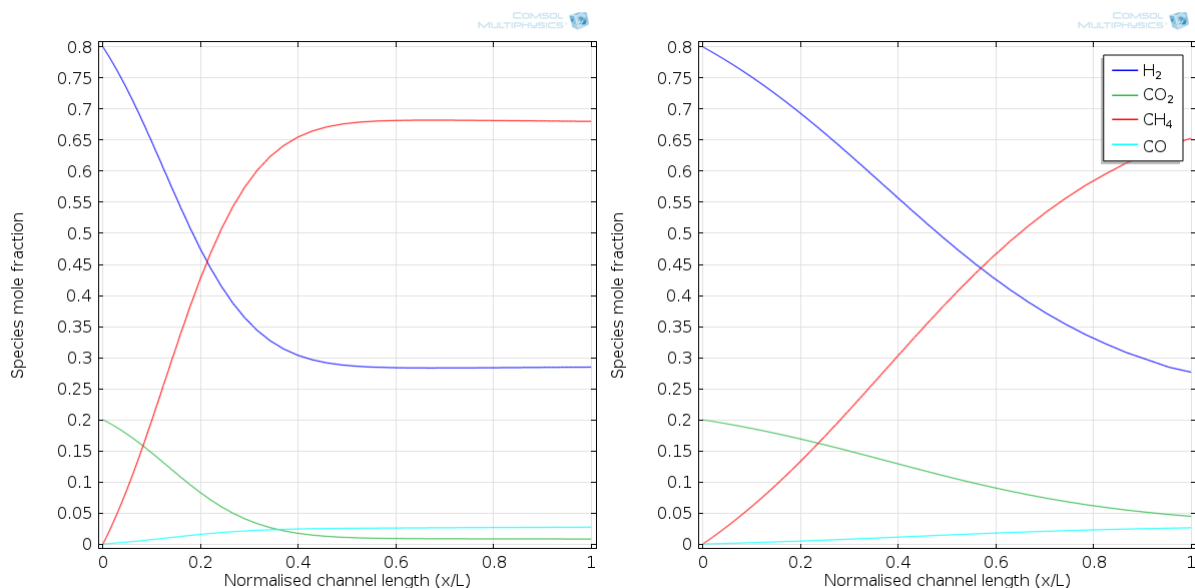


Figure 5.8: Species mole fraction (d.b.) along normalised microchannel length (x/L) for $32.6 \text{ NL.g}_{\text{cat}}^{-1}.\text{h}^{-1}$ (left) and $97.8 \text{ NL.g}_{\text{cat}}^{-1}.\text{h}^{-1}$ (right) at 400°C and 10 bar pressure

The formation of CH_4 through the Sabatier reaction was found to be the main carbon-containing product during this study as seen in Figure 5.7 (atmospheric pressure) and Figure 5.8 (10 bar). Only small amounts of CO were obtained through the RWGS reaction kinetics also included in this investigation. This observation is validated as the Sabatier reaction rate is seen to be dominant at all conditions investigated, with the magnitude of the reaction rate 10 to 20 times higher than that of the RWGS reaction at the inlet of the microchannel (Figure 5.9). Although the RWGS reaction was effectively modelled as a secondary reaction to the Sabatier reaction, its contribution to the overall conversion rate of CO_2 was still important as CO formation was observed during the experimental investigation of the microchannel reactor.

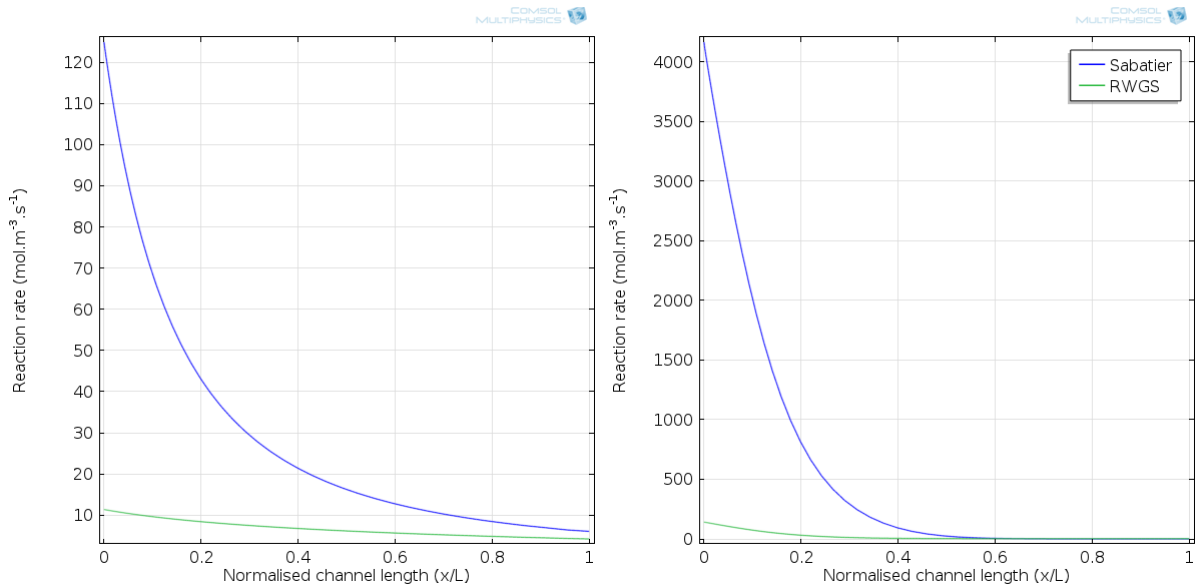


Figure 5.9: Reaction rate along normalised microchannel length (x/L) for atmospheric (left) and 10 bar pressure (right) at 400°C and 32.6 NL.g_{cat}⁻¹.h⁻¹

A closer investigation of the reaction rate can be achieved through the axial mass flux contours of the reactant CO₂ at different operational conditions. At low pressure and 400°C the residual CO₂ was evident for both 32.6 and 97.8 NL.g_{cat}⁻¹.h⁻¹ in Figure 5.10. At these conditions the lowest space velocity (Figure 5.10: left) provided the best performance, but as was shown by the CO₂ mole fractions (Figure 5.7) did not support CO₂ conversion limited by equilibrium and only managed low CH₄ fractions for all space velocities investigated.

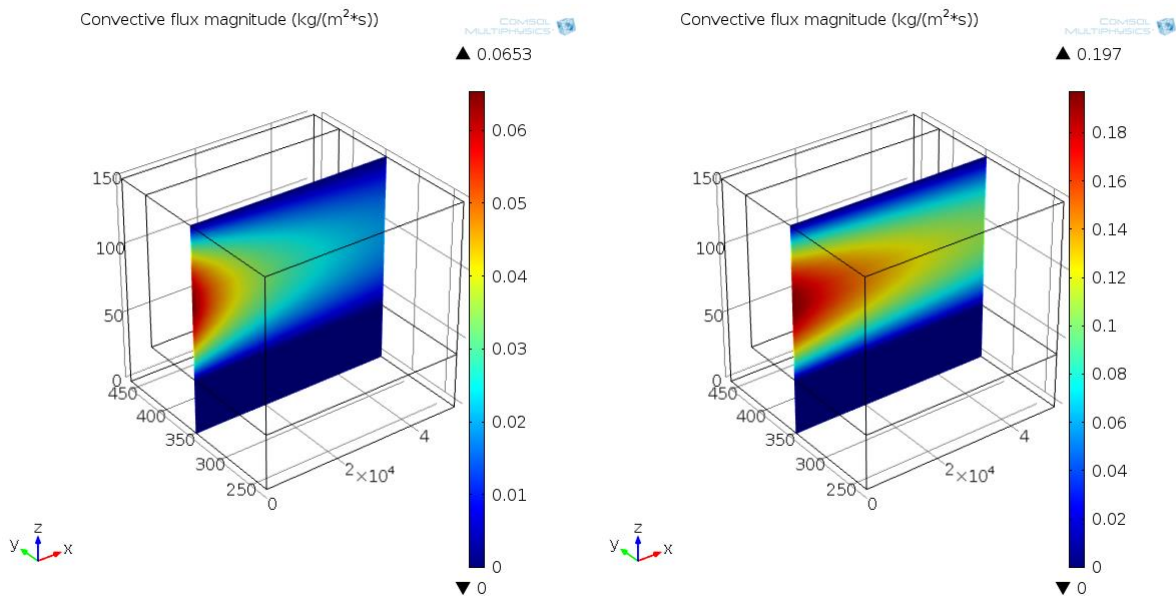


Figure 5.10: Axial CO₂ mass flux at the mid-xz plane for 32.6 NL.g_{cat}⁻¹.h⁻¹ (left) and 97.8 NL.g_{cat}⁻¹.h⁻¹ (right) at 400°C and atmospheric pressure

Confirmation of acceptable reactor performance at high-pressure and high-temperature conditions is evident in the axial CO₂ mass flux (Figure 5.11). For the lowest space velocity (32.6 NL.g_{cat}⁻¹.h⁻¹) the reduction rate of CO₂ is substantial in the first 10% of microchannel length (Figure 5.11: left) as these conditions instigate fast reaction rates. As expected, the highest space velocity (97.8 NL.g_{cat}⁻¹.h⁻¹) supports a more gradual reduction of CO₂ mass flux (Figure 5.11: right) compared to the lowest space velocity. For all pressures investigated, low axial mass fluxes of CO₂ were observed in the porous catalyst washcoat relative to the free-fluid region.

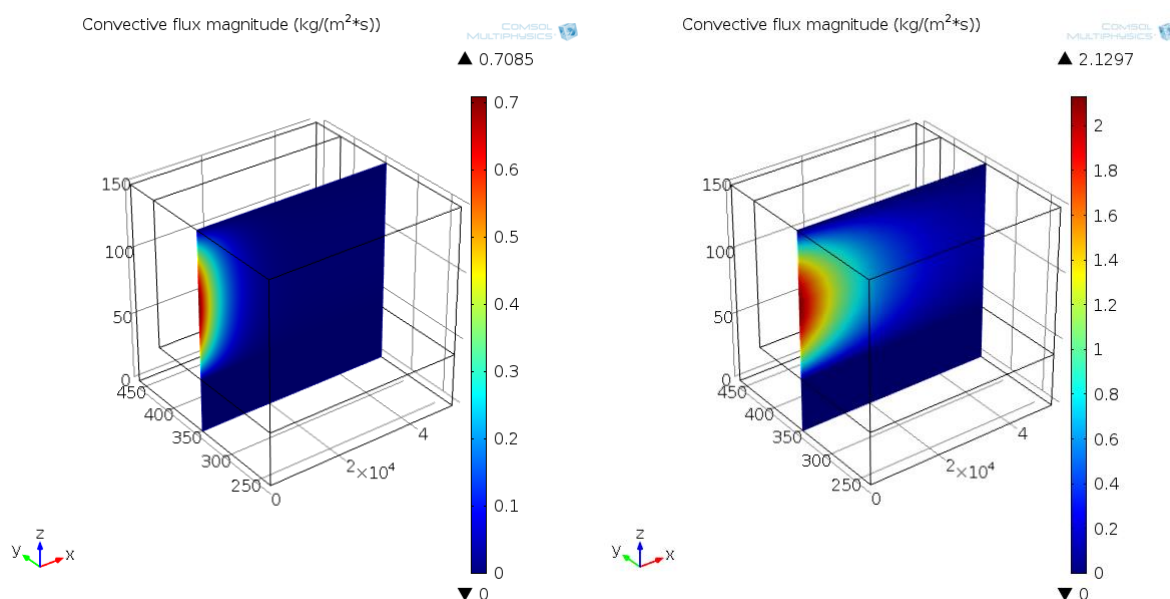


Figure 5.11: Axial CO₂ mass flux at the mid-xz plane for 32.6 NL.g_{cat}⁻¹.h⁻¹ (left) and 97.8 NL.g_{cat}⁻¹.h⁻¹ (right) at 400°C and 10 bar pressure

To obtain an understanding of CH₄ produced in the microchannel, a CH₄ concentration distribution is illustrated in Figure 5.12 along the normalised microchannel height (transverse direction to axial fluid flow) at local x-coordinates from the microchannel inlet. Close to the channel inlet (10 μm) a sharp gradient in CH₄ concentration was observed at the interface between the free-fluid and the porous catalyst phase for both atmospheric (Figure 5.12: left) and 10 bar pressure (Figure 5.12: right). This observation pointed to a high initial Sabatier reaction rate in this region of the porous catalyst washcoat. Further from the channel inlet (500 μm) a more uniform CH₄ concentration profile was apparent as a lower reaction rate occurred in the porous catalyst washcoat. Overall, higher CH₄ concentrations were obtained with increasing distance from the channel inlet. Also, the effect of a pressure increase to 10 bar not only benefited the Sabatier reaction's equilibrium CO₂ conversion, but provided a product stream much higher in CH₄ concentration (Figure 5.12: right).

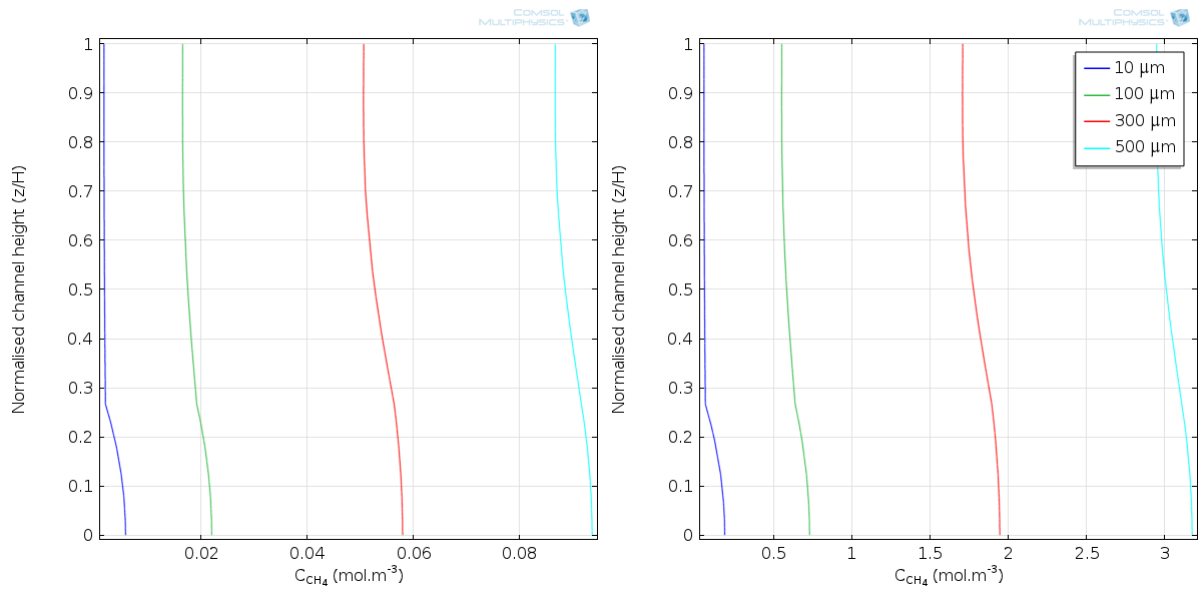


Figure 5.12: CH₄ concentration along normalised microchannel height (z/H) for atmospheric (left) and 10 bar pressure (right) at different x-coordinates (10, 100, 300 and 500 μm) from the microchannel inlet at 400°C

CHAPTER 6: CONCLUSIONS AND RECOMMENDATIONS

This chapter presents a summary of the results obtained and principal outcomes as defined by the objectives of this dissertation. In Section 6.1, the conclusions regarding the experimental and computational fluid dynamic (CFD) modelling of the microchannel reactor are made. Contributions to the current knowledge emanating from this work are given in Section 6.2. Also, the recommendations for future studies related to the use of microchannel reactor technology for CO₂ methanation purposes are given in Section 6.3.

6.1 Conclusions

- i. This investigation successfully demonstrated the methanation of CO₂ in a laboratory-scale microchannel reactor with 8.5 wt.% Ru/Al₂O₃ catalyst washcoat at varying operational conditions (reaction temperature, pressure and space velocity).
- ii. In general, the experimental microchannel reactor performed best under high-pressure, high-temperature conditions. At a pressure of 10 bar, equilibrium CO₂ conversion was achieved at numerous temperature conditions (350–400°C) for the lowest space velocity (32.6 NL.g_{cat}⁻¹.h⁻¹) considered.
- iii. To achieve optimum reactor performance, an operational trade-off between CO₂ conversion and increased space velocity was required. Ultimately, it was concluded that to maximise specific CH₄ production, a high space velocity (97.8 NL.g_{cat}⁻¹.h⁻¹) was required. Although the reactor provided the best overall performance at 10 bar pressure, the effect of a pressure increase was negligible compared to 5 bar at the highest temperature condition (400°C) investigated.
- iv. The most efficient operating point for CH₄ production therefore was 5 bar, 400°C and 97.8 NL.g_{cat}⁻¹.h⁻¹. At this condition a CO₂ conversion of 83.4%, CH₄ yield of 83.5% and specific CH₄ production of 16.9 NL.g_{cat}⁻¹.h⁻¹ was obtained.
- v. In addition to the experimentally evaluated microchannel reactor, it was deemed necessary to develop a three-dimensional mathematical model to describe the reactor. Consequently, a CFD model was developed using the COMSOL Multiphysics® software package. A free-fluid phase, as well as a porous catalyst layer was identified as computational domains to accurately describe the microchannel reactor.
- vi. For the Sabatier reaction, a reversible elementary rate law was identified to describe CH₄ formation. To describe small amounts of CO as a result of the RWGS reaction, a first order rate law was introduced. However, this first order rate law had limitations regarding its accuracy, as experimentally the RWGS reaction was equilibrium limited.

- vii. The mathematical model was subsequently validated through comparison with results obtained from the experimental investigation of the microchannel reactor. It was determined that the mathematical model represented experimental results within reasonable agreement over a wide range of operating parameters once kinetic parameter refinement was done.
- viii. The CFD model also provided an understanding of the reaction-coupled transport phenomena within the reactor. As a result, this three-dimensional modelling approach might assist future studies on the design and operation of catalytic microchannel reactors.

6.2 Contributions to current knowledge

- i. A review of open literature revealed that microchannel reactor technology offers numerous advantages related to their application in power-to-gas (P2G) scenarios. However, a lack of previously reported studies related to the use of microchannel reactors for CO₂ methanation was observed. The present work addressed this matter as a microchannel reactor was experimentally evaluated for CO₂ methanation. The reactor showed good performance in terms of CO₂ conversion and CH₄ yield at various operating conditions. Also, during the experimental evaluation of the reactor, start-stop operation was initiated to simulate the natural intermittency of renewable energies (e.g. solar or wind). The knowledge attained during this investigation therefore serves to broaden the perspective on microchannel technology for P2G applications.
- ii. The absence of three-dimensional modelling approaches on Sabatier-based microchannel reactors permitted an opportunity to elaborate on the design and operation of such reactors at the micro-scale. Model validation was done as the results obtained were fitted to data gathered through the experimental investigation. The CFD modelling study also comprised an examination of velocity and concentration profiles within the microchannel space. This investigation therefore contributed to current knowledge as a fundamental understanding of microchannel reactor operation was achieved.

6.3 Recommendations

- i. It is recommended that a separate characterisation study is done to determine the exact catalyst properties such as density, porosity, permeability and surface area. These parameters can subsequently be used to increase the precision of modelling the porous catalyst washcoat.

- ii. For future investigations, it is recommended that a multiple-reactor configuration is used to improve H₂ productivity and effectively increase CH₄ purity. A possible recommendation is a second microchannel reactor in series. A supplementary feed of pure CO₂ is added in this reaction step to increase the reaction extent in favour of CH₄ production.
- iii. To increase the accuracy of kinetic parameters, it is proposed that an experimental kinetic investigation is done. By using the obtained kinetic parameters, a more reliable modelling approach of the microchannel reactor can be accomplished.
- iv. In particular, it is proposed that a more complex rate law is used to represent the RWGS reaction, as realistically it is governed by equilibrium limitation. For this investigation, however, the first order rate law was deemed to be sufficient to describe small amounts of CO formation.

BIBLIOGRAPHY

ACTA S.P.A. 2016. Ammonia reforming catalysts.

<http://www.actaspa.com/products/ammonia-reforming-catalysts/> Date of access: 19 May 2015.

Altfeld, K. & Pinchbeck, D. 2013. Admissible hydrogen concentrations in natural gas systems. *Gas energy*, 3:1-12.

AUDI AG. 2013. Energy turnaround in the tank.

<http://www.audi.co.za/za/brand/en/vorsprung-durch-technik/content/2013/10/energy-turnaround-in-the-tank.html> Date of access: 29 Aug. 2016.

Awan, A.B. & Khan, Z.A. 2014. Recent progress in renewable energy – remedy of energy crisis in Pakistan. *Renewable and sustainable energy reviews*, 33:236-253.

Bahr, H.A. 1928. Die Kohlenoxyd-Spaltung an Nickel. *Berichte der Deutschen Chemischen Gesellschaft (A and B Series)*, 61(9):2177-2183.

Bakar, W.A.W.A. & Toemen, R.A.S. 2012. Catalytic methanation reaction over supported nickel–ruthenium oxide base for purification of simulated natural gas. *Scientia Iranica*, 19(3):525-534.

Behkish, A., Men, Z., Inga, J.R. & Morsi, B.I. 2002. Mass transfer characteristics in a large-scale slurry bubble column reactor with organic liquid mixtures. *Chemical engineering science*, 57:3307-3324.

Bensmann, A., Hanke-Rauschenbach, R., Heyer, R., Kohrs, F., Benndorf, D., Reichl, U. & Sundmacher, K. 2014. Biological methanation of hydrogen within biogas plants: a model-based feasibility study. *Applied energy*, 134:413-425.

Brooks, K.P., Hu, J., Zhu, H. & Kee, R.J. 2007. Methanation of carbon dioxide by hydrogen reduction using the Sabatier process in microchannel reactors. *Chemical engineering science*, 62:1161-1170.

Burkhardt, M. & Busch, G. 2013. Methanation of hydrogen and carbon dioxide. *Applied energy*, 111:74-79.

- Cao, C., Zhang, N., Chen, X. & Cheng, Y. 2015. A comparative study of Rh and Ni coated microchannel reactor for steam methane reforming using CFD with detailed chemistry. *Chemical engineering science*, 137:276-286.
- Chein, R.Y., Chen, W.Y. & Yu, C.T. 2016. Numerical simulation of carbon dioxide methanation reaction for synthetic natural gas production in fixed-bed reactors. *Journal of natural gas science and engineering*, 29:243-251.
- Chen, J., Yang, H., Ring, Z. & Dabros, T. 2008. Mathematical modeling of monolith catalysts and reactors for gas phase reactions. *Applied catalysis A: General*, 345(1):1-11.
- CHERIC. 2016. KDB. <https://www.cheric.org/research/kdb/> Date of access: 28 Jun. 2016.
- Chiuta, S., Everson, R.C., Neomagus, H.W.J.P., Van Der Gryp, P. & Bessarabov, D.G. 2013. Reactor technology options for distributed hydrogen generation via ammonia decomposition: a review. *International journal of hydrogen energy*, 38:14968-14991.
- Chiuta, S., Everson, R.C., Neomagus, H.W.J.P., Le Grange, L.A. & Bessarabov, D.G. 2014. A modelling evaluation of an ammonia-fuelled microchannel reformer for hydrogen generation. *International journal of hydrogen energy*, 39:11390-11402.
- Chiuta, S., Everson, R.C., Neomagus, H.W.J.P. & Bessarabov, D.G. 2015. Performance evaluation of a high-throughput microchannel reactor for ammonia decomposition over a commercial Ru-based catalyst. *International journal for hydrogen energy*, 40:2921-2926.
- Chiuta, S., Engelbrecht, N., Human, G. & Bessarabov, D.G. 2016. Techno-economic assessment of power-to-methane and power-to-syngas business models for sustainable carbon dioxide utilization in coal-to-liquid facilities. *Journal of CO₂ utilization*, 16:399-411.
- Chiuta, S., Everson, R.C., Neomagus, H.W.J.P. & Bessarabov, D.G. 2016. Hydrogen production from ammonia decomposition over a commercial Ru/Al₂O₃ catalyst in a microchannel reactor: Experimental validation and CFD simulation. *International journal of hydrogen energy*, 41(6):3774-3785.
- Choe, S.J., Kang, H.J., Kim, S., Park, S., Park, D.H. & Huh, D.S. 2005. Adsorbed carbon formation and carbon hydrogenation for CO₂ methanation on the Ni(111) surface: ASFD-MO study. *Bulletin of the Korean chemical society*, 26(11):1682-1688.

- Commenge, J.M., Falk, L., Corriou, J.P. & Matlosz, M. 2002. Optimal design for flow uniformity in microchannel reactors. *American institute of chemical engineers journal*, 48(2):345-358.
- Dagle, R.A., Platon, A., Palo, D.R., Datye, A.K., Vohs, J.M. & Wang, Y. 2008. PdZnAl catalysts for the reactions of water-gas-shift, methanol steam reforming, and reverse-water-gas-shift. *Applied catalysis A: General*, 342:63-68.
- Degaleesan, S., Dudukovic, M. & Pan, Y. 2001. Experimental study of gas-induced liquid-flow structures in bubble columns. *American institute of chemical engineers journal*, 47(9):1913-1931.
- Dellano-Paz, F., Calvo-Silvosa, A., Antelo, S.I. & Soares, I. 2015. The European low-carbon mix for 2030: the role of renewable energy sources in an environmentally and socially efficient approach. *Renewable and sustainable energy reviews*, 48:49-61.
- Delparish, A. & Avci, A.K. 2016. Intensified catalytic reactors for Fischer-Tropsch synthesis and for reforming of renewable fuels to hydrogen and synthesis gas. *Fuel processing technology*, 151:72-100.
- Deshmukh, S.R., Tonkovich, A.Y., Jarosch, K.T., Schrader, J.L., Fitzgerald, S.P., Kilanowski, D.R., Lerou, J.J. & Mazanec, T.J. 2010. Scale-up of microchannel reactors for Fischer-Tropsch synthesis. *Industrial & engineering chemistry research*, 49:10883-10888.
- Ducamp, J., Bengaouer, A. & Baurens, P. 2016?. Modelling and experimental validation of a CO₂ methanation annular cooled fixed-bed reactor exchanger. *Canadian journal of chemical engineering* (In press).
- Duyar, M.S., Ramachandran, A., Wang, C. & Farrauto, R.J. 2015. Kinetics of CO₂ methanation over Ru/γ-Al₂O₃ and implications for renewable energy storage applications. *Journal of CO₂ utilization*, 12:27-33.
- Finn, P. & Fitzpatrick, C. 2014. Demand side management of industrial electricity consumption: promoting the use of renewable energy through real-time pricing. *Applied energy*, 113:11-21.
- Fogler, H.S. 2012. Elements of Chemical Reaction Engineering. Upper Saddle River, NJ: Prentice Hall International.

Fuller, E.N., Schettler, P.D. & Giddings, J.C. 1966. A new method for prediction of binary gas-phase diffusion coefficients. *Industrial and engineering chemistry*, 58(5):19-27.

Fuller, E.N., Ensley, K. & Giddings, J.C. 1969. Diffusion of halogenated hydrocarbons in helium. *Journal of physical chemistry*, 73(11):3679-3685.

Fuller, T., Hartnig, C., Ramani, V., Uchida, H., Gasteiger, H.A., Cleghorn, S., Strasser, P., Zawodzinski, T., Jones, D., Shirvanian, P., Jarvi, T., Zelenay, P., Lamy, C. & Bele, C. 2009. Proton exchange membrane fuel cells 9: ECS transactions: Volume 25, Issue 1. Pennington, NY: The Electrochemical Society.

Gabbar, H.A., Runge, J., Bondarenko, D., Bower, L., Pandya, D., Musharavati, F. & Pokharel, S. 2015. Performance evaluation of gas-power strategies for building energy conservation. *Energy conversion and management*, 93:187-196.

Gahleitner, G. 2013. Hydrogen from renewable electricity: an international review of power-to-gas pilot plants for stationary applications. *International journal of hydrogen energy*, 38:2039-2061.

Galletti, C., Specchia, S. & Specchia, V. 2011. CO selective methanation in H₂-rich gas for fuel cell application: microchannel reactor performance with Ru-based catalysts. *Chemical engineering journal*, 167:616-621.

Gao, J., Wang, Y., Ping, Y., Hu, D., Xu, G., Gu, F. & Su, F. 2012. A thermodynamic analysis of methanation reactions of carbon oxides for the production of synthetic natural gas. *The royal society of chemistry advances*, 2:2358-2368.

Garbarino, G., Bellotti, D., Riani, P., Magistri, L. & Busca, G. 2015. Methanation of carbon dioxide on Ru/Al₂O₃ and Ni/Al₂O₃ catalysts at atmospheric pressure: catalysts activation, behaviour and stability. *International journal of hydrogen energy*, 40:9171-9182.

Garmsiri, S., Rosen, M.A. & Rymal Smith, G. 2014. Integration of wind energy, hydrogen and natural gas pipeline systems to meet community and transportation energy needs: a parametric study. *Sustainability*, 6(5):2506-2526.

Gogate, M.R. & Davis, R.J. 2010. Comparative study of CO and CO₂ hydrogenation over supported Rh-Fe catalysts. *Catalysis communications*, 11:901-906.

Goodman, D.J. 2013. Methanation of carbon dioxide. Los Angeles, CA: University of California. (Dissertation – M. Chem. Eng.).

- Görke, O., Pfeifer, P. & Schubert, K. 2005. Highly selective methanation by the use of a microchannel reactor. *Catalysis today*, 110:132-139.
- Götz, M., Bajohr, S., Graf, F., Reimert, R. & Kolb, T. 2013. Einsatz eines Blasensäulenreaktors zur Methansynthese. *Chemie Ingenieur Technik*, 85(7):1146-1151.
- Götz, M., Koch, A.M. & Graf, F. 2014. State of the art and perspectives of CO₂ methanation process concepts for power-to-gas applications. Paper presented at the International Gas Union Research Conference, Copenhagen, Denmark, 17-19 September.
- Götz, M., Lefebvre, J., Mörs, F., Koch, A., Graf, F., Bajohr, S., Reimert, R. & Kolb, T. 2016. Renewable power-to-gas: a technological and economic review. *Renewable energy*, 85:1371-1390.
- Henning, H. & Palzer, A. 2014. A comprehensive model for the German electricity and heat sector in a future energy system with a dominant contribution from renewable energy technologies – part I: methodology. *Renewable and sustainable energy reviews*, 30:1003-1018.
- Hessel, V., Hardt, S. & Löwe, H. 2004. Chemical micro process engineering: fundamentals, modelling and reactions. Weinheim: Wiley-VCH Verlag GmbH.
- Hoekman, S.K., Broch, A., Robbins, C. & Purcell, R. 2010. CO₂ recycling by reaction with renewably-generated hydrogen. *International journal of greenhouse gas control*, 4:44-50.
- Holladay, J.D., Wang, Y. & Jones, E. 2004. Review of developments in portable hydrogen production using microreactor technology. *Chemical reviews*, 104:4767-4790.
- Hwang, H., Harale, A., Liu, P.K.T., Sahimi, M. & Tsotsis, T.T. 2008. A membrane-based reactive separation system for CO₂ removal in a life support system. *Journal of membrane science*, 315(1-2):116-124.
- IEA. 2015. CO₂ emissions from fuel combustion highlights 2015. <https://www.iea.org/publications/freepublications/publication/CO2EmissionsFromFuelCombustionHighlights2015.pdf> Date of access: 26 Aug. 2016.
- Jess, A. & Kern, C. 2009. Modeling of multi-tubular reactors for Fischer-Tropsch synthesis. *Chemical engineering & technology*, 32(8):1164-1175.

- Johnston, I. 2016. Scotland just produced enough wind energy to power it for an entire day. *Independent*, 11 Aug. <http://www.independent.co.uk/environment/scotland-wind-energy-renewable-power-electricity-wwf-scotland-a7183006.html> Date of access: 19 Oct. 2016.
- Judd, R. & Pinchbeck, D. 2013. Power to gas research roadmap. Offering a solution to the energy storage problem? http://www.gerg.eu/public/uploads/files/publications/GERGpapers/SD_qfe_02_2013_fb_Judd.pdf Date of access: 30 Aug. 2016.
- Junaedi, C., Hawley, K., Walsh, D. & Roychoudhury, S. 2011. Compact and lightweight Sabatier reactor for carbon dioxide reduction. Paper presented at the 41th International Conference on Environmental Systems, Portland, OR, 17-21 July.
- Junaedi, C., Hawley, K., Walsh, D. & Roychoudhury, S. 2014. CO₂ reduction assembly prototype using microlith-based sabatier reactor for ground demonstration. Paper presented at the 44th International Conference on Environmental Systems, Tucson, AZ, 13-17 July.
- Kantarci, N., Borak, F. & Ulgen, K.O. 2005. Bubble column reactors. *Process biochemistry*, 40:2263-2283.
- Kiewidt, L. & Thöming, J. 2015. Predicting optimal temperature profiles in single-stage fixed-bed reactors for CO₂-methanation. *Chemical engineering science*, 132:59-71.
- Koohi-Kamali, S., Tyagi, V.V., Rahim, N.A., Panwar, N.L. & Mokhlis, H. 2013. Emergence of energy storage technologies as the solution for reliable operation of smart power systems: a review. *Renewable and sustainable energy reviews*, 25:135-165.
- Kopyscinski, J., Schildhauer, T.J. & Biollaz, S.M.A. 2011. Methanation in a fluidized bed reactor with high initial CO partial pressure: part I – experimental investigation of hydrodynamics, mass transfer effects, and carbon deposition. *Chemical engineering science*, 66:924-934.
- Koschany, F., Schlereth, D. & Hinrichsen, O. 2016. On the kinetics of the methanation of carbon dioxide on coprecipitated NiAl(O)_x. *Applied catalysis B: Environmental*, 181:504-516.
- Krumdieck, S., Page, S. & Dantas, A. 2010. Urban form and long-term fuel supply decline: a method to investigate the peak oil risks to essential activities. *Transportation research part A*, 44:306-322.

- Kumar, S., Kumar, R.A., Munshi, P. & Khanna, A. 2012. Gas hold-up in three phase co-current bubble columns. *Procedia engineering*, 42:782-794.
- Lebarbier, V., Dagle, R., Datye, A. & Wang, Y. 2010. The effect of PdZn particle size on reverse-water-gas-shift reaction. *Applied catalysis A: General*, 379:3-6.
- Lim, J.Y., Mcgregor, J., Sederman, A.J. & Dennis, J.S. 2016. Kinetic studies of CO₂ methanation over a Ni/ γ -Al₂O₃ catalyst using a batch reactor. *Chemical engineering science*, 141:28-45.
- Liu, B. & Ji, S. 2013. Comparative study of fluidized-bed and fixed-bed reactor for syngas methanation over Ni-W/TiO₂-SiO₂ catalyst. *Journal of energy chemistry*, 22:740-746.
- Liu, Z., Chu, B., Zhai, X., Jin, Y. & Cheng, Y. 2012. Total methanation of syngas to synthetic natural gas over Ni catalyst in a micro-channel reactor. *Fuel*, 95:599-605.
- Ludig, S., Haller, M., Schmid, E. & Bauer, N. 2011. Fluctuating renewables in a long-term climate change mitigation strategy. *Energy*, 36:6674-6685.
- Lunde, P.J. 1974. Modeling, simulation, and operation of a Sabatier reactor. *Industrial & engineering chemistry process design and development*, 13(3):226-232.
- Lunde, P.J. & Kester, F.L. 1973. Rates of methane formation from carbon dioxide and hydrogen over a ruthenium catalyst. *Journal of catalysis*, 30(3):423-429.
- Lunde, P.J. & Kester, F.L. 1974. Carbon dioxide methanation on a ruthenium catalyst. *Industrial & engineering chemistry process design and development*, 13(1):27-33.
- Luo, L., Li, S. & Zhu, Y. 2005. The effects of yttrium on the hydrogenation performance and surface properties of a ruthenium-supported catalyst. *Journal of the Serbian chemical society*, 70(12):1419-1425.
- Marwood, M., Doepper, R. & Renken, A. 1997. In-situ surface and gas phase analysis for kinetic studies under transient conditions. The catalytic hydrogenation of CO₂. *Applied catalysis A: General*, 151:223-246.
- Men, Y., Kolb, G., Zapf, R., Hessel, V. & Lowe, H. 2007. Selective methanation of carbon oxides in a microchannel reactor – primary screening and impact of gas additives. *Catalysis today*, 125:81-87.

Müller, K., Städter, M., Rachow, F., Hoffmannbeck, D. & Schmeißer, D. 2013. Sabatier-based CO₂-methanation by catalytic conversion. *Environmental earth sciences*, 70(8):3771-3778.

National Treasury. 2013. Carbon tax policy paper: reducing greenhouse gas emissions and facilitating the transition to a green economy.

<http://www.treasury.gov.za/public%20comments/Carbon%20Tax%20Policy%20Paper%202013.pdf> Date of access: 30 Aug. 2016.

NASA. 2011. The Sabatier system: producing water on the space station.

http://www.nasa.gov/mission_pages/station/research/news/sabatier.html Date of access: 1 Sep. 2016.

O'Connell, M., Kolb, G., Schelhaas, K.P., Wichert, M., Tiemann, D., Pennemann, H. & Zapf, R. 2012. Towards mass production of microstructured fuel processors for application in future distributed energy generation systems: a review of recent progress at IMM. *Chemical engineering research and design*, 90:11-18.

Ohya, H., Fun, J., Kawamura, H., Itoh, K., Ohashi, H., Aihara, M., Tanisho, S. & Negishi, Y. 1997. Methanation of carbon dioxide by using membrane reactor integrated with water vapor permselective membrane and its analysis. *Journal of membrane science*, 131:237-247.

Pandey, D. & Deo, G. 2016. Effect of support on the catalytic activity of supported Ni–Fe catalysts for the CO₂ methanation reaction. *Journal of industrial and engineering chemistry*, 33:99-107.

Park, J. & McFarland, E.W. 2009. A highly dispersed Pd–Mg/SiO₂ catalyst active for methanation of CO₂. *Journal of catalysis*, 266(1):92-97.

Pattison, R.C. & Baldea, M. 2015. Robust autothermal microchannel reactors. *Computers & chemical engineering*, 81:171-179.

Peebles, D.E. & Goodman, D.W. 1983. Methanation of carbon dioxide on Ni(100) and the effects of surface modifiers. *Journal of physical chemistry*, 87:4378-4387.

Prairie, M.R., Renken, A., Highfield, J.G., Thampi, K.R. & Grätzel, M. 1991. A Fourier transform infrared spectroscopic study of CO₂ methanation on supported ruthenium. *Journal of catalysis*, 129(1):130-144.

Pregger, T., Nitsch, J. & Naegler, T. 2013. Long-term scenarios and strategies for the deployment of renewable energies in Germany. *Energy policy*, 59:350-360.

Reid, R.C., Prausnitz, J.M. & Poling, B.E. 1987. The properties of gases and liquids. New York: McGraw-Hill.

Roberts, K. 2013. Modular design of smaller-scale GTL plants.

http://www.velocys.com/arcv/press/egs/PTQ_modular_design_of_GTL_130101.pdf Date of access: 03 Mar. 2015.

Rossi, F., Castellani, B., Morini, E., Di Giovanna, L., Corsi, N., Giuliobello, M. & Nicolini, A. 2015. Experimental apparatus for solar energy storage via methane production. Paper presented at the Third Southern African Solar Energy Conference, Kruger National Park, South Africa, 11-13 May.

Scamman, D. & Newborough, M. 2016. Using surplus nuclear power for hydrogen mobility and power-to-gas in France. *International journal of hydrogen energy*, 41:10080-10089.

Schaaf, T., Grunig, J., Schuster, M.R., Rothenfluh, T. & Orth, A. 2014. Methanation of CO₂ – storage of renewable energy in a gas distribution system. *Energy, sustainability and society*, 4(29):1-14.

Schiebahn, S., Grube, T., Robinius, M., Tietze, V., Kumar, B. & Stolten, D. 2015. Power to gas: technological overview, systems analysis and economic assessment for a case study in Germany. *International journal of hydrogen energy*, 40(12):4285-4294.

Schildhauer, T.J. & Biollaz, S.M. 2015. Reactors for catalytic methanation in the conversion of biomass to synthetic natural gas (SNG). *Chimia*, 69(10):603-607.

Schlereth, D. & Hinrichen, O. 2014. A fixed-bed reactor modeling study on the methanation of CO₂. *Chemical engineering research and design*, 92:702-712.

Schoder, M., Armbruster, U. & Martin, A. 2013. Heterogen katalysierte Hydrierung von Kohlendioxid zu Methan unter erhöhten Drücken. *Chemie Ingenieur Technik*, 85(3):344-352.

Shankleman, J. 2016. Renewable energy just provided Germany with almost all of its power. *Independent*, 19 May. <http://www.independent.co.uk/environment/germany-just-got-almost-all-of-its-power-from-renewable-energy-a7037851.html> Date of access: 19 Oct. 2016.

- Solymosi, F., Bánsági, T. & Erdöhelyi, A. 1981. Infrared study of the reaction of adsorbed formate ion with H₂ on supported Rh catalysts. *Journal of catalysis*, 72(1):166-169.
- Stambler, I. 2003. Converting dual fuel nozzles to single fuel gives Aquila 250kW. http://www.fernengineering.com/pdf/converting_dual_fuel_nozzles.pdf Date of access: 06 Mar. 2015.
- Stankiewicz, A.I. & Moulijn, J.A. 2000. Process intensification: transforming chemical engineering. *Chemical engineering progress*, 96(1):22-34.
- Sterner, M. 2009. Bioenergy and renewable power methane in integrated 100% renewable energy systems. Limiting global warming by transforming energy systems. Kassel: University of Kassel. (Thesis – Ph.D.)
- Tada, S., Ochieng, O.J., Kikuchi, R., Haneda, T. & Kameyama, H. 2014. Promotion of CO₂ methanation activity and CH₄ selectivity at low temperatures over Ru/CeO₂/Al₂O₃ catalysts. *International journal of hydrogen energy*, 39:10090-10100.
- Tonkovich, A.L.Y., Call, C.J., Jimenez, D.M., Wegeng, R.S. & Drost, M.K. 1996. Microchannel heat exchangers for chemical reactors. Paper presented at the 31st National Heat Transfer Conference, Houston, TX, 3-6 August.
- Tonkovich, A.Y., Perry, S., Wang, Y., Qiu, D., LaPlante, T. & Rogers, W.A. 2004. Microchannel process technology for compact methane steam reforming. *Chemical engineering science*, 59(22,23):4819-4824.
- U.S. DOE. 2001. Hydrogen fuel cell engines and related technologies. Module 1: hydrogen properties. http://www1.eere.energy.gov/hydrogenandfuelcells/tech_validation/pdfs/fcm01r0.pdf Date of access: 20 Mar. 2015.
- VanderWiel, D.P., Zilka-Marco, J.L., Wang, Y., Tonkovich, A.Y. & Wegeng, R.S. 2000. Carbon dioxide conversions in microreactors. Paper presented at the Fourth International Conference on Microreaction Technology, Atlanta, GA, 5-9 March.
- Vandewalle, J., Bruninx, K. & D'haeseleer, W. 2015. Effects of large-scale power to gas conversion on the power, gas and carbon sectors and their interactions. *Energy conversion and management*, 94:28-39.

- Varone, A. & Ferrari, M. 2015. Power to liquid and power to gas: an option for the German Energiewende. *Renewable and sustainable energy reviews*, 45:207-218.
- Wang, W. & Gong, J. 2011. Methanation of carbon dioxide: an overview. *Frontiers of chemical science and engineering*, 5(1):2-10.
- Wang, W., Wang, S., Ma, X. & Gong, J. 2011. Recent advances in catalytic hydrogenation of carbon dioxide. *Chemical society reviews*, 40:3703-3727.
- Weatherbee, G.D. & Bartholomew, C.H. 1981. Hydrogenation of CO₂ on group VIII metals: I. Specific activity of Ni/SiO₂. *Journal of catalysis*, 68(1):67-76.
- Weatherbee, G.D. & Bartholomew, C.H. 1982. Hydrogenation of CO₂ on group VIII metals: II. Kinetics and mechanism of CO₂ hydrogenation on nickel. *Journal of catalysis*, 77:460-472.
- Wei, W. & Jinlong, G. 2011. Methanation of carbon dioxide: an overview. *Frontiers of chemical science and engineering*, 5(1):2-10.
- Xu, J. & Froment, G.F. 1989. Methane steam reforming, methanation and water-gas shift: I. intrinsic kinetics. *American institute of chemical engineers journal*, 35(1):88-96.
- Xu, J., Lin, Q., Su, X., Duan, H., Geng, H. & Huang, Y. 2016. CO₂ methanation over TiO₂-Al₂O₃ binary oxides supported Ru catalysts. *Chinese journal of chemical engineering*, 24:140-145.
- Yang, L., Ge, X., Wan, C., Yu, F. & Li, Y. 2014. Progress and perspectives in converting biogas to transportation fuels. *Renewable and sustainable energy reviews*, 40:113-1152.
- Zamani, A.H., Ali, R. & Bakar, W.A.W.A. 2014. The investigation of Ru/Mn/Cu-Al₂O₃ oxide catalysts for CO₂/H₂ methanation in natural gas. *Journal of the Taiwan institute of chemical engineers*, 45:143-152.
- Zhang, J., Bai, Y., Zhang, Q., Wang, X., Zhang, T., Tan, Y. & Han, Y. 2014. Low-temperature methanation of syngas in slurry phase over Zr-doped Ni/γ-Al₂O₃ catalysts prepared using different methods. *Fuel*, 132:211-218.
- Zhao, Y., Zhang, Z., Wang, S. & Zhang, Y., Liu, Y. 2015. Linkage analysis of sectoral CO₂ emissions based on the hypothetical extraction method in South Africa. *Journal of cleaner production*, 103:916-624.

ZSW. 2016. Power-to-Gas. <https://www.zsw-bw.de/en/research/renewable-fuels/topics/power-to-gas.html> Date of access: 01 Sep. 2016.

APPENDIX A: GAS CALIBRATION CURVES

Standard gas mixtures were used to produce GC calibration curves for H₂, CO₂, CH₄ and CO. The gas calibration curves, based on peak area counts, were subsequently used to determine the product gas composition during experiments on the microchannel reactor. The respective calibration curves are illustrated for H₂ (Figure A.1), CO₂ (Figure A.2), CH₄ (Figure A.3) and CO (Figure A.4).

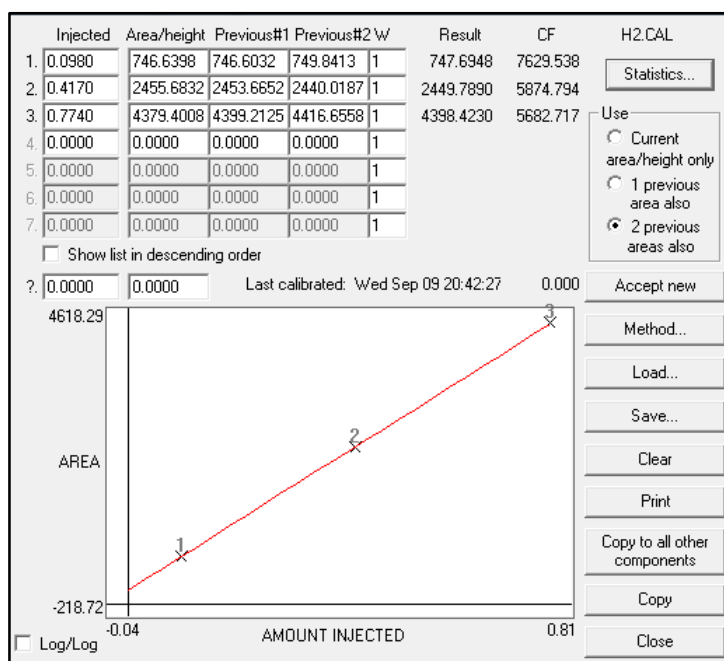


Figure A.1: Hydrogen calibration curve used to calculate H₂ mole fraction in product gas during experiments

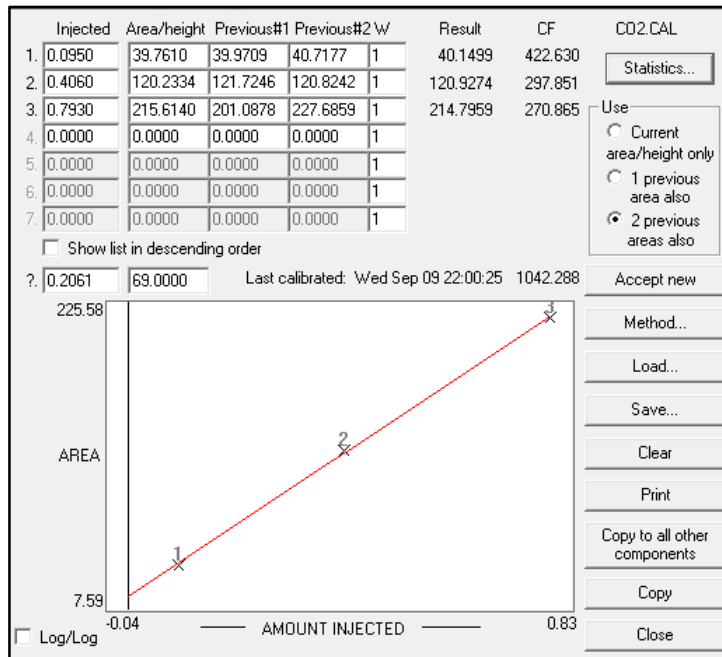


Figure A.2: Carbon dioxide calibration curve used to calculate CO₂ mole fraction in product gas during experiments

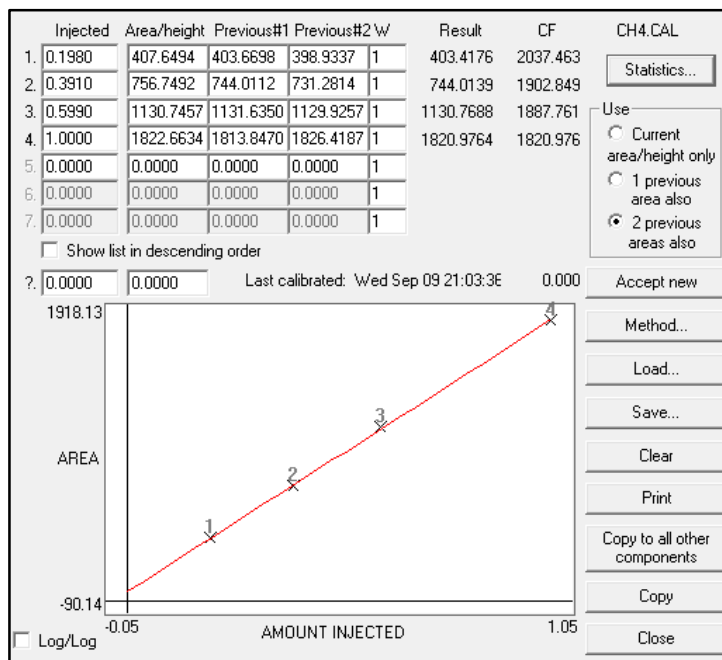


Figure A.3: Methane calibration curve used to calculate CH₄ mole fraction in product gas during experiments

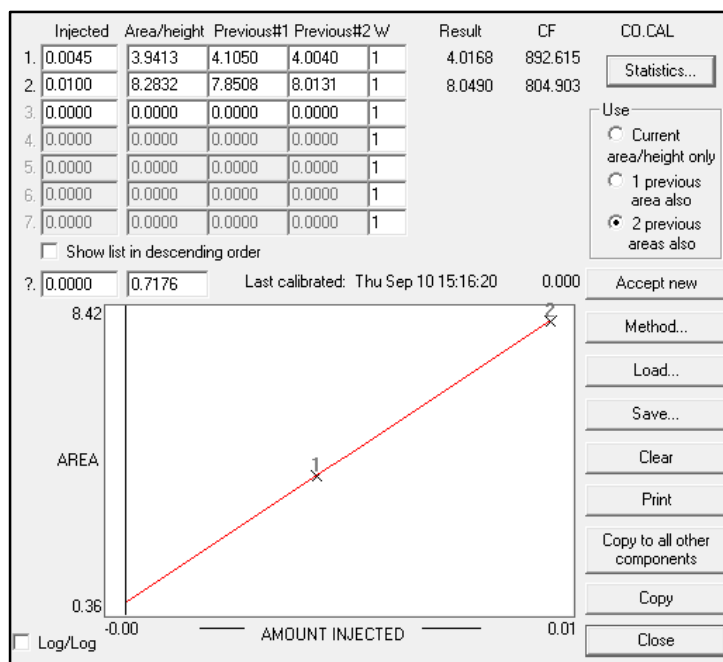


Figure A.4: Carbon monoxide calibration curve used to calculate CO mole fraction in product gas during experiments

An example of the data collection table used during the experimental investigation is given in Table A.1. Once data was collected and fed into a MS Excel spreadsheet, the performance parameters defined as CO₂ conversion and CH₄ yield was calculated for each experimental run.

Table A.1: Example of the data collection table used during the experimental investigation

Time (h)	CO ₂ Flow rate (Nml.min ⁻¹)	H ₂ Flow rate (Nml.min ⁻¹)	Thermocouple 1 Temp (°C)	Thermocouple 2 Temp (°C)	Pressure drop (kPa)	Flow rate (Nml.min ⁻¹)	H ₂ mole fraction	CO ₂ mole fraction	CH ₄ mole fraction	CO mole fraction
0.25										
0.5										
0.75										
1										
1.25										
1.5										
1.75										
2										
2.25										
2.5										
0.25										
0.5										
0.75										
1										
1.25										
1.5										
1.75										
2										
2.25										
2.5										

APPENDIX B: FULL SET OF EXPERIMENTAL DATA

The effect of a variation in reactor temperature is illustrated on CO₂ conversion and CH₄ yield at all five GHSVs investigated at atmospheric (Figure B.1), 5 bar (Figure B.2) and 10 bar pressure (Figure B.3).

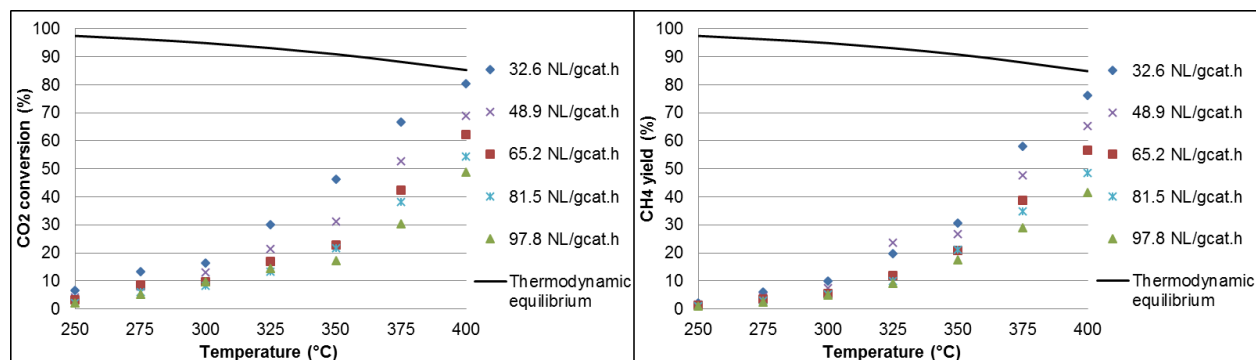


Figure B.1: Effect of reactor temperature on CO₂ conversion (left) and CH₄ yield (right) at atmospheric pressure and GHSVs of 32.6, 48.9, 65.2, 81.5 and 97.8 NL.g_{cat}⁻¹.h⁻¹

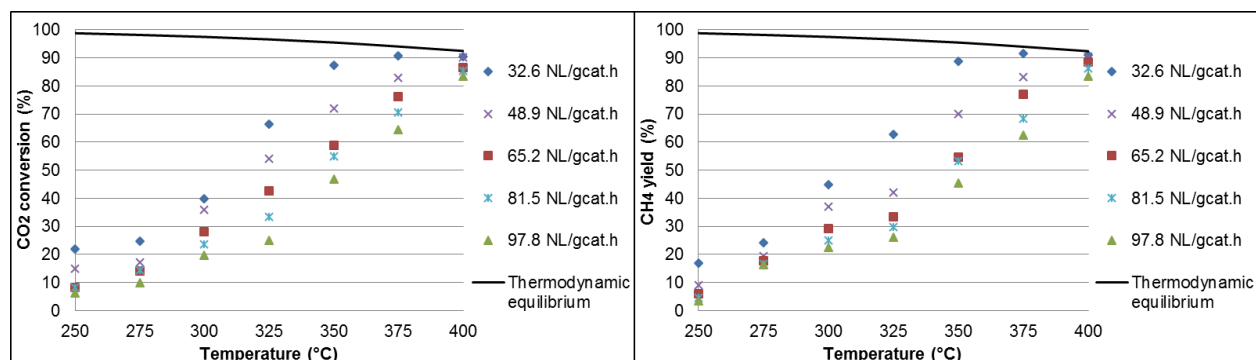


Figure B.2: Effect of reactor temperature on CO₂ conversion (left) and CH₄ yield (right) at 5 bar pressure and GHSVs of 32.6, 48.9, 65.2, 81.5 and 97.8 NL.g_{cat}⁻¹.h⁻¹

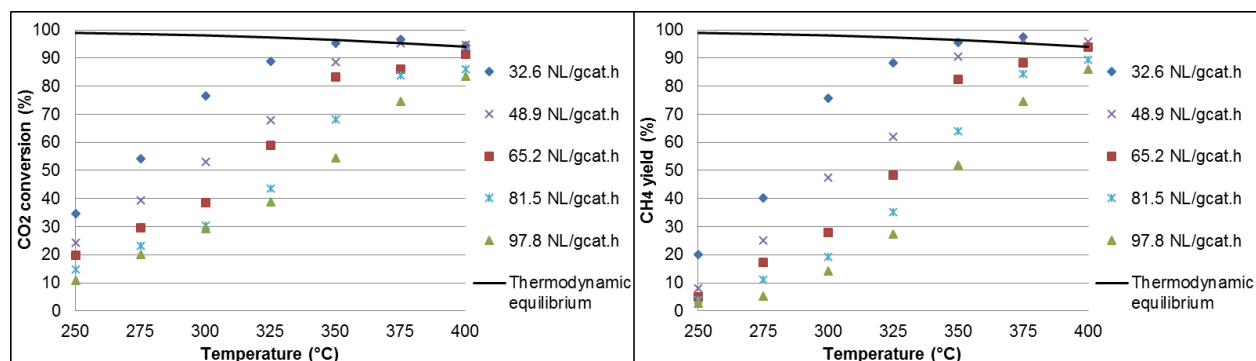


Figure B.3: Effect of reactor temperature on CO₂ conversion (left) and CH₄ yield (right) at 10 bar pressure and GHSVs of 32.6, 48.9, 65.2, 81.5 and 97.8 NL.g_{cat}⁻¹.h⁻¹

APPENDIX C: PARITY PLOTS

Parity plots of model-determined CO₂ conversion vs. experimental CO₂ conversion is presented for atmospheric (Figure C.1), 5 bar (Figure C.2) and 10 bar (Figure C.3) pressure, respectively. These parity plots demonstrate the degree of accurateness of the sum of least squares method used by the optimisation strategy for kinetic parameter estimation. R² values of 0.973, 0.989 and 0.953 were obtained for the respective operating pressures.

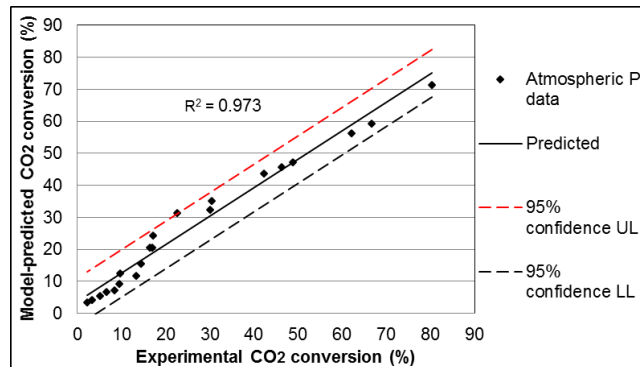


Figure C.1: Parity plot of model predicted vs experimental CO₂ conversion at atmospheric pressure

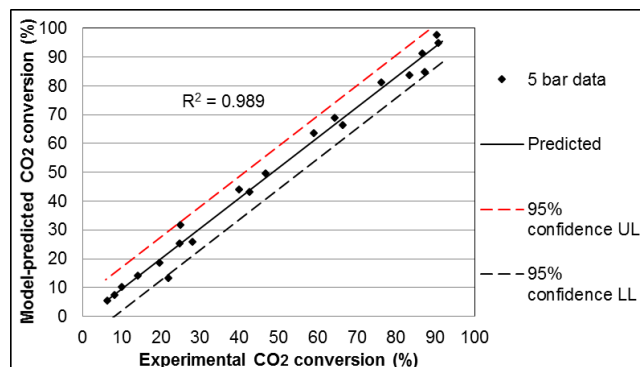


Figure C.2: Parity plot of model predicted vs experimental CO₂ conversion at 5 bar pressure

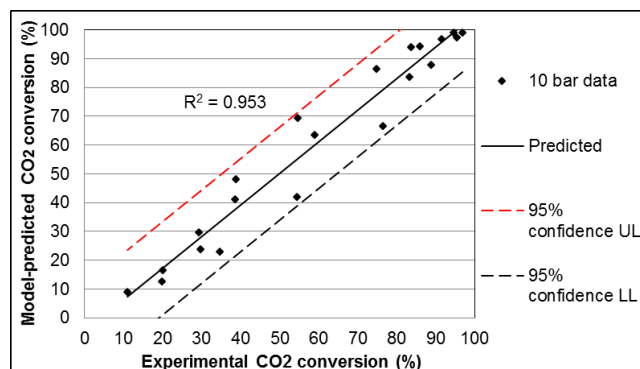


Figure C.3: Parity plot of model predicted vs experimental CO₂ conversion at 10 bar pressure